SCK•CEN/27622175
ER-0505

Dissolution behaviour of spent nuclear fuel at highly alkaline conditions

Phenomenological synthesis report

Karel Lemmens, Christelle Cachoir and Thierry Mennecart

Publication date : January 2019

Contract name: ONDRAF/NIRAS, Contrat de R&D "Gestion à long terme des déchets radioactifs" (2015-2020)

Contract number:
SCK•CEN: CO-90-14-3690-00
ONDRAF/NIRAS: CCHO 2015-0304/00/00
Specification sheet 15-SCK-SPF-06

SCK•CEN
Boeretang 200
BE-2400 Mol
Belgium

Studiecentrum voor Kernenergie
Centre d'Etude de l'énergie Nucléaire
Boeretang 200
BE-2400 Mol
Belgium

Phone +32 14 33 21 11
Fax +32 14 31 50 21

http://www.sckcen.be

Contact:
Knowledge Centre
library@sckcen.be

Configuration Control

Document History

Revision	Status	Author	Date	Changes

Document Approval

	Name	Date	Signature
Author: (Function)	Karel Lemmens (Scientific collaborator)	23-01-2019	
Reviewed by: (Function)	Thierry Mennecart (Scientific collaborator)	23.01.2019	
Approved by: (Function)	Elie Valcke (Head of Unit RDW)	23.01.2019	
Approved for QA: (Function)	Elke Jacops (QA coordinator)	24/01/2019	
Security approval: (Function)			

Distribution List

Name	Affiliation/Expert Group/Unit	Number of copies	Format
Roberto Gaggiano	NIRAS/ONDRAF	5 1	 On vignette

Table of Content

List of figures

List of tables

Glossary of Abbreviations

BE	Best Estimate
BWR	Boiling Water Reactor
CANDU	Canada Deuterium Uranium fuel
CEC	Contained Environment Concept
C-S-H	Calcium-Silicate-Hydrate
DIW	Distilled Water
ECW	Evolved Cement Water
FG	Fission Gas
FIAP	Fraction of the Inventory in the Aqueous Phase
FP	Fission Product
HTR	High Temperature Reactor
IRF	Instant Release Fraction
MIMAS	Micronized Master blend
MOX	Mixed Oxide fuel
OCW	Old Cement Water
OPC	Ordinary Portland Cement
PE	Pessimistic Estimate
PWR	Pressurized Water Reactor
SA/V	Surface Area to leachate Volume
SCK•CEN	Studiecentrum voor Kernenergie / Centre d'Etude de l'Energie Nucléaire
SNF	Spent Nuclear Fuel
SYF	Simple Young Fluid
UOX	Uranium Oxide fuel
VHLW	Vitrified High-Level Waste
YCW	Young Cement Water without Ca
YCWCa	Young Cement Water with Ca

Preface

This report was written in close cooperation with, and with the financial support of ONDRAF/NIRAS, the Belgian Agency for Radioactive Waste and Fissile Materials, as part of the programme on geological disposal that is carried out by ONDRAF/NIRAS.

The report is a deliverable of specification sheet 15-SCK-SPF-06 of Research package 'Spent Fuel' (SPF) in the framework of the ONDRAF/NIRAS R&D contract "Gestion à long terme des déchets radioactifs" (2015-2020). The ONDRAF/NIRAS reference number for the contract is CCHO 2015-0304/00/00. The SCK•CEN contract number is CO-90-14-3690-00.

Abstract

This report gives a summary of literature data pertaining to the dissolution behaviour of spent nuclear fuel in generic geological disposal conditions, with special attention to the highly alkaline systems that are dominated by the presence of Ordinary Portland Cement (OPC).

It contains a description of the spent fuel alteration and dissolution mechanisms, leading to the release of radionuclides. The report focuses on the release of radionuclides that are incorporated in the UO_2 matrix. Both results found in the open literature and results generated in the framework of the Belgian R&D programme are presented.

The available information shows that the dissolution behaviour of spent fuel in a system dominated by the presence of OPC (contact with high pH cement water) is similar to the dissolution expected in other conditions (contact with near-neutral pH ground waters), both in terms of mechanisms and in terms of the resulting dissolution rate.

Extended summary

This report gives a summary of literature data pertaining to the dissolution behaviour of spent nuclear fuel in generic geological disposal conditions, with special attention to the highly alkaline systems that are dominated by the presence of Ordinary Portland Cement (OPC).

It contains a description of the spent fuel alteration and dissolution mechanisms, leading to the release of radionuclides. The report focuses on the release of radionuclides that are incorporated in the UO_2 matrix. Both results found in the open literature and results generated in the framework of the Belgian R&D programme are presented.

The available information shows that the dissolution behaviour of spent fuel in a system dominated by the presence of OPC (contact with high pH cement water) is similar to the dissolution expected in other conditions (contact with near-neutral pH ground waters), both in terms of mechanisms and in terms of the resulting dissolution rate. In the expected geological disposal conditions (reducing chemical conditions, low temperature, very little water replacement), the UO_2 matrix of the spent fuel will be very stable. Significant dissolution of the spent fuel is possible only when the UO_2 matrix is oxidized to more soluble UO_{2+x}, releasing in solution U(VI) species and other radionuclides incorporated in the uranium matrix. In absence of airborne oxygen gas, UO_2 matrix oxidation can occur only through formation of radiolytic oxidants in the surrounding pore water. The resulting matrix dissolution rate is expected to decrease spontaneously because of the decreasing α-activity. In the presence of hydrogen gas, generated as a result of anaerobic corrosion of metallic near-field materials, the dissolution rate will be low even on the short term, when the α-activity is still high. This was confirmed by tests with spent nuclear fuel at high pH and a H_2 pressure of 3.2 bar. The stabilizing effect of H_2 at high pH still has to be confirmed for a lower H_2 pressure.

In the expected chemically reducing geological disposal conditions the fuel dissolution will be non-oxidative, and thus controlled by saturation of the solution with U(IV). The strongest evidence for this comes from the tests with real spent fuel. Other experiments were done with depleted or UO_2 doped with alpha emitters (^{238}Pu, ^{233}U) to simulate real spent fuel thousands or tens of thousands of years after the discharge from the reactor. Most of these experiments still show a residual dissolution rate in cement water. This is, however, not expected to occur under the foreseen geological disposal conditions, as the experimentally observed residual dissolution rate may be ascribed to oxidation by contamination with traces of atmospheric O_2. For more active UO_2 there is also a radiolytic oxidation due to the low reducing capacity of the high pH water that was used. Moreover, there is evidence that the presence of fission products stabilizes the fuel, so (α-doped) UO_2 would be less stable than the real, more complex UOX matrix.

The dissolution rate with spent fuel in the presence of hydrogen gas is low, and probably similar as in near-neutral pH conditions, but a precise quantification of the long-term dissolution rate is difficult. The dissolution rates measured so far with fresh fuel and with depleted or Pu-doped UO_2 thus probably overestimate the real long term matrix dissolution rate we can expect in geological disposal conditions. This rate is expected to be very low, as suggested by the natural analogues like uraninite, which are very stable in spite of their activity.

The effective surface area of the spent fuel is not expected to depend much on the disposal design. Its long-term evolution is difficult to assess experimentally. For this reason, the surface area of today's fuels is used to estimate the surface area after disposal.

Keywords

Spent fuel, dissolution, supercontainer, cement, phenomenology

1 Introduction

1.1 General background

In Belgium, the radioactive waste is categorized according to its activity level and life span into three categories (ONDRAF/NIRAS, 2013):

- category 'A' waste, i.e. short-lived low- and intermediate-level conditioned waste
- category 'B' waste, i.e. low- and intermediate-level conditioned waste contaminated by long-lived radionuclides
- category 'C' waste, i.e. high-level conditioned waste containing large quantities of long-lived radionuclides. For the Belgian case, this corresponds basically to vitrified high-level waste and non-reprocessed spent fuel declared as waste.

The national Agency for Radioactive Waste and Enriched Fissile Materials – ONDRAF/NIRAS – is responsible for the management of all radioactive materials (currently existing and future waste) generated in Belgium. One of the main concerns is to find a safe and sustainable solution for the final management of this radioactive waste in such a way that it will protect people and the environment from potential hazards, to ensure their safety now and in the future.

Disposal in deep stable geological formations is, at present, accepted at an international level to be the most promising option for the long-term management of high-level and/or long-lived radioactive waste (Chapman et al., 2012; NEA, 2008; IAEA, 2011). Geological disposal relies on a combination of engineered (man-made) barriers and a natural barrier (the host rock), in order to avoid that radionuclides and other contaminants can reach concentrations at which they could present an unacceptable risk for man and the environment. The engineered barriers should be designed to provide complete containment of the heat-generating waste at least throughout the thermal phase, which is assumed to last for at least several hundreds of years for vitrified high-level waste and possibly up to a few thousand years for spent fuel, to avoid coping with complex behaviours of radionuclide transport during this period (Chapman et al., 2012; IAEA, 2011).

ONDRAF/NIRAS currently recommends underground disposal in a geological stable and poorly indurated clay formation as the reference to steer their RD&D research programmes. The reference host formations for the geological disposal are poorly indurated argillaceous formations. They have been the subject of extensive studies over the last years. Schist rock (shales or slates) are studied as a further potential alternative option. The clays have favourable properties such as a low hydraulic conductivity (Yu et al., 2013), a high sorption capacity for many radionuclides (Maes et al., 2004) and self-healing properties because of its elasto-plastic behaviour (Maes et al., 2004; Bastiaens et al., 2007; Van Geet et al., 2008). All of these properties help to retard the migration of radionuclides released from the waste after breaching of the primary containment barrier (the overpack) (Weetjens et al., 2012). It should be noted, that currently there is no national policy regarding the long-term management of category B waste and category C waste in Belgium.
The *supercontainer concept* is currently being considered as reference design for the final disposal of Vitrified High-Level radioactive waste (VHLW) and Spent Nuclear Fuel (SNF) in

Belgium, i.e. the category C waste. In this design (see Figure 1-1), the VHLW or SNF is first encapsulated in a stainless steel drum, i.e. *the waste canister*, and then placed in a watertight carbon steel container (*the overpack*). In the case of the SNF assemblies a cast iron insert is emplaced within the overpack for criticality purposes. The overpack is afterwards inserted into a cylindrical prefabricated concrete block (*the buffer*). The cavity between the carbon steel overpack and the concrete buffer is filled with a cementitious material (*the filler*). In the presently preferred design option, the concrete block is fitted into an outer stainless steel casing (*the envelope*). These supercontainers are placed in concrete lined disposal galleries. The void space between the gallery lining and the supercontainer is also filled with a cement-based backfill material (ONDRAF/NIRAS, 2017). This design is based on the Contained Environment Concept (CEC) (ONDRAF/NIRAS, 2004), which aims to establish an engineered environment around the metallic overpack that would ensure chemically favourable conditions under which corrosion processes are very slow and well understood and thereby guaranteeing full containment of the overpack during at least the thermal phase, when the heat emitted by the waste form is still significant.

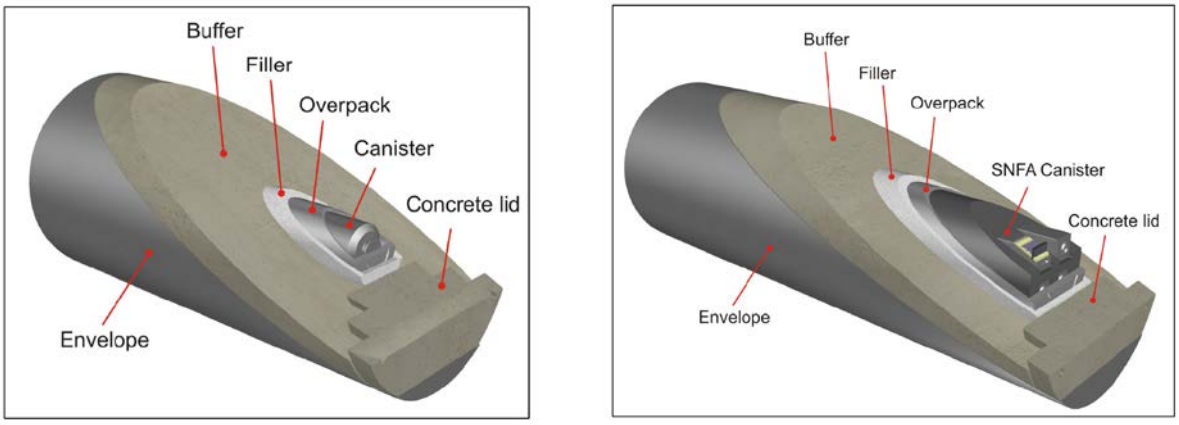

Figure 1-1: Top: 3D representation of a supercontainer containing 2 vitrified waste canisters (left) and a supercontainer containing 4 UOX spent fuel assemblies (right) (ONDRAF/NIRAS, 2017)

Low carbon steel (mild steel) has been chosen as material for the overpack. The function of the overpack is to provide total containment of the radionuclides during at least the thermal phase by preventing contact between the waste form and pore water coming from the host formation (ONDRAF/NIRAS, 2013).

An Ordinary Portland Cement based (OPC) self-compacting concrete is currently the preferred option for the choice of the concrete buffer. The primary role of the concrete buffer is to create a chemically favourable environment around the carbon steel overpack with regards to corrosion (ONDRAF/NIRAS, 2013). Indeed, the highly alkaline conditions that exist in OPC concrete (pH ~ 13.6) will protect carbon steel against corrosion by the presence of a thin "passive" layer, which significantly minimizes corrosion, leading to very low uniform corrosion rates in the absence of aggressive species (Kursten, 2018). An additional buffer function is to provide permanent radiological shielding, which eliminates the need for remotely controlled underground operations and intrinsically better protects the workforce during handling and transportation operations of the supercontainers (ONDRAF/NIRAS, 2013).

1.2 Scope and objectives

This report gives a summary of knowledge pertaining to the dissolution behaviour of spent nuclear fuel in generic disposal conditions, with the focus on the systems that are dominated by the presence of Ordinary Portland Cement.

It contains a description of the phenomena that are expected to take place in the waste form and as a result of the interaction of the waste form and the disposal environment, and that may – or may not – have an impact on the dissolution behaviour of the waste form. It also gives a summary of experiments that were performed to quantify these effects, including data on natural analogues. The level of detail is such that it should be understandable to readers with a general scientific background.

The data discussed in this report have been gathered from two main sources:

- Data reported in the literature originating from studies in the framework of various national nuclear waste management programmes. The experiments used in these studies were conducted in conditions (chemical and environmental) that were considered to be relevant to those expected in the supercontainer.
- Data generated during the RD&D experimental programmes that have been funded by ONDRAF/NIRAS. These studies were conducted in conditions that simulated the supercontainer conditions as closely as possible. In this report we will further refer to these studies as the *Belgian R&D programme*.

The dissolution mechanisms and rates that are presented in this report should be used as a scientific basis to assess the behaviour of spent fuel in disposal conditions that are comparable with the supercontainer conditions. For this, we frequently refer to the so called 'long-term geological disposal conditions'. The most relevant characteristics of these conditions are:

- the high pH (due to the concrete),
- the absence of airborne O_2,
- a low temperature, not much higher than the host rock,
- very little water replacement (diffusion controlled transport to the near-field).

1.3 Structure of the report

The report is structured as follows:

- Chapter 2 presents a generic description of the reference spent nuclear fuel types considered in this report, including information about the microstructure of these spent fuel types.
- Chapter 3 presents a review of published data on spent fuel dissolution in aqueous conditions that are relevant for the Belgian context. We show a general model for the spent fuel alteration in water, making clear the most relevant release mechanisms, we present the main parameters affecting the dissolution behaviour of

the spent fuel, we give an overview of the literature data on spent fuel matrix dissolution rates, and we present evidence from natural analogues.

- Chapter 4 presents an overview of the materials and methods that were applied in the Belgian R&D programme.
- Chapter 5 presents the main results of the Belgian R&D programme.
- Chapter 6 gives a discussion of the data. It compares the fuel behaviour as described in the open literature with the findings of the related tests in the Belgian R&D programme and discusses the consequences for the long term evolution of the spent fuel
- Chapter 7 gives the open issues and recommendations.
- Chapter 8 contains the list of literature references.
- Chapter 9 is an annex presenting literature data related to the specific surface area of the spent fuel, this is a parameter for which the Belgian R&D programme did not foresee specific studies.

2 Description of the spent nuclear fuel

In this section, we give a short overview of the characteristics of the main spent nuclear fuel types relevant in the Belgian context. We focus on aspects that are relevant for the dissolution behavior of spent fuel in water. A more complete overview is given in (Govers et al., 2018).

Worldwide, a variety of nuclear fuel types exists, including pressurized water reactor fuels, boiling water reactor fuel, Canada Deuterium Uranium fuel, High Temperature Reactor fuel, and advanced gas cooled reactor fuel. Most of these designs use uranium dioxide fuel (UO_2). Uranium dioxide fuel (referred to as UOX) is the most important fuel also in the the Belgian spent fuel inventory, which includes enriched natural uranium dioxide, enriched reprocessed uranium dioxide, and mixed uranium-plutonium dioxide (MOX).

The UOX or MOX fuel is prepared as pellets. The fuel pellets are contained in a tight zirconium alloy cladding, for confinement purpose. The fuel pellet stack and the cladding form the fuel rod. These fuel rods are not manipulated individually, but as bundles of rods maintained at fixed spacing by a rigid structure, forming a so-called fuel assembly. An example of such a fuel assembly is shown in Figure 2-1. In Belgium, a wide range of fuel assemblies has been used, with different geometries, differing in fissile column length and number of fuel rods loaded. More information about this can be found in (Govers et al., 2018).

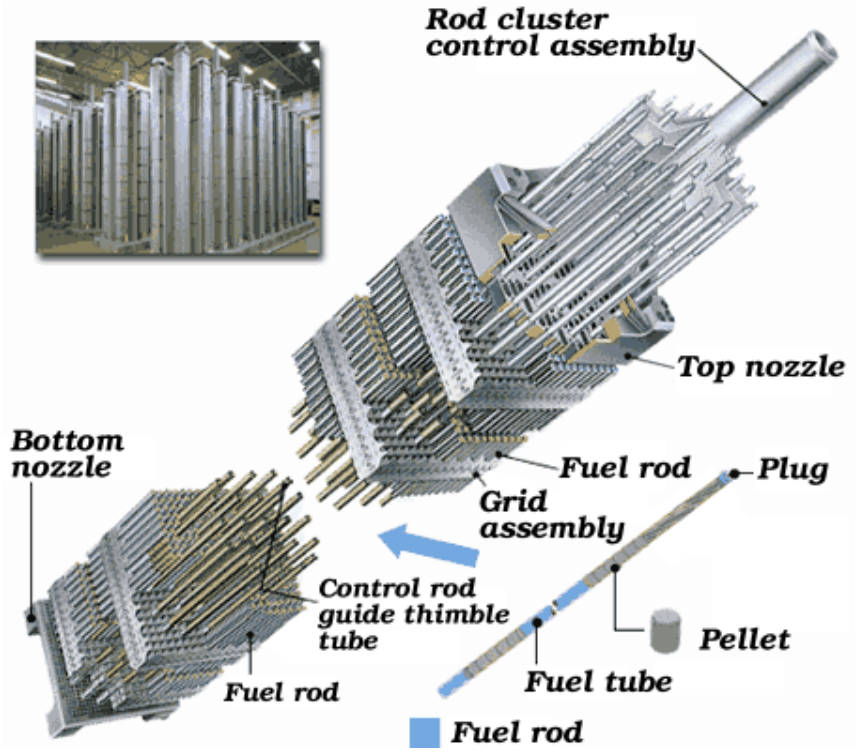

Figure 2-1 : Structural components of a UOX and MOX fuel assembly. Source: Mitsubishi Nuclear Fuel 2017 [WNA 2017]

Apart from unavoidable impurities, the as-fabricated UOX pellets consist of uranium oxide, with a U/O ratio close to 2. The oxidation state of the uranium increases slightly during the irradiation and afterwards, by fission and by beta-decay (Govers et al., 2018). During the irradiation, fission and activation reactions take place, resulting in the presence of fission products and other actinide nuclides. Apart from this, activation of non-actinide nuclides in the fuel, cladding and structural materials results in the production of activation products. Although the irradiated fuel can still be described as a uranium dioxide matrix, it thus has a chemical composition that is different from the as-fabricated fuel. This is relevant for the interpretation of experiments that use pure (unirradiated) UO_2 to simulate real spent fuel.

The distribution of nuclides within the spent fuel and the related microstructure are influenced mainly by the temperature during irradiation and the burnup (the definition of burnup is given in the last paragraph of this section). A distinction is made between elements that readily form solid solutions with UO_2 and thus remain fully dissolved in the fuel matrix and those which have a solubility limit that is low compared to the concentration at which they are typically present in spent nuclear fuel and which thus have a tendency to segregate from the matrix. Due to the radial temperature gradient in the fuel, the radionuclides that are volatile in the temperature range occuring during their irradiation will move towards the narrow gap between the fuel pellet and cladding (thermal migration). This has consequences for the dissolution behavior in geological disposal conditions. Nuclides which remain inside the UO_2 matrix are released only in events where the UO_2 matrix itself disintegrates, while nuclides present e.g. in the gap may be released already upon simple cladding breach. This is relevant also for the interpretation of leaching experiments with spent fuel described further in this report.

Unirradiated UOX fuel consists of crystalline UO_2 grains with an average diameter of 9 µm, separated by grain boundaries. MOX fuel also consists of crystalline grains, but typically still show Pu-rich agglomerates resulting from the MIMAS fabrication process. The UO_2 grain size of MOX fuel is about 6 µm (for MIMAS MOX) (Poinssot et al., 2001). During irradiation the cylindrical fuel pellets in the fuel rod undergo a range of physical modifications including cracking, grain growth and formation of new solid and gaseous phases. An external zone is formed (the rim), with a structure that is very different from the internal part. This so called *High Burnup Structure* (HBS) is highly porous and characterized by a very small grain size (0.1 µm). The thickness of the rim increases with the pellet-average burnup. The (micro)structure of the irradiated fuel is illustrated in Figure 2-2. The inner part of the fuel pellets still shows the UO_2 grains and the grain boundaries like in the unirradiated fuel. In the pellet periphery the HBS structure (rim) is clearly visible. The figure also illustrates the corrosion of the zircaloy cladding that takes place during irradiation.

All these in-reactor fuel changes are governed by the *irradiation history* of the fuel: the instantaneous power and the time-integration thereof. The power is generally expressed per unit length of a fuel rod: Watt per cm ($W \cdot cm^{-1}$). Time integration of the power yields the total energy delivered by the fuel, called the "burnup" (BU) of the fuel, and this is conventionally expressed in terms of energy delivered per unit mass of the fuel. By convention, this is expressed as gigawatt day per metric ton of "heavy metal" (uranium or uranium and plutonium): $GWd \cdot t_{HM}^{-1}$. While the burnup defines the composition of the irradiated fuel, it is the instantaneous power which principally determines the in-reactor temperature of the fuel (temperatures exceeding 1500 °C are not exceptional) and thus defines the mobility and possible segregation of fission products.

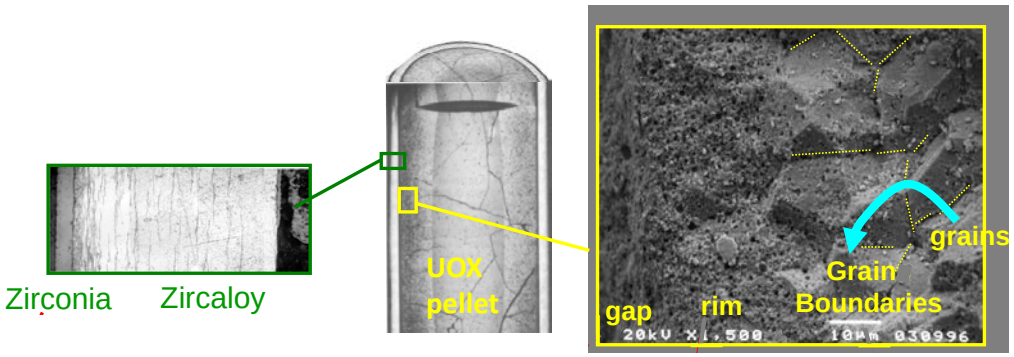

Figure 2-2 : View of the main structures of PWR spent fuel, showing the transition of the large grains and grain boundaries in the inner part of the pellet to the fine grains in the rim and the gap between the rim and the cladding (Ferry et al., 2007)

3 Spent fuel alteration and dissolution in water : review of data

The extensive research on the spent fuel dissolution behaviour at neutral pH has led to a relatively good understanding of the dissolution mechanisms, and their interaction. A general model describing the alteration of spent fuel in water, as described in (Poinssot et al., 2005; Poinssot et al., 2006; Eriksen et al., 2012), is shown in Section 3.1. The main parameters affecting the radionuclide release processes are discussed in Section 3.2. The release kinetics (dissolution rates) reported in literature in conditions relevant to geological disposal is summarized in Section 3.3. In Section 3.4, we summarize the evidence from natural analogues of spent fuel.

3.1 General model for spent fuel matrix alteration and dissolution in water

Upon contact with water, the spent fuel will start to release its radionuclides via different mechanisms. The amount of radionuclides that is released at a certain rate is generally called the *radionuclide source term*. The release mechanism will be different for radionuclides that are dissolved and those that are not dissolved in the UO_2 matrix.

Most radionuclides (fission products, actinides, activation products) are incorporated in the spent fuel matrix. They will be released only by fuel matrix alteration or dissolution and will constitute the vast majority of the radionuclide source term. This release by matrix dissolution is the focus of this report.

Because the matrix of the spent fuel consists basically of UO_2 (or rather UO_{2+x}), the terms *UO_2 matrix dissolution* and *spent fuel matrix dissolution* are further used as synonyms.

3.1.1 Mechanisms of spent fuel matrix dissolution

The *fuel matrix dissolution* consists of the sum of oxidative U(VI) dissolution and non-oxidative U(IV) dissolution, as shown by many studies at neutral pH.

Oxidative dissolution

The oxidation of the fuel surface typically results in the formation of U(VI). This U(VI) can remain attached to the surface, but the higher solubility of U(VI) phases promotes the release of U(VI) species into solution, with an increasing solubilization in the presence of carbonates (Casas et al., 2009). The oxidation is not stopped by saturation of the solution. At saturation, secondary U(VI) phases are formed and the oxidation continues. However, the formation of a dense layer of precipitated phases on the fuel surface could possibly slow down the oxidation (Shoesmith et al., 1996; Jerden et al., 2015). Because of the changes in the uranium oxide fluorite crystal structure and the dissolution of the U(VI), the radionuclides included in the uranium oxide matrix are no longer retained after matrix oxidation and they are released to the solution as well. Their dissolution will depend on their solubility in the leaching solution. They can coprecipitate with secondary uranium phases.

Oxidative dissolution occurs in the presence of oxidizing species, such as airborne oxygen, but can also be enhanced in anoxic conditions in deep groundwaters, by oxidative radiolytic molecules or radicals.

In anoxic conditions, the oxidizing effect of radiation will become smaller with disposal time, due to the radioactive decay. At a sufficiently low dose ('threshold' dose) radiation seems to become unable to sustain oxidative dissolution. The dose rate at which the oxidation becomes negligible is the so called 'threshold for oxidative dissolution'. The threshold is reached sooner when the conditions are more reducing. In the presence of H_2 gas at sufficiently high concentration, the threshold is reached even for very high α–β–γ doses, corresponding to young spent fuel (see Section 3.2.4 and Figure 6-3). When the threshold has been reached, the further fuel dissolution may be governed by the fuel solubility, but the influence of local water radiolysis needs to be assessed better (Poinssot et al., 2006). A slow continued oxidative dissolution, followed by reduction and precipitation of the dissolved uranium species would offer a way for the embedded radionuclides to become released further into the intruding water. In (SKB, 2010), this process is called 'fuel conversion'.

Non-oxidative dissolution

Under anoxic or reducing conditions, at a sufficiently low dose rate, the oxidative dissolution will be negligible, while the non-oxidative dissolution can continue as long as the solution is undersaturated with U(IV) relative to the fuel surface.

Removal of U(IV) from solution by transport, sorption or precipitation can delay the saturation of the solution and hence trigger the non-oxidative dissolution (Grambow et al., 2006).

Even under the threshold and in a U(IV)-saturated solution, there may be slow remaining non-oxidative transformation processes at the UO_2 surface, involving exchange with U in solution, as suggested by isotope dilution tests (Ollila et al., 2007), but the existence of such mechanism is still questioned.

3.1.2 Spent fuel matrix dissolution models

The existing fuel dissolution models (and codes) focus on the oxidative matrix dissolution (Grambow et al., 2010). They typically consider the following steps: (i) modelling of the generation of oxidants and reductants by a kinetic model of radiolysis, (ii) oxidation of spent fuel surface, (iii) reduction of the aqueous oxidants and finally (iv) dissolution of the spent fuel matrix and radionuclide release according to the uranium speciation and groundwater composition with or without consideration of electrochemical processes. The oxidized U(VI) can reprecipitate in secondary phases. This is illustrated in Figure 3-1.

Models that account for the spatial dose distribution and the diffusion of species to and from the surface tend to predict oxidative dissolution rates nearly an order of magnitude lower than models not considering the transport of species (Eriksen et al., 2012).

Simplified models (and codes) assume for example that all produced oxidants will react with the fuel and that all fuel oxidation will lead to fuel dissolution.

More recent models focus on how to take into account the beneficial effect of hydrogen counteracting oxidative radiolytic dissolution. This includes radiolytic reactions of hydrogen in solution and at the UO_2 surface.

A specific class of models uses electrochemical equations to describe the system, such as the MPM model (Shoesmith et al., 1998) and the recent FMDM model (Jerden et al., 2015). The latter model also includes the effect of the epsilon particles and diffusion through a precipitation layer.

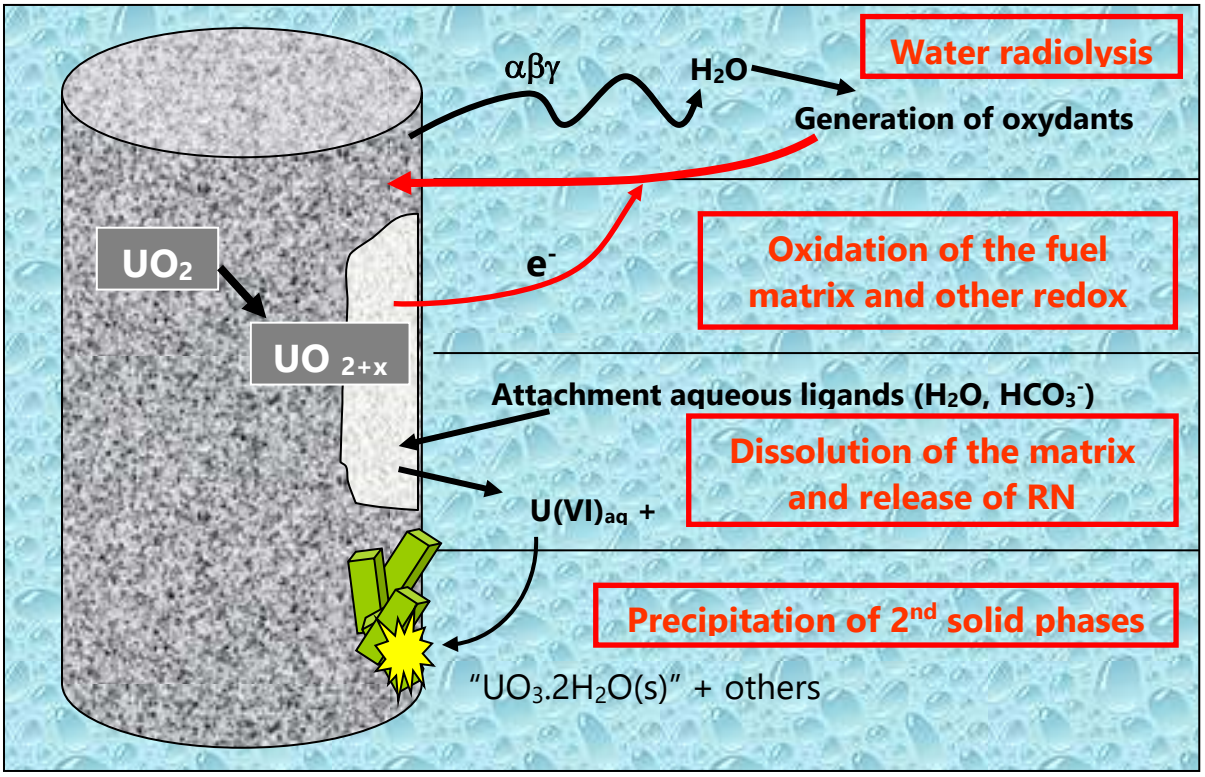

Figure 3-1: Elementary processes governing the spent fuel alteration (Poinssot et al., 2005).

Much less attention is given to the kinetic modelling of non-oxidative fuel dissolution. In reducing static test conditions, equilibrium with the U(IV) solution is quickly reached, and the further dissolution rate, based on the dissolved uranium concentrations, cannot be distinguished from zero. There are indications that the non-oxidative dissolution proceeds even under U(IV) saturation, but this is still debated, and the mechanisms and implications are not clear (Ollila et al., 2007).

Modelling of the interaction with near-field materials is hampered by the lack of precise data about the interaction of U(IV) species with the near-field materials. Data for U(VI) are less scarce. Moreover, the number of experimental data allowing to develop or validate coupled models is very limited. Because the interaction of uranium with common near-field materials like iron corrosion products or concrete is very limited anyway (see Section 3.2.8), it is not expected to cause a significant increase of the fuel dissolution rate. It can, however, play a role on the (very) long term.

On the long term oxidative dissolution is believed to become negligible, because the long term conditions are reducing. The remaining non-oxidative dissolution is probably solubility controlled, but it cannot be excluded that it is controlled by a slow constant conversion, lower than the experimental detection limits. In the case of a model based on solubility control, coupled with transport into the near-field, the predicted fuel alteration rate will become very small (depending on the exact model parameters, including the sorption on the near-field and host rock materials), resulting in very long fuel life times. In the case of a model with a low constant residual conversion rate, the fuel life time will depend on the value of the assumed constant rate.

3.2 Parameters affecting the dissolution behaviour of the spent fuel

The main parameters or processes with an effect on the spent fuel dissolution and the related radionuclide release are the fuel characteristics, the radiation dose emitted by the fuel, related to the so called threshold for radiolytic oxidative dissolution, the pH and redox conditions, the concentration of H_2 gas, water composition, temperature and the specific surface area of the spent fuel. Probably less important on the short term but relevant on the long term are the sorption of uranium on surrounding materials and the secondary phase formation. The effect of these parameters on the dissolution of spent fuel is discussed in the following sections.

3.2.1 Impact of fuel characteristics

The relevant fuel characteristics are the fuel type (UOX or MOX), and the conditions during the reactor operation, mainly the fuel burnup, the irradiation temperature and the linear power rating, which have an impact on the microstructure of the fuel.

MOX fuels have been studied much less intensively than UOX fuels. The basic dissolution mechanisms are believed to be the same, but the dissolution rate may be different. A medium burnup MOX appeared to dissolve 7 to 8 times faster than a UO_2 fuel with similar burnup in aerated carbonated groundwater (Jégou et al., 2004b; Roudil et al., 2007), but in the presence of dissolved H_2, the oxidation and dissolution is inhibited like for UOX, as shown by the stable U concentration of 7×10^{-10} mol·L^{-1} (Carbol et al., 2009a). In the latter case (with H_2), the uranium oxide matrix of the spent MOX fuel appeared to be the main contributor to the measured dissolution, while the corrosion of the high burnup Pu rich islands was negligible. There are indications that the uranium oxide matrix dissolves faster than the Pu-islands also in argon atmosphere without H_2 (Carbol et al., 2009a).

The main effect of the burnup on the matrix dissolution is due to the specific α-β-γ activity (Bq per gram of UO_2), which increases with increasing burnup, leading to higher radiation dose rates of the surrounding water, and hence potentially higher radiolytic oxidative dissolution (see Section 3.2.2). The effect of the burnup on the α-activity of UO_2 and MOX at the time of discharge from the reactor and further in the future is illustrated in Figure 3-2.

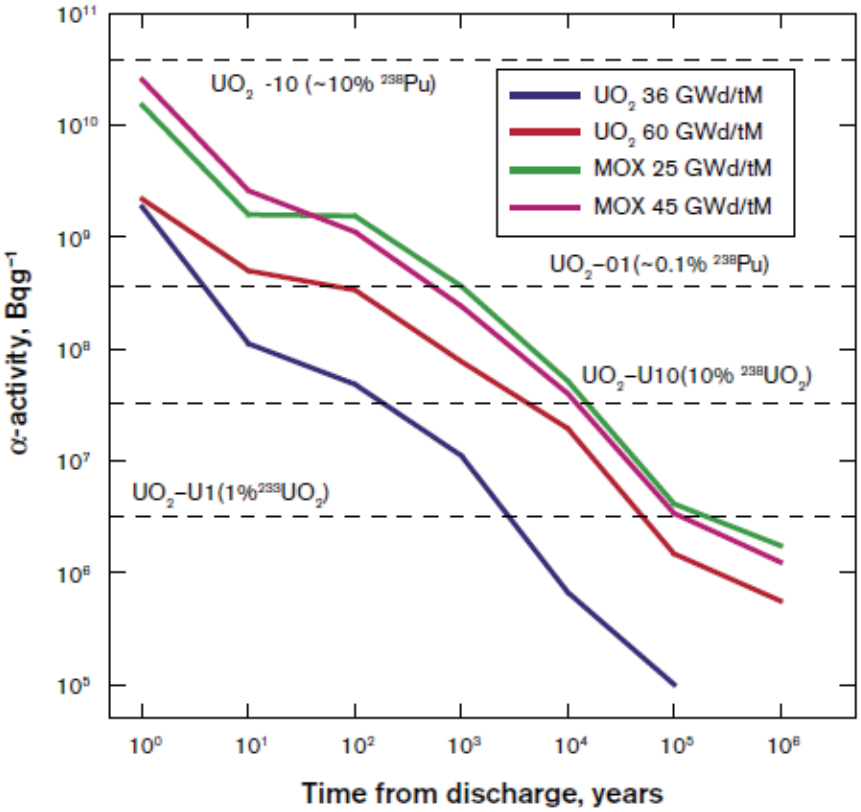

Figure 3-2: Decreasing α-activity of spent fuel as a function of time. The graph shows that the α-activity is higher for UOX with higher burnup. The horizontal lines correspond to the α-activity of α-doped UO_2 types (UO_2 doped with 10% ^{238}Pu, 0.1% ^{238}Pu, 10% ^{233}U and 1% ^{233}U) that were used as test material in foreign research programmes (Carbol et al., 2005).

The radiation after discharge from the reactor has further effects on the fuel structure and composition, but without a significant impact on the matrix dissolution. The only radiation effect on the structure with possible long-term consequences is the opening of grain boundaries due to increasing He accumulation. This is discussed in the chapter 7.

3.2.2 Impact of fuel activity

A higher α-β-γ activity of the fuel leads to higher radiation dose rates of the surrounding water. The ionizing radiation causes the formation of radiolysis products and the products that are formed in the first stage (physicochemical stage) can recombine in the second stage (chemical stage). This leads to the formation of both oxidizing and reducing species, which can be radicals or molecular species. In oxygen-free water, the products are e^-_{aq} (solvated electrons), H•, •OH, H_2, H_2O_2 (hydrogen peroxide), OH^- and H_3O^+ (Choppin et al., 2013). In oxygenated water the perhydroxyl radical HO_2• is formed. The H_2O_2 is formed by recombination of •OH following reaction Equation 1.

$$\bullet OH + \bullet OH \rightarrow H_2O_2 \qquad \text{(Equation 1)}$$

H_2O_2 can decompose into O_2 and H_2O:

$2\ H_2O_2 \rightarrow O_2 + 2\ H_2O$ (Equation 2)

O_2 can further be formed by Equation 3:

$\bullet OH + HO_2\bullet \rightarrow H_2O + O_2$ (Equation 3)

O_2 can also be formed by various other reactions involving recombination of radicals (Roth et al., 2011; Pastina et al., 2001).

The O_2 can react with the solvated electrons and hydrogen radicals to form other oxidants ($O_2\bullet$, $HO_2\bullet$). Reaction of •OH with dissolved carbonate can lead to the formation of an oxidizing carbonate radical ($HCO_3^- + \bullet OH \rightarrow CO_3\bullet^- + H_2O$) (Ekeroth et al., 2006). Formation of reducing H_2 is possible via several recombination reactions, such as Equation 4:

$H\bullet + H\bullet \rightarrow H_2$ (Equation 4)

Extensive lists of radical reactions can be found in literature (e.g. Pastina et al., 2001)

The yield of the various radiolytic products depends on the radiation type and energy. The primary yield of a particular radiation product is commonly referred to as G value, this is the amount of product per unit of absorbed energy. It depends on the linear energy transfer (LET) of the ionizing particle, which is the amount of energy that the particle transfers to the material traversed per unit distance. For α-radiation (high LET), the energy is absorbed in a very small volume. In water, this results in a track with a high density of radicals, increasing the probability for recombination reactions. Therefore, α-radiation produces mainly molecular products (H_2O_2), whereas beta or gamma-radiation (low LET) produce more radicals.

The oxidizing products can react with the UO_2 and hence cause radiolytic oxidative dissolution. Oxidation by H_2O_2 is the most important reaction (Ekeroth et al., 2006)

$UO_2\ (s) + H_2O_2 \rightarrow UO_2^{2+}\ (s) + 2\ OH^-$ (Equation 5)

O_2 can also oxidize the UO_2, but the oxidation by H_2O_2 is 200 times faster (Shoesmith et al., 2000). The oxidation results in the formation of an oxidized surface layer, which has a higher solubility than the UO_2, leading to the dissolution of the matrix.

The effect of increasing specific α-activity on the dissolution rate is illustrated in Figure 3-3. The spent fuels currently available for experiments have a very high α-β-γ activity (>100 $MBq{\cdot}g^{-1}$, see Figure 3-2). To study the impact of lower dose rates, α-doped UO_2 is used with lower activity (1 – 100 $MBq{\cdot}g^{-1}$). This is mostly ^{238}Pu or ^{233}U doped UO_2, as illustrated also in Figure 3-2. The rates corresponding to the lower α-activities in Figure 3-3 were obtained with such α-doped UO_2.

Figure 3-3 also shows that, when the α-activity reaches a certain minimum, the measured dissolution rate does not decrease further, this is the so called 'threshold for oxidative dissolution'. Below this threshold, the radiolytic generation of oxidants is too weak to cause oxidation of the fuel even in absence of reducing agents. Below the threshold, the dissolution would be solubility controlled (non-oxidative dissolution). According to (Muzeau et al., 2009), the threshold value lies between 18 and 33 $MBq{\cdot}g^{-1}$ in a carbonate solution (10^{-3} $mol{\cdot}L^{-1}$) under anoxic conditions ($pO_2 < 1 \times 10^{-5}$ %). This threshold depends on the environmental conditions:

in a carbonate solution in the presence of hydrogen (P_{H2} = 1 bar), the threshold rises above 385 MBq·g^{-1}.

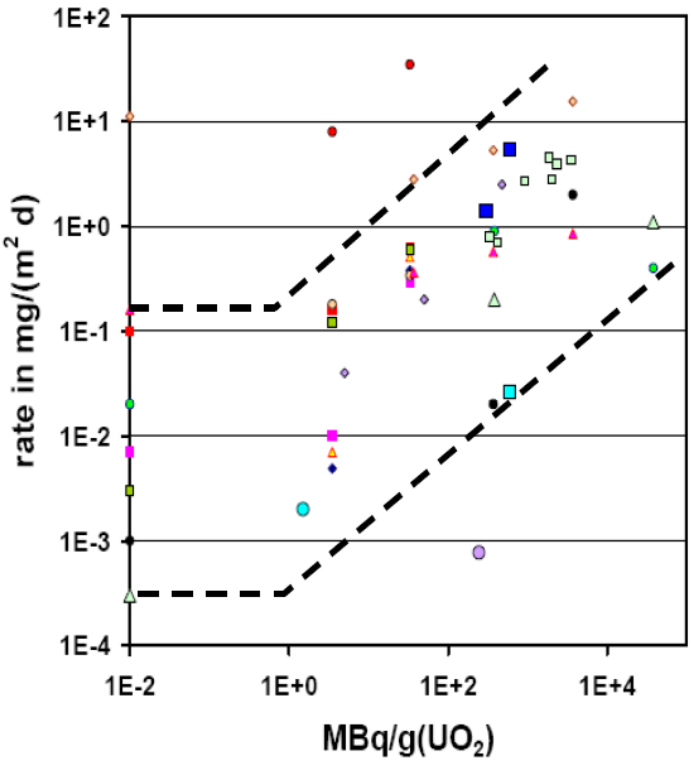

Figure 3-3: Dissolution rates measured for α-doped UO_2, non-doped UO_2 (0.01 MBq·g^{-1}) and spent fuel specimens as a function of specific α-activity (Poinssot et al., 2005). The sources of the individual data points are given in the reference. The dashed lines are arbitrary and drawn to emphasize the approximate α-strength below which no influence of α-radiation is observed (Shoesmith et al., 2008).

3.2.3 Impact of redox conditions and pH

Because the oxidative dissolution of the UO_2 is a redox process, the redox conditions have an evident impact on the fuel stability. Electrochemical studies have given important insight in the oxidation mechanisms. Figure 3-4 illustrates how the UO_2 is stepwise oxidized at increasing redox potential (Shoesmith et al., 1997). A critical step is the oxidation from $UO_{2.33}$ to higher oxidation states. Uranium dioxide appears to be capable of taking up oxygen at interstitial sites in the crystal lattice until a limiting stoichiometry of $UO_{2.33}$ is achieved. The further oxidation requires a major crystallographic rearrangement from the fluorite to the orthorombic structure and is accompanied by extensive dissolution and release of incorporated radionuclides (Lutze et al., 1988, p. 359).

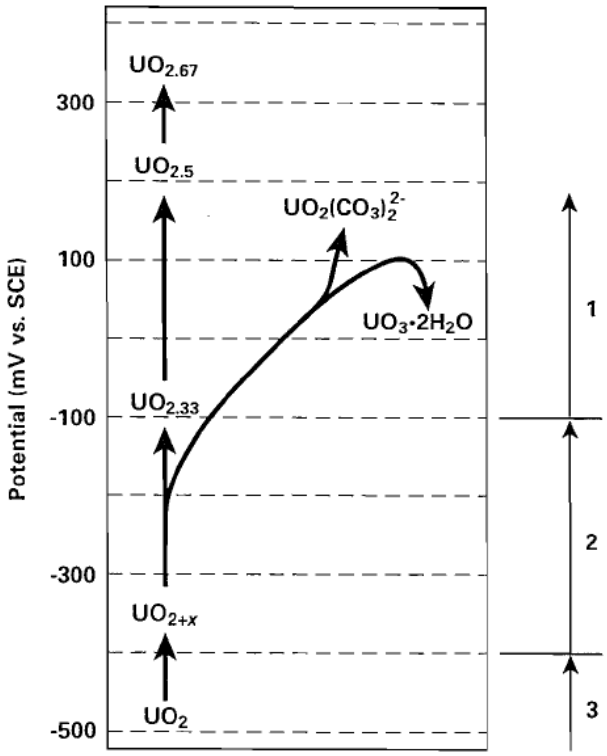

Figure 3-4: Chemistry/Electrochemistry of UO_2 oxidation and dissolution as a function of corrosion potential (Shoesmith et al., 1997)

Because the oxidized uranium U(VI) phases are much more soluble than the U(IV) phases, the oxidized uranium tends to dissolve. The dissolution is promoted by carbonate ions. When saturation is reached, the oxidized uranium can reprecipitate as a solid phase, such as $UO_3 \cdot 2H_2O$ in Figure 3-4. Exposure of spent fuel or UO_2 to water in the presence of oxygen will thus cause oxidative dissolution. This can be counteracted by the addition or reducing species, such as metallic iron or Fe(II), sulphide, or H_2 (Ollila et al., 2011).

The redox potential and pH will affect both the solid state and the dissolved species of the UO_2. This is discussed further hereunder. Moreover, literature data about the effect of pH on radiolysis and on the dissolution rate is summarized.

Effect of E_h/pH on the solid state

Redox potential and pH are coupled, as illustrated already by Equation 5 (the oxidation of UO_2 causes a pH increase). The relation between the two parameters is often graphically presented in Pourbaix diagrams, showing the E_h/pH ranges in which the various species with difference valence are thermodynamically prevailing (Pourbaix, 1974). Thermodynamic calculations suggest that a very high pH could decrease the UO_2 matrix stability by favouring U(VI) oxidation. At high pH, U(VI) is more stable than U(IV) even under nominally reducing conditions. This is illustrated by the Pourbaix diagram of Figure 3-5 (Duro et al., 2010). This is due to the high stability of the hydroxocomplexes of U(VI) formed at high pH values.

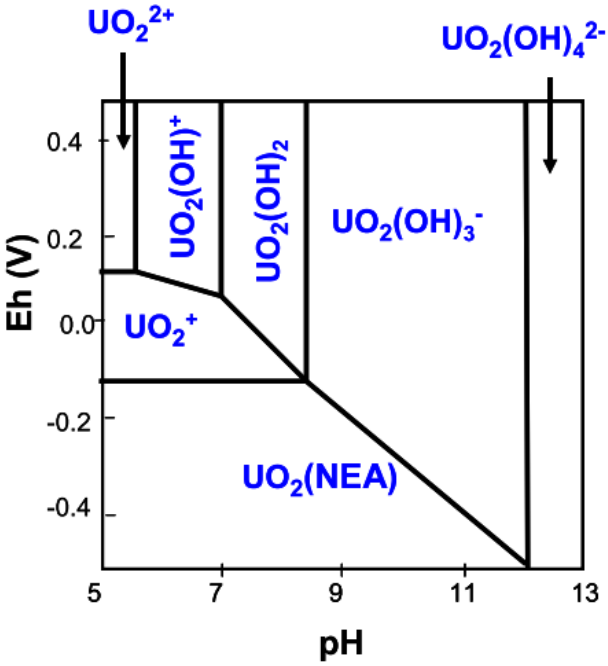

Figure 3-5: Predominance diagram of uranium in the absence of complexants in solution for a total uranium concentration of 10^{-8} mol·L^{-1}. Thermodynamic database used: Hatches NEA 18 avoiding the precipitation of crystalline UO_{2+x} (Duro et al., 2010)

Effect of the E_h/pH on the solubility of UO_2

Literature also provides data about the effect of pH on the UO_2 solubility.

- A review of solubility data by Neck (Neck et al., 2001) shows no clear change of the measured U(IV) concentrations in equilibrium with amorphous or microcrystalline $UO_2 \cdot xH_2O$ at higher pH (Figure 3-6). Above pH 6 and up to pH 13, the U(IV) concentrations are around an average of $10^{-8.5}$ mol·L^{-1}. The observed variations are probably due mostly to varying redox control.

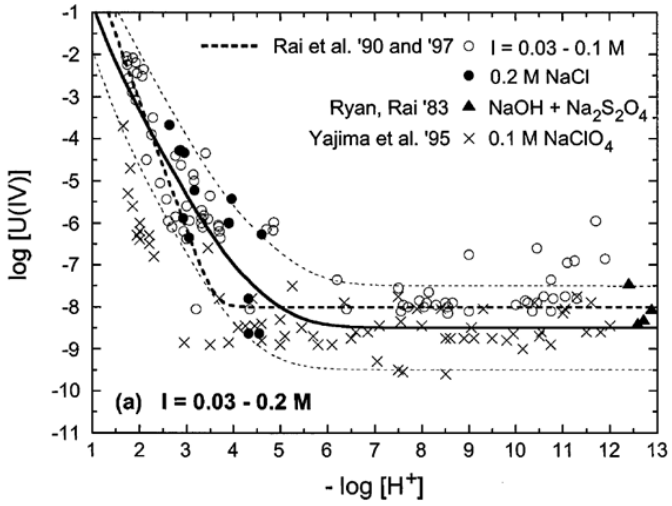

Figure 3-6: Solubility of amorphous or microcrystalline $UO_2 \cdot xH_2O$ as a function of pH (Neck et al., 2001)

- U(IV) concentrations of 10^{-7} mol·L^{-1} or higher have been reported for pH >10 (Wang 2009, p. 206; Ewart et al., 1992; Fujiwara et al., 2005), but because redox control is very difficult with U(IV), it is difficult to exclude the presence of U(VI) by oxidative dissolution. Also formation of polymeric species is not excluded.
- In some other tests with low-activity UO_2 containing 2.8% ^{235}U, the U(IV) concentration seemed to increase with pH between pH 9 and pH 13 under reducing conditions (Figure 3-7) (Ollila et al., 2008). It was suggested that this might be due to the formation of polynuclear U(IV) complexes, but this hypothesis needs confirmation. The measured concentrations are, however, all lower than the $10^{-8.5}$ mol·L^{-1} suggested in Figure 3-6.

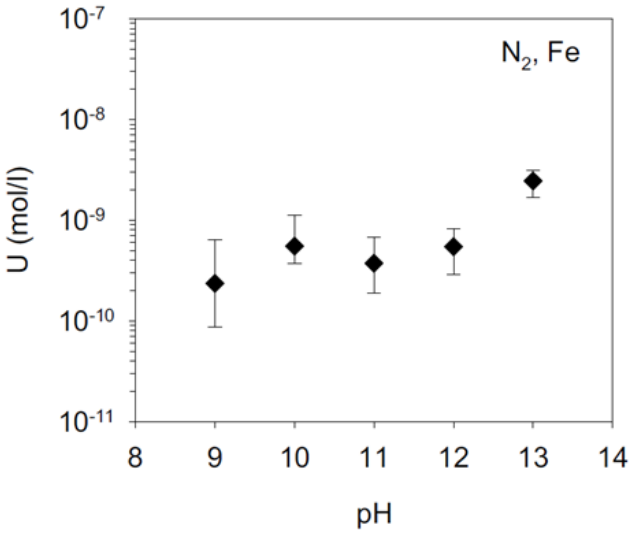

Figure 3-7: Stable U concentration in tests with UO_2 in NaCl/KOH solution of various pH (Ollila et al., 2008)

- The solubility of tetravalent actinides Th(IV), Np(IV) and Pu(IV) can increase at pH >11 in the presence of >1 mol·L^{-1} of Ca by the formation of $Ca_4[An(OH)_8]^{4+}$ complexes; a similar behaviour is expected for U(IV) (Fellhauer et al., 2010).
- The presence of H_2 gas can further lower the U concentrations. The concerning literature data are presented in Section 3.3.2.

Effect of the E_h/pH on radiolysis

The radiolytic oxidation rate might be different at high pH, if the yield for formation of radiolytic species (G-values, see Section 3.2.2) is affected by the pH. The available data suggest, however, that this is not the case.

- Roth (Roth et al., 2011) showed that H_2O_2 production in the radiolysis of water was not affected by pH (in the pH range 1-13). Around pH 13, the H_2O_2 production was even lower than at neutral pH.
- An important pH effect on the production of H_2O_2 was not observed either by Auclair (Auclair, 2001).

- The radiolytic H_2 production was not affected by a high pH (Loida et al., 2006; Kelm et al., 2002).
- The production of the oxidizing hypochlorite and chlorate species was higher at pH 12 than at pH 8 in 5 M NaCl solutions (Kelm et al., 2002)

A low redox potential due to the presence of reducing species can have an effect on the yield of radiolytic species. The main reducing species involved is H_2 gas. Related data are given in Section 3.2.4.

Effect of the E_h/pH on the spent fuel dissolution rate

The collection of literature data presented in Figure 3-3 was obtained for tests with varying pH, but also different media, atmosphere and experimental methods. For this reason, the net effect of the pH cannot be distinguished. A systematic study of the effect of pH was performed by Röllin (Röllin et al., 2001). Dissolution rates of spent UOX fuel were investigated using flow-through experiments under oxidizing, anoxic and reducing conditions in carbonate solutions. The results are shown in Figure 3-8. For oxidizing conditions, the U dissolution rates were about 3 $mg \cdot d^{-1} \cdot m^{-2}$ for pH > 6. For pH < 6, dissolution rates were strongly increasing with decreasing pH. The dissolution rates with H_2 saturated solutions dropped by up to four orders of magnitude when compared to oxidizing conditions and were largely independent of pH. For anoxic conditions, both redox potential and dissolution rate approached the values under oxidizing conditions, but this was not tested for the whole pH range.

These results confirm that the pH has little effect on the fuel dissolution at near-neutral pH (6 < pH < 9.3), but no tests were performed at pH >9.3. On the other hand, the results illustrate the huge effect of the redox potential on the stability of the UO_2 matrix (these data are not shown in Figure 3-8).

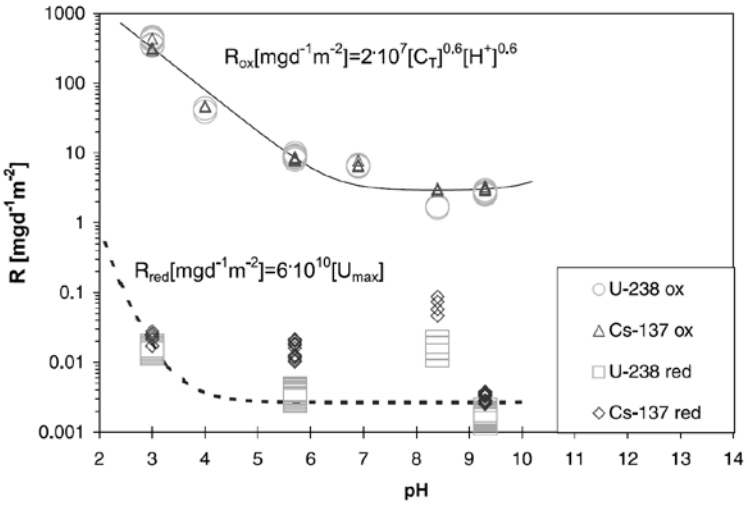

Figure 3-8: Dissolution rate of spent UOX fuel based on ^{238}U and ^{137}Cs as a function of pH for oxidizing and reducing conditions. Different dissolution rates for an isotope at a particular pH correspond to different flow rates. The dissolution rate at pH 8.3 in reducing conditions was possibly interrupted before reaching the reducing conditions in the fuel cell (Röllin et al., 2001).

3.2.4 Impact of H_2 gas pressure

Hydrogen gas is a very effective reducing agent, suppressing the oxidative dissolution. An overview of the involved mechanisms is given in (Eriksen et al., 2012).

Several processes can take place, either in the solution or on the UO_2 surface.

In the solution, hydrogen gas can consume •OH, necessary to form H_2O_2 by Equation 1, as indicated in Equation 6.

$H_2 + \bullet OH \rightarrow H_2O + H\bullet$ (Equation 6)

This process is relevant mostly for gamma radiation, with a high yield of •OH radicals (low LET).

Hydrogen gas would also be able to reduce oxidized uranium on the UO_2 surface, thereby preventing its dissolution, and to reduce already dissolved U(VI) back, in the presence of a catalyzing UO_2 surface (Spahiu et al., 2004; Carbol et al., 2009b; Muzeau et al., 2009; Bauhn et al., 2017).

Catalysis on a UO_2 surface is considerably enhanced on defective surfaces. Alpha emission will also produce surface defects, which would lead to the formation of H• available to scavenge radiolytic oxidants (Shoesmith et al., 2008).

The strongest H_2 effect is observed, however, with the epsilon particles in spent fuel, consisting of noble metals, which can catalyze the reaction between H_2O_2 and H_2 to produce water (Equation 7) (Shoesmith et al., 2008).

$H_2 + H_2O_2 \rightarrow 2\ H_2O$ (Equation 7)

As a result, even small amounts of dissolved H_2 ($\leq 10^{-4}$ mol·dm^{-3}) can be sufficient to suppress the U release rate of spent fuel to effectively immeasurable levels.

A summary of the dissolution rates measured in the presence of H_2 gas is given in Section 3.3.

3.2.5 Impact of water composition

As summarized in (SKB, 2010), the experimental evidence allows to conclude that ionic strength has little influence on the fuel dissolution in oxidizing, anoxic and reducing conditions.

Carbonate concentrations can enhance the oxidative dissolution, depending on the concentration of oxidants and pH (SKB, 2010). Casas (Casas et al., 2009) proposed a model in which the rate of oxidative dissolution r is calculated as follows:

$$r = \frac{r_{ox}\, r_{dis}}{r_{ox} + r_{dis}}$$ (Equation 8)

With

r_{ox} = partial oxidation rate

$r_{ox} = \rho \cdot k_1 \cdot [H_2O_2]$

r_{dis} = partial dissolution rate

$r_{dis} = \rho \cdot (k_2 \cdot [H^+] + k_3 \cdot [HCO_3^-])$

k_1, k_2 and k_3 are kinetical constants

ρ is density of reactive sites on the UO_2 surface.

This means that $r \approx r_{dis}$ for high oxidant concentration (young fuel) even at low carbonate concentrations. In the $[H_2O_2]$ range 10^{-6} mol·L^{-1} to 5 x 10^{-4} mol·L^{-1}, corresponding to young fuel, carbonate concentrations of 10^{-4} – 10^{-2} mol·L^{-1} can thus increase the UO_2 dissolution rate according to Casas. For old fuel the expected H_2O_2 concentrations are however much smaller. Dependent on the geometry of the fuel particles, H_2O_2 concentrations of order of magnitude 10^{-8} to 10^{-10} mol·L^{-1} are expected after 10^3 years (Martinez Esparza et al., 2005). With such low H_2O_2 concentrations, the rate of oxidative dissolution is controlled by oxidation even at carbonate concentrations of 10^{-4} – 10^{-6} mol·L^{-1}, like in cement water.

Carbonates have no influence on the non-oxidative dissolution (SKB, 2010), although there may be some effect when the carbonate concentration is higher than 0.1 mol·L^{-1}.

Trace groundwater components can reduce the favourable H_2 effect in the presence of β,γ-radiation, but with α-radiation, the effect is expected to be negligible (Pastina et al., 2001).

The presence of Ca (and Mg) is expected to be favourable, because the Ca is adsorbed on the UO_2 surface and thus inhibits the oxidation/dissolution (Santos et al., 2006; Cui et al., 2003b). The precipitated layer may offer partial protection against further fuel oxidation and dissolution. This was suggested also by tests with UO_2 in Ca containing solutions at neutral pH (Cerrato et al., 2012).

3.2.6 Impact of temperature

In principle, a temperature increase will cause an increase of the fuel alteration rate. Most experiments that measure the fuel matrix dissolution rate have been performed at low (ambient) temperature, but there are also some literature data for higher temperatures. In oxidizing conditions (air-saturated granite groundwater), a temperature increase from 25 to 150 °C suggested a rate increase by a factor of 10 to 20 for irradiated CANDU fuel (Johnson et al., 1982; IAEA, 1991, p.42). In the presence of H_2 gas, at temperatures up to 70 °C, there are no indications for elevated dissolution rates, but rather higher rates of reduction and precipitation of U(VI) and other oxidized radionuclides (SKB, 2010). Also according to SKB (SKB, 2010), there are no published data from fuel leaching at temperatures over 70 °C under reducing conditions, but in a paper by Johnson (Johnson et al., 1982), tests with irradiated CANDU fuel under 100 kPa H_2 gas in granitic groundwater at 150 °C are reported. Both uranium and ^{99}Tc concentrations in solution decreased to the detection limit or to the background level, confirming that the high temperature did not increase the dissolution rate. According to Parks (Parks et al., 1988), referred to by Neck (Neck et al., 2001), the temperature has a negligible effect on the solubility of crystalline UO_2 (uraninite) between 25 and 300 °C in reducing conditions, with the remark that the solubilities measured with crystalline UO_2 may refer rather to an amorphous surface layer. So we do not expect an effect of the temperature on the matrix solubility and – indirectly – on the non-oxidative dissolution rate. Papers from Le Lous, Johnson and Sunder support the small impact of a temperature increase on the stability of UO_2 or spent

fuel in reducing conditions (Le Lous et al., 1998; Johnson et al., 1988; Sunder et al., 1990; Sunder et al., 1991).

3.2.7 Impact of the specific surface area of the spent fuel or UO_2

The ***effective specific fuel surface area*** is the specific fuel surface area that is contributing to the release of radionuclides (see also Section 3.3.1). This includes the external surface area of the fuel pellets and the internal surface of the cracks and accessible grain boundaries of the pellets. It is expressed in units of surface area per unit of fuel mass. The fuel surface is an important parameter for the dissolution behaviour of spent fuel or UO_2, if the dissolution step is rate determining in the case of oxidative matrix dissolution. For solubility controlled non-oxidative dissolution, the surface area is irrelevant. Because the effective specific surface area is very difficult to estimate for spent fuel, dissolution rates are often expressed as fractional dissolution rates, i.e. the fraction of the initial inventory that is dissolved.

The burnup and surface area are in principle correlated. A higher burnup leads to a higher fuel activity and the formation of a rim zone with a different structure (see Section 2). Intergranular bubbles may interconnect and form a network within the fuel offering an escape path for the gas and increasing the surface area, as illustrated in Figure 3-9, showing the specific surface area of spent fuel in cm^2 per cm^3 fuel derived from the release of short-lived gaseous isotopes (Govers et al., 2018). In practice, the fine structured rim surface may not contribute to the matrix dissolution, because the porosity would not be interconnected (see Section 2). The estimation of the effective surface area of spent fuel for leach tests does not explicitly consider the burnup effect.

Literature data about the specific surface area of UO_2 and spent fuel are given in chapter 9.

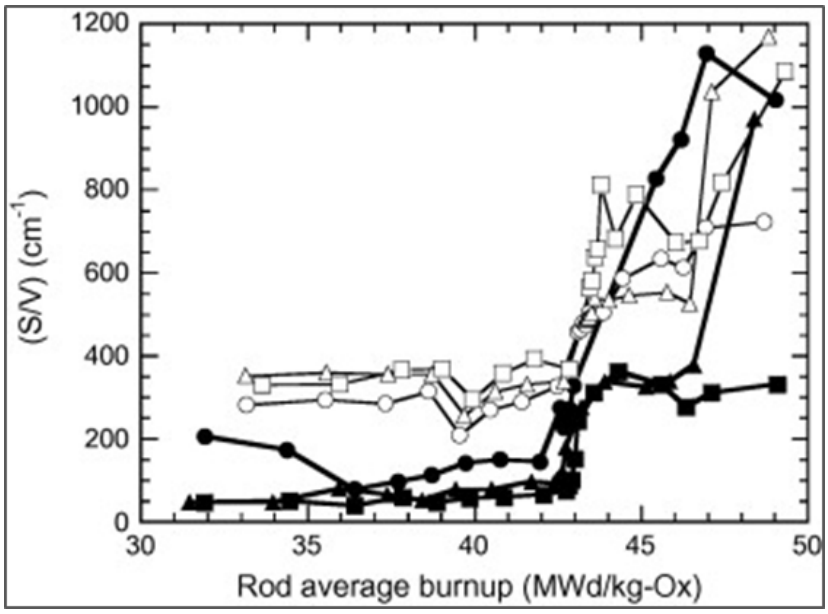

Figure 3-9: Surface-to-volume ratio of spent nuclear fuel derived from the release of short-lived gaseous isotopes (Govers et al., 2018), originally in paper from Amaya (Amaya et al., 2010)

3.2.8 Impact of the presence of solids with a sorption capacity for U

Near-field or host rock materials with a sorption capacity for U could have an impact on the spent fuel or UO_2 dissolution because the sorption removes U from the solution and may thus postpone the evolution towards chemical equilibrium with the UO_2 surface. Sorption of U(VI) would mainly affect the oxidative dissolution and sorption of U(IV) would affect the non-oxidative dissolution.

The oxidative dissolution requires the preceding oxidation of UO_2 to U(VI). An increase of the U(VI) concentration can lead to the formation of a layer of oxidized U phases that could – at least theoretically – protect the UO_2 to some extent from further oxidation. Sorption of U(VI) on other materials might delay or prevent the formation of a protective layer, but there is no clear evidence for such protection by an oxidized layer, nor for a counteracting effect of U(VI) sorption. The situation may be different when a thick layer of oxidized secondary phases covers the surface (see Section 3.2.9).

Without external oxidants (e.g. no traces of airborne O_2), the radiolytic fuel oxidation should be the rate determining step in the oxidative dissolution process, so any sorption of generated U(VI) should be a secondary phenomenon with little effect on the fuel dissolution rate. Sorption of U(IV) on other materials could in principle trigger the non-oxidative matrix dissolution. For instance sorption of U(IV) on clay appeared to cause a measurable increase of the non-oxidative dissolution rate, but the effect was of short duration, probably because the sorption capacity of the clay for U(IV) is too small (Salah et al., 2006). In the final report of the MICADO project (Grambow et al., 2010; Grambow et al., 2011), sorption is considered as a potential mechanism that may control the long-term dissolution, but it is difficult to quantify. The potential effect will depend on the sorption equilibria and capacity of the solids, which will be material dependent, and is in general a function of pH. We will in this short overview thus refer to materials that are relevant to the Belgian disposal conditions, this means OPC and magnetite.

A distribution ratio R_d of $>2.2 \times 10^5$ L·kg^{-1} was measured for U(IV) on OPC in sodium hydroxide solution at pH ~10.5 (Clacher et al., 2010). A R_d for U(IV) of 2.2×10^4 L·kg^{-1} measured on magnetite in sodium hydroxide solution at pH ~10.5 (Clacher et al., 2010). Sorption of U(VI) on C-S-H phases has been described as well, for instance in a paper from Tits (Tits et al., 2008). So sorption of U(IV) or U(VI) on these materials occurs, but the distribution ratios for U(IV) are indicative of a very limited sorption, and we are not aware of any experiments that have demonstrated that this has an effect on the UO_2 dissolution rate. It is probably very difficult to demonstrate that such effect would exist, because of the low solubility of UO_2 in reducing conditions (around 10^{-9} mol·L^{-1}), implying that a large amount of solid is required to have a significant effect on the UO_2 dissolution rate.

If concrete undergoes a thermal stage, the cement phases may evolve. This may affect the sorption of uranium. We did no look for sorption data on altered cement phases, but anyway much higher distribution ratios would be required to have a potentially significant effect on the spent fuel stability.

3.2.9 Impact of secondary phase formation

Secondary phase formation with U(IV) could in principle lead to a conversion of the fuel to another U(IV) or UO_{2+x} phase. The formation of a layer of oxidized uranium phases might have some protective effect for further oxidation. There is some discussion on the question whether or not a precipitation layer could suppress radiolytic oxidation. Apart from Cerrato (Cerrato et al., 2012), also Shoesmith observed the apparent blocking of the oxidative dissolution by accumulation of secondary phases in grain boundaries (tests performed in $NaClO_4$ at pH ~9.5) (Shoesmith et al., 1996). The mechanism is considered also in the recent FMDM model (Jerden et al., 2015).

We distinguish the formation of secondary U(IV) phases and secondary U(VI) phases.

- *U(IV) phases*

Indications for U(IV) formation come mainly from natural analogue studies. Laboratory experiments and natural analogue studies have indicated that the most likely solid phases to form from uraninite (UO_{2+x}) alteration under reducing conditions are secondary uraninite and coffinite ($USiO_4 \cdot nH_2O$). All the coffinitization processes observed in nature occurred at high temperatures (>80 °C). Coffinite formation also requires high Si concentrations. Calcium incorporation has been observed in many natural uraninite samples (Duro et al., 2010). Some other phases are mentioned as well (nigyoite, secondary uraninite). The formation of these phases appears to have no destabilizing effect. We refer to the Section 3.4 on 'natural analogues' for this.

- *U(VI) phases*

According to thermodynamic calculations, fuel oxidation could be favoured by a high pH (Figure 3-5), with the appearance of U(VI) aqueous species and solid phases depending on the composition of the solution in contact with the solid (Duro et al., 2010). The dissolved U(VI) could reprecipitate as a U(VI) phase. This would mean that the mere alkalinisation of the system might favour the oxidation of the spent fuel matrix at a given redox potential, and the precipitation of secondary U(VI) phases would trigger the further oxidation. There is, however, no experimental evidence for such pH-promoted conversion of U(IV) into U(VI). Secondary phases with U(VI) at high pH are reported only in tests where the U is in the U(VI) valence from the start. For instance, Ca-diuranate formation was observed in very concentrated Ca solutions (Ca concentration of 4 to 160 $g \cdot L^{-1}$) at pH 10 –11, starting from already oxidized U (metaschoepite) (Altmaier et al., 2005). Other U(VI) phases, like $CaUO_4$ (Moroni et al., 1995), and $K_2U_2O_7$ (Sutton et al., 1999) have been observed at high pH, but again only in experiments that start with U(VI). Starting from UO_2, the oxidation of U(IV) to U(VI) requires the continuous availability of oxidizing species.

3.3 Literature data on matrix dissolution rates

For the safety of the disposal system, it is important to know the release rate of the various radionuclides in the spent fuel. The radionuclides that are homogeneously incorporated in the UO_2 waste matrix have different chemical properties, and therefore also a dissolution behaviour that may be different from the dissolution behaviour of the UOX matrix.

The most relevant literature data on spent fuel dissolution at high pH and its relation with the radionuclide release is discussed below. This review of literature date does not include the tests performed within the Belgian R&D programme, which are presented in Section 5.

3.3.1 Relation between the matrix dissolution rate and radionuclide release rate

As discussed in Section 3.1, the radionuclides that are embedded in the UOX matrix of the spent fuel will become available for dissolution only after dissolution of the surrounding UOX matrix.

Fuel matrix dissolution is a specific type of ***fuel matrix alteration***. *Fuel matrix alteration* refers to any process that causes the release of radioactive components from the fuel matrix in contact with water. This can be the dissolution of the uranium from the matrix, but the oxidation of the fuel matrix can also cause the release of the trapped radionuclides without uranium dissolution, because of a change in the UOX lattice structure (see Section 3.2.3). For the release rate of the radionuclides in the context of this report, the formal distinction between fuel dissolution and fuel alteration is not very relevant. In most experiments, the fuel matrix alteration is monitored by following the fuel matrix dissolution, based on the dissolution of uranium or fission products. Therefore, the term 'fuel (matrix) dissolution' is more commonly used.

The ***release rate of radionuclides*** is the rate at which the radionuclides are released from the fuel matrix. The radionuclides are by definition considered to be released when the surrounding UO_2 matrix has been altered (= dissolved or oxidized). This means that the normalized release rate of the radionuclides is the same as the normalized release rate of the uranium, which is essentially the fuel matrix dissolution rate. This does not mean that all incorporated radionuclides dissolve at the same rate as the fuel matrix. The less soluble radionuclides can remain undissolved, can reprecipitate or can be incorporated in secondary phases with or without uranium.

There will be a relation between the matrix dissolution rate and the release of segregated isotopes, because the radionuclides that are segregated or concentrated along the deeper grain boundaries will be released only after the partial dissolution of the UO_2 matrix, which may open the grain boundaries and make them accessible for water, affecting thus the effective fuel surface area (see chapter 7).

When the uranium oxide at the fuel surface is in chemical equilibrium with a uranium (IV) saturated solution, there will be no net matrix dissolution, but because this is a dynamic equilibrium between the forward and backward dissolution reaction, the included radioactive components might still be released. There are some indications that this can happen (Ollila et

al., 2007), but it probably affects only the outer layers of the fuel, and the release rate is expected to decrease when the depleted layer gets thicker until a steady state equilibrium is reached with the progressing matrix dissolution front.

Therefore, on the long term, the dissolution rate of the fuel matrix is a good approximation of the release rate of the included radionuclides.

We distinguish the ***surface normalized dissolution rate*** from the ***fractional dissolution rate***.

- The ***surface normalized dissolution rate*** is the mass of fuel altered per unit of fuel surface area and per unit of time;
- The ***fractional dissolution rate*** is the fraction of the fuel mass altered per unit of time.

Similarly, we distinguish the ***surface normalized radionuclide release rate*** from the ***fractional radionuclide release rate***.

- The ***surface normalized release rate*** is the amount of radionuclide released per unit of fuel surface area and per unit of time;
- The ***fractional release rate*** is the fraction of the radionuclide inventory released per unit of time for a specified initial radionuclide inventory.

The fractional dissolution or release rate is related to the surface normalized dissolution or release rate via **the *effective fuel surface area***, which is the specific fuel surface area that is contributing to the dissolution or the release of radionuclides. This includes the external surface area of the fuel and the internal surface of the cracks and accessible grain boundaries. It is expressed in units of surface area per unit of mass of the fuel.

The fractional dissolution or release rate (1/time) depends on the surface normalized dissolution or release rate $R_{surface}$ (= mass divided by surface area and time) and the effective specific fuel surface area SA_{spec} (= surface area divided by mass).

Fractional dissolution or release rate = $R_{surface}$ x SA_{spec} (Equation 9)

In most tests with unirradiated UO_2, the specific surface area can be estimated, and the dissolution rate can thus be expressed as a surface normalized dissolution rate. In practice, a uranium isotope (for instance ^{233}U) is used as a dissolution indicator and the released amount of this isotope is divided by the mass fraction of the isotope in the UO_2 to convert it to the equivalent UO_2 matrix dissolution. When the specific surface area of a tested fuel (or UO_2) is not well known, experimental results are often expressed directly as fractional rates, based on the measurement of the amount of radionuclides released and the initial inventory. To convert this to a surface normalized release rate, the specific surface area has to be measured (or estimated). Although the fractional dissolution rate can thus be calculated without knowing the surface area, it gives less information and is less useful in mechanistic modeling where a surface area must be defined where the dissolution/precipitation processes take place. To interpret correctly fractional dissolution rates, one should have information about the geometry of the sample. A similar fractional dissolution rate can correspond to fast dissolution

if it measured on a large fragment (with a small sample surface area / sample volume ratio) or to slow dissolution if it is measured on a small fragment (with a large sample surface area / sample volume ratio. Direct comparison of fractional dissolution rates is meaningful only when the samples have a similar geometry.

3.3.2 Dissolution rates in reducing conditions

From the preceding sections, it is clear that the matrix dissolution rate of spent fuel or simulated spent fuels such as UO_2 or α-doped UO_2 depends on several parameters. Hence, a wide range of dissolution rates is observed in the literature, as illustrated by Figure 3-3. Not all test conditions are relevant to geological disposal conditions, though. In most geological disposal media, and certainly also in the Belgian context, reducing conditions are expected to prevail, due to the presence of iron near-field materials, but also to the reducing capacity of the host rock. On the short term, this situation may be disturbed by the effects of radiolysis, which generates oxidizing species (molecular species such as H_2O_2 or O_2, radical species such as the hydroxyl radical OH•), but also reducing species (such a H_2 gas). This might cause oxidative dissolution as long as the threshold for radiolytic oxidation is not reached, but afterwards, the chemical, not-oxidizing dissolution would be the main dissolution path. Dissolution rates measured in reducing conditions are thus more relevant to geological disposal conditions, than rates measured in oxidizing conditions.

Because the spent fuel is close to thermodynamic equilibrium in reducing conditions, the non-oxidative dissolution rate should be very small. On the very long term, it may be driven by conversion to other minerals (like observed for natural analogues). Sorption on the near-field materials or the host rock may trigger the non-oxidative dissolution, but probably only to a minor extent, because of the small sorption capacity for U(IV). It is, however, not evident to reproduce the stable reducing conditions expected in a geological environment in the experiments, and to take into account correctly the sorption of U(IV) on the internal surfaces of the leach test equipment. Reducing conditions can be imposed by making use of the natural reducing capacity of the ground water used for the experiment (e.g. Boom Clay water), by addition of reducing components to the solution (metallic iron, sulphide), or by addition of H_2 gas.

The MICADO project (Grambow et al., 2010) proposed ranges for the dissolution rates for the most representative test conditions, considering only reducing conditions, and distinguishing the situation with H_2 gas and without H_2 gas. Tests with real spent fuel in the presence of H_2 gas are the most representative tests for realistic geological disposal conditions, because both the test material (real spent fuel) and the test conditions (presence of H_2 gas) simulate relatively well the expected conditions. Indeed, the H_2 gas will be effectively present as a result of the anaerobic corrosion of steel components. Tests in absence of H_2 gas are thus less realistic. On the other hand the currently available real young spent fuel used in the experiments is a relatively realistic representation of real old spent fuel, because the fuel microstructure and complex composition should be rather similar for young and old real spent fuel, even if young fuel has a higher β - γ activity. This higher activity is expected to increase the oxidative dissolution rate in absence of an effective reducing agent (the oxidative dissolution rate of real old spent fuel is expected to be smaller than for real young spent fuel in otherwise similar conditions). The fractional dissolution rate of 10^{-9} day^{-1} measured in the presence of corroding

iron, generating H_2 gas (Grambow et al., 2000) was taken as a representative minimum rate, but because the specific surface area of the fuel pellets is not well known, the conversion of this fractional dissolution rate in surface normalized dissolution rates induces an extra uncertainty. Assuming a minimum accessible surface area of 10^{-3} $m^2 \cdot g^{-1}$, the surface normalized dissolution rate would be 1 $\mu g \cdot m^{-2} \cdot d^{-1}$. With the maximum surface area of 0.0071 $m^2 \cdot g^{-1}$, it would be 0.1 $\mu g \cdot m^{-2} \cdot d^{-1}$. The result of a flow-through experiment, 3 ± 2 $\mu g \cdot m^{-2} \cdot d^{-1}$ (Röllin et al., 2001) was proposed as a maximum rate in MICADO (Grambow et al., 2010). The many tests performed with α-doped UO_2 simulating old spent fuel (i.e. with low β - γ activity) were also considered to estimate the dissolution rate of spent fuel in reducing conditions, but because H_2 gas is less effective in suppressing the oxidation of α-doped UO_2 than it is for real spent fuel, the dissolution rates measured in tests with other reducing agents (natural Boom Clay water, sulfide, iron) were considered as most representative. The MICADO project further suggested that experiments with minimum sorption would be most representative for the long term dissolution rate. This would result in a range of 0.03 to 2.6 $\mu g \cdot m^2 \cdot d^{-1}$ at near neutral pH. This range also takes into account the uncertainty due to the specific surface area (Grambow et al., 2010).

The conclusions of the MICADO project were drawn in 2010. Since then, more experiments were performed with H_2 gas, which allow to estimate the minimum H_2 concentration required to suppress the radiolytic oxidative dissolution. Hereunder we give a more complete list of rates that were collected from literature., including data that were used in MICADO, but also more recent data. They all refer to tests at near-neutral pH. Sometimes, the dissolution rate was below the detection limit because there was no significant increase of the U concentrations, which were very low, indicating absence of oxidative dissolution. For such cases, the U concentration is reported.

- In short-term tests (<15 days) with Pu-doped UO_2 simulating the specific α-activity of 50 and 10000 year old fuel (385 and 18 $MBq \cdot g^{-1}$, resp.) and 1 bar H_2 gas ($[H_2(aq)]$ = 0.78 $mmol \cdot L^{-1}$), the U concentration in 10^{-3} $mol \cdot L^{-1}$ $NaHCO_3$ slightly decreased and stabilized around 10^{-8} $mol \cdot L^{-1}$, whereas in similar experiments in Ar atmosphere without H_2 gas, the U concentration showed a clear increase to 10^{-6} $mol \cdot L^{-1}$ due to oxidative dissolution (Muzeau et al., 2009).
- With α-doped UO_2, simulating an α-activity of 3000 year old fuel, very low U concentrations (10^{-11} $mol \cdot L^{-1}$) were found for H_2 concentrations as low as 0.02 $mmol \cdot L^{-1}$ (Carbol et al., 2009a).
- With irradiated MOX, H_2 concentrations in the range 1-42 $mmol \cdot L^{-1}$ stabilized the U concentrations around 7 x 10^{-10} $mol \cdot L^{-1}$ (Carbol et al., 2009b).
- U concentrations of <10^{-9} $mol \cdot L^{-1}$ were observed with spent fuel at 5 bar (4 $mmol \cdot L^{-1}$) H_2 (Spahiu et al., 2004).
- Spent UOX fuel with high burn-up (67 $GWd \cdot t_{HM}^{-1}$) showed low U concentrations (1.5 10^{-10} $mol \cdot L^{-1}$) with 33 $mmol \cdot L^{-1}$ H_2 gas (Fors et al., 2009). These concentrations are lower than the solubility limit of around $10^{-8.5}$ $mol \cdot L^{-1}$ in Figure 3-6 (Neck et al., 2001). This could be caused by the precipitation of a more crystalline UO_2 phase.
- Tests with spent fuel of burnup 50 $GWd \cdot t_{HM}^{-1}$ in NaCl brine with 2.75 bar H_2 (~ 2 $mmol \cdot L^{-1}$) resulting from corroding iron (co-dissolution with metallic iron) showed a clear dissolution

suppression, with a rate of $<10^{-9}$ day^{-1}, although the U concentrations were relatively high at 2.8 x 10^{-8} mol·L^{-1} (Grambow et al., 2000). This rate was taken as the minimum rate of the estimated rate range in the presence of H_2 in the MICADO project. In parallel tests with spent fuel in NaCl brine with only 0.2 bar of H_2 (0.16 mmol·L^{-1}), the H_2 did not have much effect (dissolution rate of 4.6 x 10^{-7} day^{-1} and U concentration of 1.5 10^{-6} mol·L^{-1}). (Grambow et al., 2000). This seems to contradict the findings by Carbol (Carbol et al., 2009a), which were, however, obtained for a much less active material.

- In dynamic tests on spent fuel with H_2 bubbling (presumably about 1 bar, i.e. 0.8 mmol·L^{-1} H_2), a relatively high dissolution rate of 3 ± 2 µg·m^{-2}·d^{-1} was measured (Röllin et al., 2001; Grambow et al., 2010), but here the contact with the H_2 gas may have been not sufficient to block all radiolytic processes. This rate was taken as the maximum rate of the estimated rate range in the presence of H_2 in the MICADO project.
- In tests with Pu-doped UO_2 in deionized water under Ar + 4 % H_2 gas (~0.04 bar H_2, 0.03 mmol·L^{-1} H_2) under gamma irradiation, the dissolution rate was still very high at 6 mg·m^{-2}·d^{-1}. Similar tests with gamma irradiated spent fuel (60 GWd·t_{HM}^{-1}) showed a similar dissolution rate of 6.5 mg·m^{-2}·d^{-1} (Jégou et al., 2005). The effect of gamma radiation cannot be simply extrapolated to α-radiation, because different radiolytic species are generated.
- Pastina followed the evolution of the H_2O_2 concentration at several H_2 pressures under γ and α irradiation. Under γ irradiation complete H_2O_2 consumption was observed at 0.1 bar H_2 pressure (0.08 mmol·L^{-1}), but not at 0.01 bar H_2 (0.008 mmol·L^{-1}). Because H_2O_2 is the most important radiolytic oxidant for the UO_2 matrix, this might imply that the threshold H_2 gas pressure for oxidation suppression lies between 0.01 and 0.1 bar (0.008 and 0.08 mmol·L^{-1}). With α radiation, the rate reduction effect of H_2 was much smaller (Pastina et al., 2001).
- The review paper by (Eriksen et al., 2012) mentions that ≤ 0.1 mmol·L^{-1} of dissolved H_2 is sufficient to suppress the U release rate to effectively immeasurable levels (at near neutral pH).
- Based on an electrochemical model, Wu predicts a critical H_2 concentration of 0.015 mmol·L^{-1}, above which the fuel oxidation should be completely suppressed (Wu et al., 2012)
- According to the Fuel Matrix Dissolution Model (FMDM), a gradually increasing effect is expected for H_2 concentrations higher than 0.001 mmol·L^{-1} when epsilon particles are present. The effect is stronger in absence of carbonate. At H_2 concentrations greater than 1 mmol·L^{-1}, the matrix dissolution rate is predicted to be 4 or 5 orders of magnitude lower than that for the oxidative dissolution case in typical crystalline and clay-rock/shale repository settings. This would mean that an important effect would be expected also in the range 0.8 – 2.5 mmol·L^{-1} that was tested in cement water (see Section 5.5), but the possible effect of high pH is not considered in the model (Jerden et al., 2015).

3.3.3 Dissolution rates measured at high pH (literature data)

Because the objective of this report is to provide data about the spent fuel dissolution behaviour at high pH, the literature data for these conditions are highlighted hereunder.

- Tests with partly oxidized spent fuel (50 GWd·t_{HM}^{-1}) in 5 mol·L^{-1} NaCl solution under argon atmosphere (Loida et al., 2001) showed that a gradual increase of the pH from 5.8 to pH 11 by adding NaOH did not change the fuel dissolution rate, based on the release of Cs. With Sr as a dissolution indicator, the fuel dissolution rate even appeared to decrease, but this may be due to Sr precipitation (Figure 3-10). The resulting fractional dissolution rate was 2.1 x 10^{-4} d^{-1} for Cs and 1.7 x 10^{-4} d^{-1} for Sr. These rates are not directly applicable to long-term reducing conditions, because the fuel was partly oxidized. The use of an argon atmosphere without hydrogen gas is also pessimistic and not representative of the expected geological disposal conditions. The tests nevertheless show that the pH increase did not have much effect on the dissolution rate.

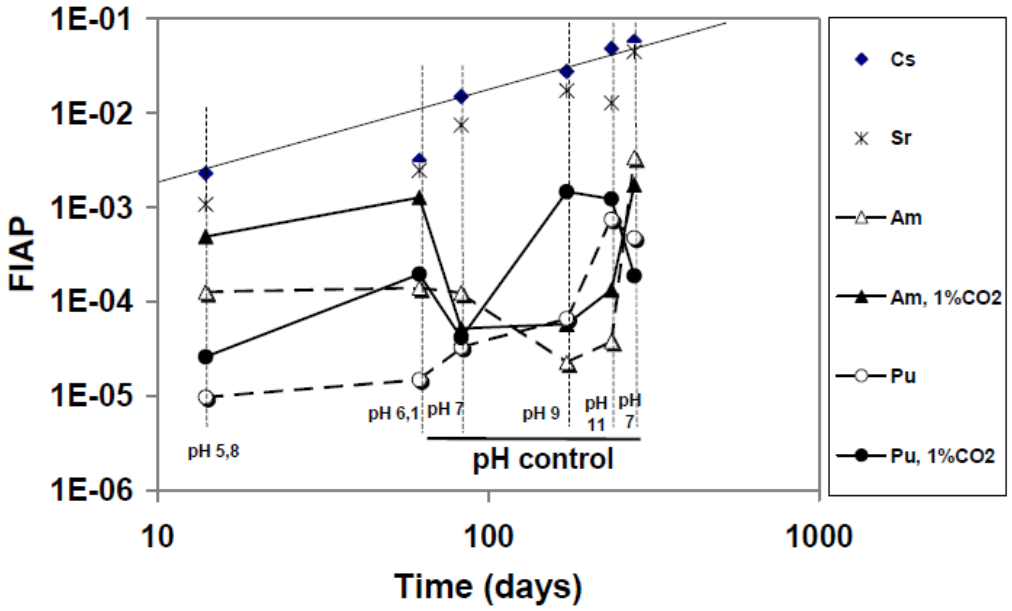

Figure 3-10: Cs and Sr release from partly oxidized spent fuel in 5 mol·L^{-1} NaCl solution with gradual pH increase (Loida et al., 2001)

- Tests under argon atmosphere with spent fuel (50 GWd·t_{HM}^{-1}) in cementitious water ('Simple young fluid'), composed of KOH, NaOH and $Ca(OH)_2$, with an initial pH 13.2, and with addition of a small amount of Bure Clay (Loida et al., 2006), showed a fractional dissolution rate of 4 x 10^{-8} d^{-1}, which was much lower than in brine media with lower pH, where the fuel dissolved at 2 to 7 x 10^{-6} d^{-1} (Figure 3-11). So these tests suggest a favourable effect of the high pH.

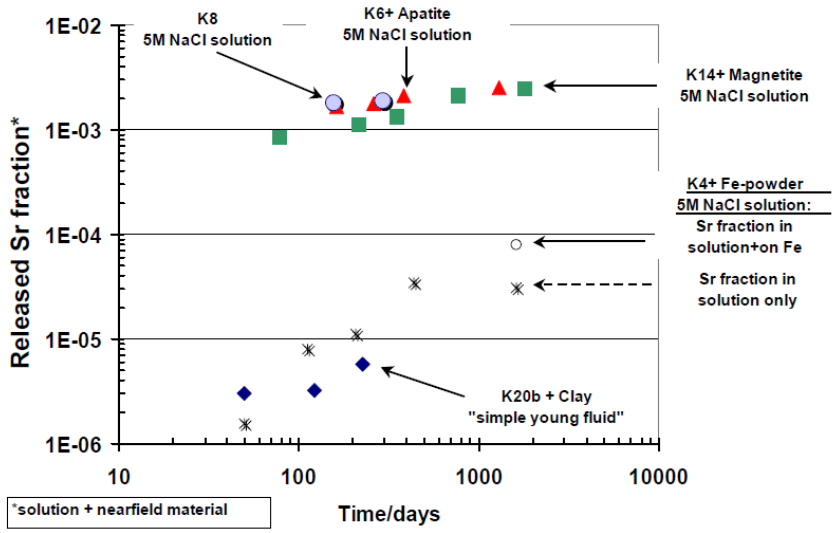

Figure 3-11: Sr release from spent fuel in various media, showing the lowest released fraction with the 'simple young fluid' (Loida et al., 2006)

- Tests with UO_2 pellets in KOH water and in cement water of pH 12.7 (Lawrence solution, composed of NaOH, KOH and $Ca(OH)_2$) in anoxic conditions showed stable long term U concentrations, suggesting a low, but not quantified dissolution rate (Figure 3-12) (Cui et al., 2003b). The U concentration was higher for the KOH solution (~10^{-6} mol·L^{-1}) than for the Lawrence solution (~10^{-7} mol·L^{-1}), which may be an indication for the favourable Ca effects mentioned in Section 3.2.5.

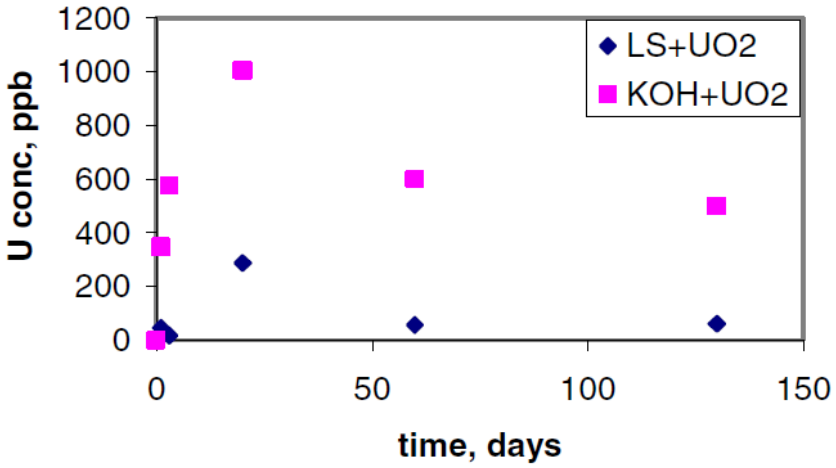

Figure 3-12: U concentration with UO_2 in KOH and Lawrence solution (LS) of pH 12.7 (Cui et al., 2003a)

- Tests with UO_2 fragments (2 –4 mm) with 2.8% ^{235}U (so with a low specific activity) in 0.01 mol·L^{-1} NaCl, adjusted to alkaline pH 11, 12 and 13 with NaOH, under argon atmosphere and in the presence of iron strips or sulphide (Ollila et al., 2008) also showed stable long term U concentrations, suggesting a low, but not quantified dissolution rate (shown in Figure 3-13 for pH 13). The U concentration seemed to increase with pH between pH 9 and pH 13 as shown already in Figure 3-7. It was suggested that this might be due to the formation of polynuclear U(IV) complexes, but this hypothesis needs confirmation.

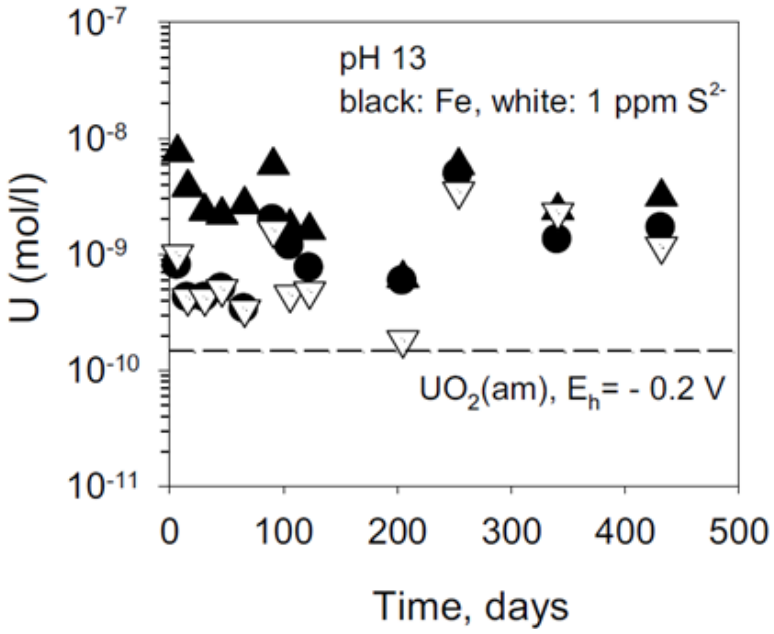

Figure 3-13: U concentration in tests with UO_2 in NaCl/KOH solution of pH 13 (Ollila et al., 2008)

Based on the data available in the open literature, we can thus conclude that a high pH does not appear to be particularly unfavourable for the stability of the tested spent fuels or UO_2.

3.4 Evidence from natural analogues

A comparison with natural analogues is relevant to estimate the potential fuel stability of spent fuel on geological time scales, although the chemical conditions to which the natural analogues have been exposed, may be different from the high pH conditions in cement waters.

Relevant natural analogues for spent fuel in cement water conditions are not reported in literature. Highly alkaline groundwaters are found in the Maqarin area of northern Jordan, but these contain only traces of uranium (10^{-11} – 10^{-10} mol·L^{-1}), while there is no direct evidence for the existence of a solid U phase. This natural analogue gives thus no information about the potential stability of U(IV) phases (Linklater et al., 1996). The absence of U(IV) phases in these conditions can be interpreted as an indication for the destabilization as a result of the high pH, with the transformation of U(IV) into U(VI) phases, even in reducing conditions (Duro et al., 2010), as shown by the Eh/pH diagram of Figure 3-5. Geological disposal conditions, in the presence of H_2 gas, will however be reducing enough to avoid this transformation.

Literature provides several recent evaluations of the UO_2 stability based on natural analogues for other environments (Grambow et al., 2010, Duro et al., 2010, SKB 2011). The most relevant analogue for spent nuclear fuel is the natural mineral uraninite. It has many similarities with UO_2-based spent nuclear fuel. It has the same crystallographic structure, forms solid solutions with oxides of Th, Ca and rare earth elements, is resistant to radiation damage, and is similarly affected by oxidation. Such uraninite is found for instance in *Cigar Lake* (an ore body), *Oklo* (a

natural fission reactor) and at several other locations. A good overview is given by Duro (Duro et al., 2010).

These natural analogue studies show that UO_2 may be partially converted into other uranium phases under reducing conditions, but that the U(IV) minerals have remained more or less stable over extended periods of time (>10^9 years), despite contact with water with a variety of pH values and compositions. In Cigar Lake, uraninite has remained stable even in slightly oxidizing conditions. The mobility of U(IV) phases must have been minimal in reducing conditions, even in cases where contact with significant water flow has taken place. Oxidant production by radiolysis may have been largely neutralized by reducing components, while oxidative dissolution did apparently not occur. A major factor in the stability of the Cigar lake ore body may be the presence of dissolved hydrogen in the groundwaters contacting the ore body. The hydrogen would be activated on the surface of the Cigar Lake uraninites by α-radiation consuming the generated radiolytic oxidants (Bruno et al., 2014).

The physical appearance of the natural analogues is variable. Uranite occurs as cubic, cubo-octahedral and octahedral crystals and as massive, well crystalline aggregates. Uraninite (also called pitchblende) occurs as fine-grained collomorphic, massive dendritic aggregates and is poorly crystalline (Janeczek et al., 1996). The fact that these materials are all very stable in nature shows that the specific surface area is little relevant in reducing conditions.

The following conclusion, drawn by Grambow (Grambow et al., 2010), is applicable in principle also for spent fuel in supercontainer conditions: *"The observations of the stability of uraninite over geological time provide qualitative and semi-quantitative indications of the long-term stability of spent fuel in a geological repository. The direct application of such observations to performance assessment models in any quantitative sense is difficult and has not been achieved despite extensive efforts. However, these observations are useful in building confidence for performance assessment for disposal of spent fuel, in particular for the period beyond several hundred thousand years after disposal of spent fuel. In this time period, the α-emitter content of spent fuel has decayed to a level approaching that of rich natural uraninite ores. As the dissolution rate of natural uraninites must be extremely low under reducing conditions or they would not be preserved over geological time, the dissolution rate of spent fuel after several hundred thousand years would likewise be expected to be similarly low in a reducing geological environment."*

So, the fraction of the fuel that is not dissolved in the first few hundred thousand years, will probably remain undissolved for millions of years.

4 Materials and methods applied for the spent fuel dissolution studies

In Section 4, we present the materials and methods that were used for the dissolution studies in the framework of the Belgian R&D programme. We successively explain the applied test conditions (Section 4.1) and the experimental methods used to determine matrix dissolution rates (Section 4.2). In this report, results are described that were reported in official references that appeared not later than in 2015. Since then, complementary experiments have been performed, but the results of these tests are not included.

4.1 Test conditions in the Belgian R&D programme

The tests in the framework of the Belgian R&D programme have been performed at ambient temperature in cement waters with depleted UO_2, with UO_2 doped with ^{238}Pu and ^{233}U, and with real spent fuel.

4.1.1 Tests with doped UO_2

Four types of doped UO_2 have been used, i.e. batches F1, F2, F4, and F6, with specific α-activities as shown in Table 4-1 and in Figure 4-1. The α-activity of these batches covers the range from very young fuel (150 years) to relatively old fuel (89000 years) with a burnup of 45 – 55 $GWd \cdot t_{HM}^{-1}$, and includes the range where the threshold activity for oxidative dissolution in anoxic conditions is believed to be situated, based on tests at near-neutral pH.

Table 4-1: Batches of UO_2 doped with ^{238}Pu and ^{233}U available for testing in cement water conditions in the Belgian R&D programme

Batch	Specific Activity ($MBq \cdot g^{-1}$)	Simulated age (years)
F1	244	150
F2	36	2000
F4	17	11000
F6	1.4	89000
Depleted UO_2	0.01	$>10^8$

The depleted and doped UO_2 was added as pellets or in powder form of various grain sizes <200 µm. The amount of powder was varied to test various ratios of *fuel Surface Area to leachate Volume* (SA/V). The tests with UO_2 and doped UO_2 were performed by SCK•CEN in glove boxes with anoxic atmosphere, without addition of reducing redox agents, unless mentioned otherwise (iron or magnetite were added in some other tests, but the results were not coherent).

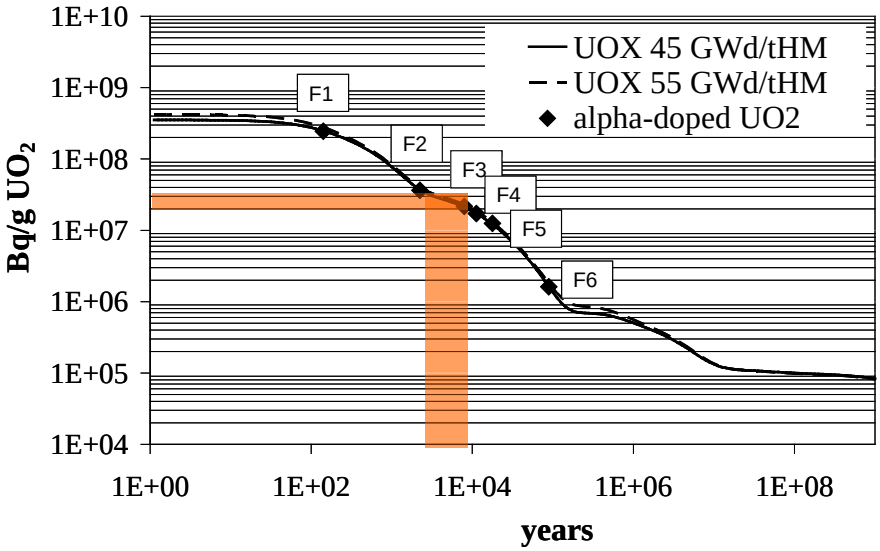

Figure 4-1: Evolution of the specific α-activity of spent UOX fuel, and comparison with various batches of ^{238}Pu - ^{233}U doped UO_2 (F1 to F6) available for testing in the Belgian R&D programme. Batches F1, F2, F4 and F6 were tested in the framework of the Belgian R&D programme. The colored range indicates the threshold activity for oxidative dissolution in anoxic conditions (18 to 33 MBq·g^{-1}) and the corresponding fuel age (2500 to 10000 years), based on experiments at near-neutral pH (Muzeau et al., 2009)

The tests were performed in three types of leaching media, representative of the expected three main stages of OPC concrete evolution in a Boom Clay host rock (Wang, 2009). These media are called *Young Cement Water* with calcium (YCWCa), *Evolved Cement Water* (ECW), and *Old Cement Water* (OCW). A few tests were done also with a *Young Cement Water without Ca* addition (YCW), to study the effect of Ca by comparison with tests in YCWCa, but this is no realistic cement water. The detailed composition of typical batches of cement water is given in Tabme 4-2. These are the compositions and pH values for the media at room temperature, which is the temperature at which the experiments were performed.

Table 4-2: Types of synthetic cement waters used in the experiments with depleted UO_2, α–doped UO_2 and spent fuel in the Belgian R&D programme

		Na	K	Ca	Al	Si	SO_4^{2-}	CO_3^{2-}
YCWCa pH 13.5	mol·L^{-1}	1.4×10^{-1}	3.3×10^{-1}	6.5×10^{-4}	$< 7\times10^{-6}$	2.0×10^{-4}	2×10^{-3}	9.3×10^{-4}
	mg·L^{-1}	3300	12900	26	< 0.2	5.5	186	11.2
ECW pH 12.5	mol·L^{-1}	1.6×10^{-2}	2.2×10^{-4}	$1.3.10^{-2}$	1.1×10^{-5}	1.8×10^{-4}	3×10^{-6}	4.8×10^{-4}
	mg·L^{-1}	370	8.7	520	0.3	4.9	0.28	5.8
OCW pH 11.7	mol·L^{-1}	3.7×10^{-3}		7.3×10^{-4}	3.7×10^{-6}	1.5×10^{-4}	4×10^{-5}	1.4×10^{-4}
	mg·L^{-1}	84		29.2	0.1	4.3	3.5	1.68

Most tests were performed with YCWCa, for the following reasons:

- This medium has the highest pH, so if there is a pH effect, it should be most obvious in this medium.
- The medium is relatively stable for a long time, compared to the other media.
- It appears to promote the dissolution of U(VI) from the UO_{2+x} surface, so the U concentration in solution is a better indicator of the fuel alteration (oxidation).

The matrix dissolution rate of the (doped) UO_2 has been determined in static tests (depleted UO_2, doped UO_2, spent fuel) and in dynamic tests (depleted and doped UO_2). These are explained in Section 4.2. The details can be found in the topical reports (Cachoir et al., 2015b; Cachoir et al., 2015c; Mennecart et al., 2012).

4.1.2 Tests with spent fuel

The tests with the real spent fuel were done by KIT (Karlsruher Institute für Technologie).

Three types of tests were performed:

- Tests with clad fuel *segments* in ECW without an applied H_2 gas overpressure
- Tests with clad fuel *segments* in ECW and YCWCa with an applied H_2 overpressure up to 3.2 bar
- Tests with fuel *fragments* in ECW and YCWCa with an applied overpressure of 3.2 bar

The tests were done with high burnup LWR-UO_2 SNF from the PWR power plant Gösgen, Switzerland (initial enrichment ^{235}U 3.8%, burnup 50.4 $GWd \cdot t_{HM}^{-1}$, ~26 $kW.m^{-1}$ average power rating). The details can be found in the references (Loida et al., 2009a; Loida et al., 2009b; Loida et al., 2010; Loida et al., 2011; Loida et al., 2012; González et al., 2014).

4.2 Methods to determine matrix dissolution rates

The estimation of the dissolution rate of (doped) UO_2 or spent fuel is not straightforward. Different methods are used for depleted and Pu-doped UO_2 on the one hand, and spent fuel on the other hand.

4.2.1 Depleted and Pu-doped UO_2

The tests performed to determine the matrix dissolution rate were partly 'static' and partly 'dynamic'. Figure 4-2 shows a scheme of the setup for the two types of experiments. For both methods, the uranium concentration in the leachate is used as dissolution indicator. Uranium analyses were performed on unfiltered samples of the solution and on samples that were ultrafiltered with filters that let pass only the fraction with molecular weight smaller than 30000 dalton. Analysis of the unfiltered samples thus gives the total uranium concentration, including

both the dissolved and colloidal uranium, while the analysis of the ultrafiltered samples only gives the dissolved uranium.

- In 'static tests', the UO_2 stays in contact with the same volume of leaching solution for the entire test duration, at a fixed UO_2 surface area to solution volume (SA/V). This implies that U concentrations can build up and reach (over)saturation. In these conditions, dissolved U can potentially reprecipitate on the UO_2 surface. The dissolution rate is calculated, based on the increase of the uranium concentration in the leaching solution. If U reprecipitates, the thus calculated dissolution rate will underestimate the real dissolution rate. Because the non-oxidative dissolution rate should decrease quickly as soon as the solution is saturated with U(IV), static tests give measurable rates (different from zero) only if there is also oxidative dissolution, causing increasing U(VI) concentrations, which are much less solubility limited. Fast dissolution can lead to colloid formation in the leachate, which may lead to the aforementioned reprecipitation.
- In 'dynamic tests', the volume of leaching solution in contact with the UO_2 is continuously renewed by means of a pump that imposes a fixed flow rate of the leaching solution through the cell with the UO_2. This implies that U concentrations stay low and – at a sufficiently high flow rate – reprecipitation on the UO_2 surface is less likely. Another advantage is that any preoxidized layer will be removed in the first period. On the other hand, the continuous flow of undersaturated water can increase the non-oxidative dissolution, and make it higher than expected in geological disposal conditions, where the water flow should be negligible. The dissolution rate is calculated based on a combination of the flow rate and the uranium concentration.

  To obtain useful results, the flow rate of the solution has to be optimized. The dissolution rate in a dynamic test close to uranium saturation increases with the flow rate. With very high flow rates, the system becomes undersaturated, and the resulting rate becomes in principle independent of the flow rate. A high rate determined in this way would, however, not be realistic for geological disposal conditions with stagnant water. To simulate these conditions the flow rate must be low. In practice, the flow rate range in which statistically significant measurements are possible is determined by the detection limit of the chemical analyses. Therefore, flow rates are selected that give uranium concentrations slightly above the detection limit. Even when the solution is close to saturation, the resulting rates are still higher than expected in geological disposal conditions, because of the continuous removal of dissolved U.

Static tests thus not always give results that are suitable for dissolution rate determination. With very inactive UO_2 (little or no radiolytic oxidation), the dissolution rate determined from the evolution of the U concentration may be statistically not different from zero, or even apparently negative, i.e. lower than the detection limit of the method. With too much oxidation, reprecipitation can bias the result. Dynamic tests do not present these problems, but they are more complicated to perform. On the other hand, static tests better reproduce the geological disposal conditions with stagnant water and increasing U concentrations, so the two types of tests are complementary. The reliability of the experimental results as indicator of the matrix dissolution rate has to be evaluated case by case. High concentration of colloidal uranium imply a higher risk of reprecipitation and increase the uncertainty on the derived dissolution rate.

High oxidative dissolution rates for inactive UO_2 in supposed anoxic or reducing conditions can be the result of presence of a layer of pre-oxidized uranium or of a contamination with traces of oxygen. To avoid an overestimation of the (short term) dissolution rate by a pre-oxidized layer, the UO_2 is annealed before the leaching. During the annealing, the UO_2 is heated for 6 hours at 1000 °C in a furnace with argon/5% H_2 atmosphere inside a glove box under N_2 atmosphere. This reduces the oxidized U(VI) back to the U(IV) state.

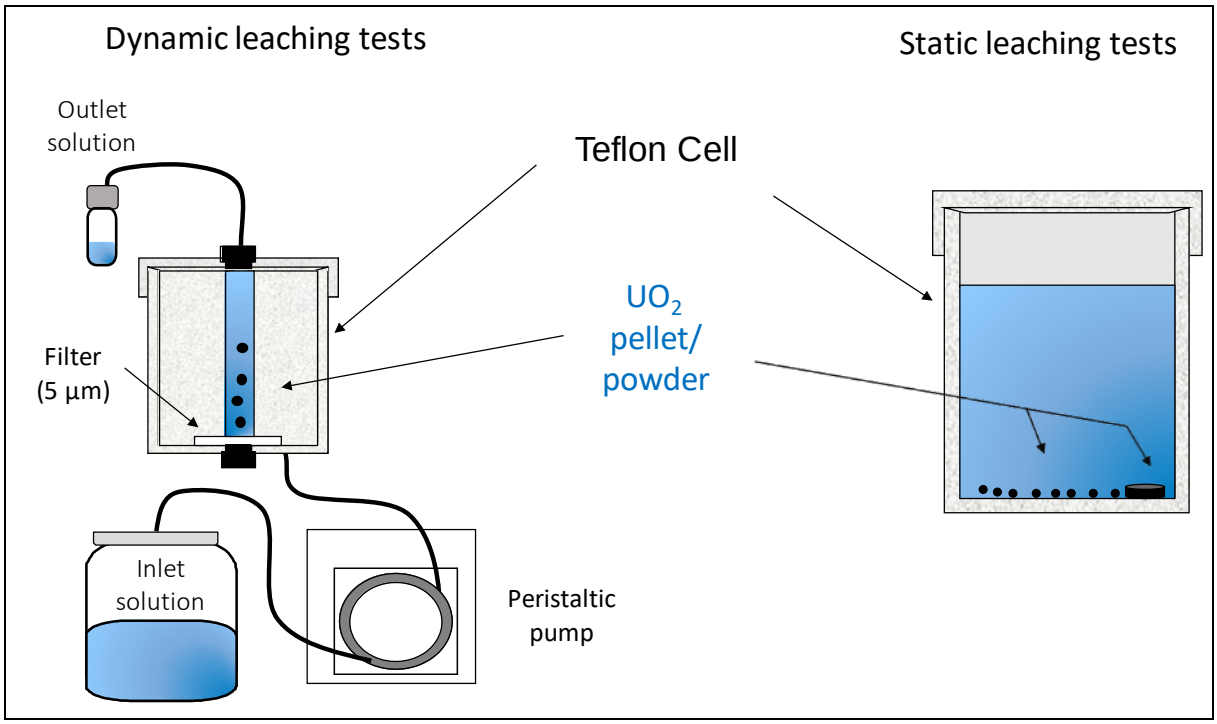

Figure 4-2: Scheme of experimental set-up for dynamic and static leach tests performed with (α-doped) UO_2

4.2.2 Tests with spent fuel

The tests that were performed with spent fuel by KIT were static tests in autoclaves that allow to impose a H_2 overpressure and to analyze also the composition of the atmosphere above the leachate in the autoclave. Because spent fuel contains many different chemical elements, uranium is not the only dissolution indicator. Other, more soluble elements, like Sr or Cs can be used as well, but these may overestimate the matrix dissolution rate, because they are precipitated in open structures that may be leached faster than the UO_2 matrix.

4.2.3 Uncertainty on the dissolution rates

The dissolution rates derived from the tests with (Pu-doped) UO_2 in the next section are given with an experimental uncertainty expressed as the 95% confidence interval, and correspond to the cumulated uncertainties due to the weighing of the samples leachate volumes, and (most important) the chemical analyses. The uncertainty related to the exposed surface area is not included. As explained in the next paragraph, this uncertainty is poorly known, and it probably adds little to the statistical scatter of the results, but it may cause a systematic bias.

Uncertainty on the exposed surface area of the (α-doped) UO_2 or spent fuel samples

As mentioned in Section 3.2.7, the exposed surface area of the (α-doped) UO_2 or spent fuel segments used in the experiments is an important test parameter.

For tests with unirradiated pellets with a simple geometry, the exposed surface area can be calculated relatively accurately as the geometric surface area. Because the surface of such polished pellets is smooth, the surface roughness is assumed to be small compared to the surface roughness of UO_2 powder or fragments, for which a surface roughness factor of 3 is used (see next paragraph). Hence a correction of the geometric surface area with a surface roughness factor is not performed. By not considering any surface roughness the actual pellet surface area involved in the dissolution process may be somewhat underestimated. This implies that the given surface normalized dissolution rates may be overestimated. The overestimation should be in the worst case a factor 3. This leads to a systematic bias, that should be considered when the surface normalized dissolution rates are interpreted. The remaining experimental uncertainty related to the (geometric) surface area estimation (due to measurement of the dimensions of the pellet) is small compared to other sources of uncertainty of the surface normalized dissolution rate.

For unirradiated UO_2 powder or fragments, obtained by crushing of pellets, the surface roughness is much larger. A surface roughness factor of 3 was proposed in the MICADO project, as a proportionality factor between the BET surface area and the geometric surface area (Grambow et al., 2010). In the Belgian R&D programme, UO_2 powders of various size fractions were used, and the specific surface area (S_{sp}) was estimated based on an equation that correlates the BET surface area of UO_2 particles to the average particle size (Cachoir et al., 2015b, Annex II):

$$S_{sp}(UO_2) = 3.8748 \cdot (\text{average particle size})^{-1.1161} \qquad \text{(Equation 10)}$$

This equation gives the specific surface area of the UO_2 in $m^2 \cdot g^{-1}$ if the particle size is given in µm.

Particle size distribution analyses on some UO_2 powders used in the experiments showed that the average size of the particles tended to be larger than assumed. For a sample of depleted UO_2 powder 50 – 100 µm, the average particle size was 88 µm ± 33 µm instead of the 75 µm assumed. With the given equation, this implies that the actual surface area was about 20% smaller than the one used in the calculations. For a sample of F1 powder 50 – 100 µm, the average particle size was 115 µm ± 39 µm instead of 75 µm, implying that the surface area was

about 40% smaller than estimated. For a sample of F2, a similar result (111 µm ± 42 µm) was obtained (Cachoir et al., 2015a). Because only one particle size distribution measurement was performed per batch, there is no statistics on the possible differences in particle size distribution between different powder samples of the same type. For some tests (e.g. the static tests with F1), a 100 – 200 µm fraction was used. For this fraction, no particle size distribution measurement was performed. Because the particle distribution is assumed to be the main source for statistical variation of the specific surface area of the powders, the corresponding uncertainty on the specific surface area cannot be given, and is thus not included in the error bars. Variations in particle size distribution should, however, have little effect on the specific surface area of the powder, as long as the average particle size is similar. The measurements done suggest that the use of the theoretical mathematical average for the particle size (for instance, 75 µm for the fraction of 50 – 100 µm) tends to underestimate the actual average particle size, thus overestimates the specific surface area and underestimates the surface normalized dissolution rates by 20 or 40 %.

For real spent fuel fragments, the effective specific surface area depends not only on the surface roughness, but also on the accessibility of the internal cracks and of grain boundaries. Because of the difficulty to determine the accessible surface area, dissolution rates of spent fuel pellets or fragments are often expressed as fractional dissolution rates, i.e. not normalized with regard to the surface area (see Section 3.3.1). For the first series of tests performed with spent fuel for the Belgian R&D programme, clad fuel segments were used. Also for these samples, the accessible surface area was difficult to estimate. There, the normalization was done with a low (10 $cm^2 \cdot g^{-1}$) and a high (80 $cm^2 \cdot g^{-1}$) specific surface area, derived from literature, which should cover the uncertainty. The background for this selection is explained in section 9.

5 Results from the spent fuel dissolution studies in the framework of the Belgian R&D programme

As discussed in Section 3.2, the characteristics of the pore water contacting the spent fuel in the expected long-term geological disposal conditions can have certain effects on the fuel dissolution mechanisms. In this Section 5, we will illustrate and discuss the matrix dissolution rates that have been measured in high pH conditions in the framework of the Belgian R&D programme. The leach tests with (α-doped) UO_2 and spent fuel performed in this programme were described in research plans (RP.WD.0034, 2004) and (RP.W&D.0060, 2009). An overview of the fractional and surface normalized matrix dissolution rates of UO_2 and spent fuel at high pH determined in the Belgian R&D programme and found in the open literature is given in Table 5.2 at the end of Section 5.

We successively present the dissolution rates measured in

- static tests with depleted UO_2 in cement waters (Section 5.1)
- dynamic tests with depleted UO_2 in cement waters (Section 5.2)
- static tests with Pu-doped UO_2 in cement waters (Section 5.3)
- dynamic tests with Pu-doped UO_2 in cement waters (Section 5.4)
- tests with spent fuel in cement waters (Section 5.5)

5.1 Static tests with depleted UO_2 in cement waters

In most static tests with depleted UO_2, the ultrafiltered uranium concentration stops increasing after some time. This suggests that the uranium in solution reaches an equilibrium with the UO_2 surface. The remaining dissolution measured in these experiments is probably due to the slow oxidation by traces of oxygen, and is not expected under the expected geological disposal conditions.

The presence of colloids in the tests with UO_2 powders complicates the interpretation, and may lead to an underestimation of the dissolution rate, if the colloids reprecipitate onto the UO_2 surface. This colloid formation is considered as an artifact (see Section 6.8). For this reason, we do not give a detailed overview of all rates that have been obtained in static tests with UO_2 powder in the topical reports (Cachoir et al., 2015a; Cachoir et al., 2015b; Cachoir et al., 2015c); we show only the more reliable dissolution rate measured with pellets of depleted UO_2.

The dissolution rate thus measured in YCWCa, based on uranium concentrations in leachates that were not filtered, is shown in Figure 5-1. The resulting long term dissolution rate, obtained between the two last data points, is 0.23 ± 0.21 $\mu g \cdot m^{-2} \cdot d^{-1}$. The higher short term rate is probably biased by the dissolution of preoxidized uranium. The dissolution rate thus clearly decreases with time. A continuation of the test might have shown a still lower rate, so it seems likely that the rate of 0.23 $\mu g \cdot m^{-2} \cdot d^{-1}$ overestimates the long term dissolution rate under the given test conditions. Similar results were obtained with depleted UO_2 pellets in ECW and OCW (Cachoir et al., 2015b; Cachoir et al., 2015c).

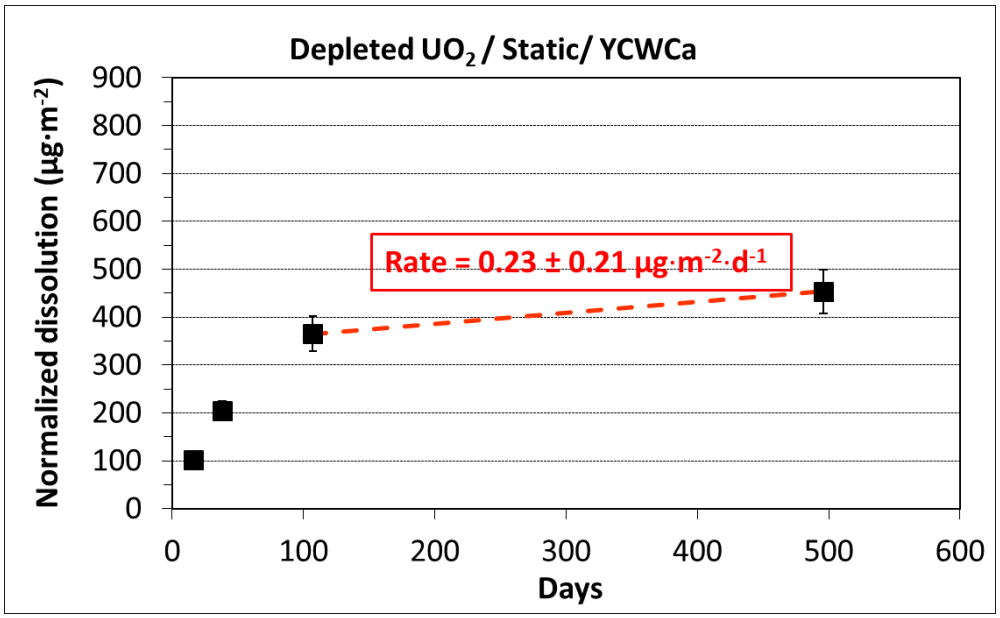

Figure 5-1: Evolution of the amount of uranium dissolved per m^2 of UO_2 in a static test with a pellet of depleted UO_2 in YCWCa at ambient temperature for a surface/volume ratio of 6 m^{-1} (Cachoir et al., 2015b; Cachoir et al., 2015c)

5.2 Dynamic tests with depleted UO_2 in cement waters

Dynamic tests with depleted UO_2 powder (50 – 100 µm) were performed in the three reference cement waters of Table 4-2. Detailed results are given in the topical reports (Cachoir et al., 2015b and Cachoir et al., 2015c).

- In ECW (pH 12.5), two flow rates were tested, resulting in dissolution rates of 1.0 ± 0.3 $\mu g \cdot m^{-2} \cdot d^{-1}$ and 1.8 ± 0.9 $\mu g \cdot m^{-2} \cdot d^{-1}$.
- In OCW (pH 11.7), only one flow rate was tested, resulting in a dissolution rate of 2.3 ± 1.0 $\mu g \cdot m^{-2} \cdot d^{-1}$.
- In YCWCa (pH 13.5), tests were done at two different flow rates, giving a dissolution rate of 0.10 ± 0.02 $\mu g \cdot m^{-2} \cdot d^{-1}$ (Figure 5-2) and 0.8 ± 0.2 $\mu g \cdot m^{-2} \cdot d^{-1}$, but the latter value was considered as less reliable as a result of CO_2 intrusion in the glove box during the experiment. The former rate is derived from the uranium concentrations higher than the detection limit measured after more than 40 days. These rates are shown by the dark squares (■) in Figure 5.2. The dissolution rates from uranium concentrations below the detection limit are shown by the empty squares (□). In this case, the detection limit was used as an upper estimation. The detection limit varies, amongst others because of different dilutions made for the analysis. The higher uranium concentration (and apparent dissolution rate) measured after 60 days is considered as an artefact. It is probably due to the presence of a small UO_2 particle in the analysed leachate.

These rates were calculated with the uranium concentrations in leachates that were not filtered.

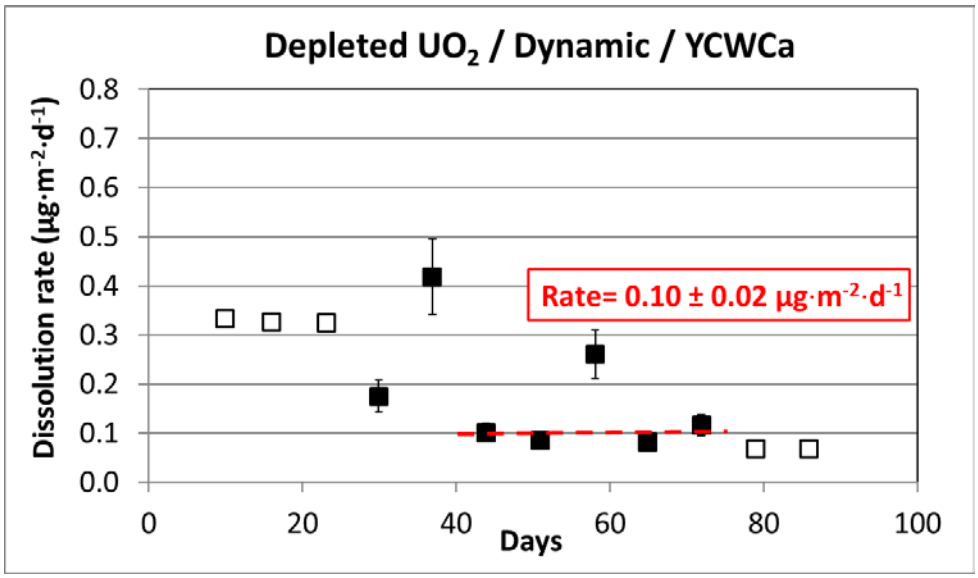

Figure 5-2: Evolution of the dissolution rate for the dynamic tests with depleted UO_2 powder 50 – 100 µm in YCWCa at ambient temperature (flow rate 8.4 µl·min^{-1}), based on uranium concentrations in leachates that were not filtered. The empty squares (□) on the graphs correspond to uranium concentrations below detection limit.

Because the duration of the tests in OCW and ECW was very short (≤ 10 days), the reported rates for these media may have been biased by remaining U(VI). The tests in YCWCa were performed for longer periods. Moreover the YCWCa dissolves better the U(VI) from the UO_2 surface and the medium is more stable. For these reasons, the dynamic dissolution rate in YCWCa is considered as more reliable. The rate of 0.10 ± 0.02 µg·m^{-2}·d^{-1} probably approaches better the steady state dissolution rate for the given flow rate. In these tests, the uranium concentrations are approximately 10^{-9} mol·L^{-1}. This suggests that we have mainly non-oxidative dissolution, driven by the continuous water flow with cement water that is undersaturated with U(IV) before it reaches the UO_2 powder.

The good agreement between the dissolution rate measured in the static tests (0.23 ± 0.21 µg·m^{-2}·d^{-1}) and in dynamic tests (0.10 ± 0.02 µg·m^{-2}·d^{-1}) increases the confidence in the measured rates. Although the difference between the two rates may be statistically not significant (because of the large uncertainty for the static dissolution rate) the slightly higher static dissolution rate may be due to the dissolution of a remaining preoxidized layer or oxidation by traces of oxygen. The uranium concentration in this static test was indeed close to 10^{-8} mol·L^{-1}, suggesting a small fraction of oxidative dissolution. The slow remaining dissolution in the dynamic tests is probably due to the oxidation by traces of oxygen and by the water flow. Under geological disposal conditions, there will be no traces of oxygen, and the flow rate will be much lower than the experimental flow rate. In such conditions, the dissolution rate should be still lower than 0.10 ± 0.02 µg·m^{-2}·d^{-1}.

The given 95% confidence intervals do not include the possible overestimation of the dissolution rate for the static test with the pellet and the possible underestimation for the dynamic test with powder, which is due to the uncertainty concerning the precise surface area involved in the dissolution (see Section 4.2.3).

Because the number of tests with depleted UO_2 in cement waters is still small, the results obtained within the Belgian R&D programme until 2014 need confirmation by supplementary experiments.

5.3 Static tests with Pu-doped UO_2 in cement waters

The tests with Pu-doped UO_2 were all done with powders, because Pu-doped pellets were not available. In the tests with Pu-doped UO_2 powders, the ultrafiltered uranium concentration tends to stabilize, like for depleted UO_2, but at a higher concentration, because the radiolytic UO_2 oxidation increases the U(VI) concentration. For the Pu-doped UO_2, almost all uranium in solution is colloidal. Like for the depleted UO_2, the presence of these colloids induces uncertainties. The colloid formation was particularly high in tests at high surface area/volume (SA/V) ratio (257 m^{-1}). This was probably an artefact, due to the presence of oxidized U on the large UO_2 surface at the start of the tests. It led to unstable total concentrations, making it difficult to derive a dissolution rate. This was less a problem for tests at moderate SA/V (6 m^{-1} and 130 m^{-1}). Therefore, the tests at moderate SA/V were considered as more reliable for the determination of the UO_2 dissolution rate. In these tests at moderate SA/V with Pu-doped UO_2, the total uranium concentrations tend to increase with time because of the radiolytic oxidation. The dissolution rate determined by linear regression thus gives a positive result, with a dissolution rate that can statistically be distinguished from zero. The dissolution rate was tested for different media and different α-activities of the UO_2. Static tests have thus been performed with Pu-doped UO_2 F1 (Section 5.3.1), and with F2, F4 and F6 (Section 5.3.2). The detailed results can be found in the topical reports (Cachoir et al., 2015a; Cachoir et al., 2015b; Cachoir et al., 2015c). The dissolution rates determined with the Pu-doped UO_2 are probably biased by the fact that all batches were available only in powder form, produced by crushing of pellets. This powder has a large specific surface area and probably many surface defects. This may accelerate the dissolution, especially for the very active fuel F1, generating a high dose rate, and thus a high concentration of oxidizing species in the solution.

5.3.1 Results for static tests with Pu-doped UO_2 F1

Tests were performed at high SA/V (257 m^{-1}) and low SA/V (6 m^{-1}), but only the latter gave measurable dissolution rates and are reported here. Tests were done in YCWCa, ECW and OCW. The regression for the test with F1 at 6 m^{-1} in YCWCa is shown in Figure 5-3. A detailed analysis suggests that fuel dissolution may occur in three steps. A fast initial dissolution of the preoxidized U(VI) (0 –10 days) followed by a stabilization due to the time needed to form a new radiolytically oxidized layer. Afterwards, the dissolution starts again (100 – 150 days). In order to consider the longer-term influence of α-radiation on the dissolution rate, regressions were made not only for the period 0 – 500 days, but also for the period 100 – 500 days. The

resulting dissolution rates were 42 ± 12 µg·m^{-2}·d^{-1} (0 – 500 days) and 45 ± 22 µg·m^{-2}·d^{-1} (100 – 500 days). These rates were calculated with the uranium concentrations in leachates that were not filtered.

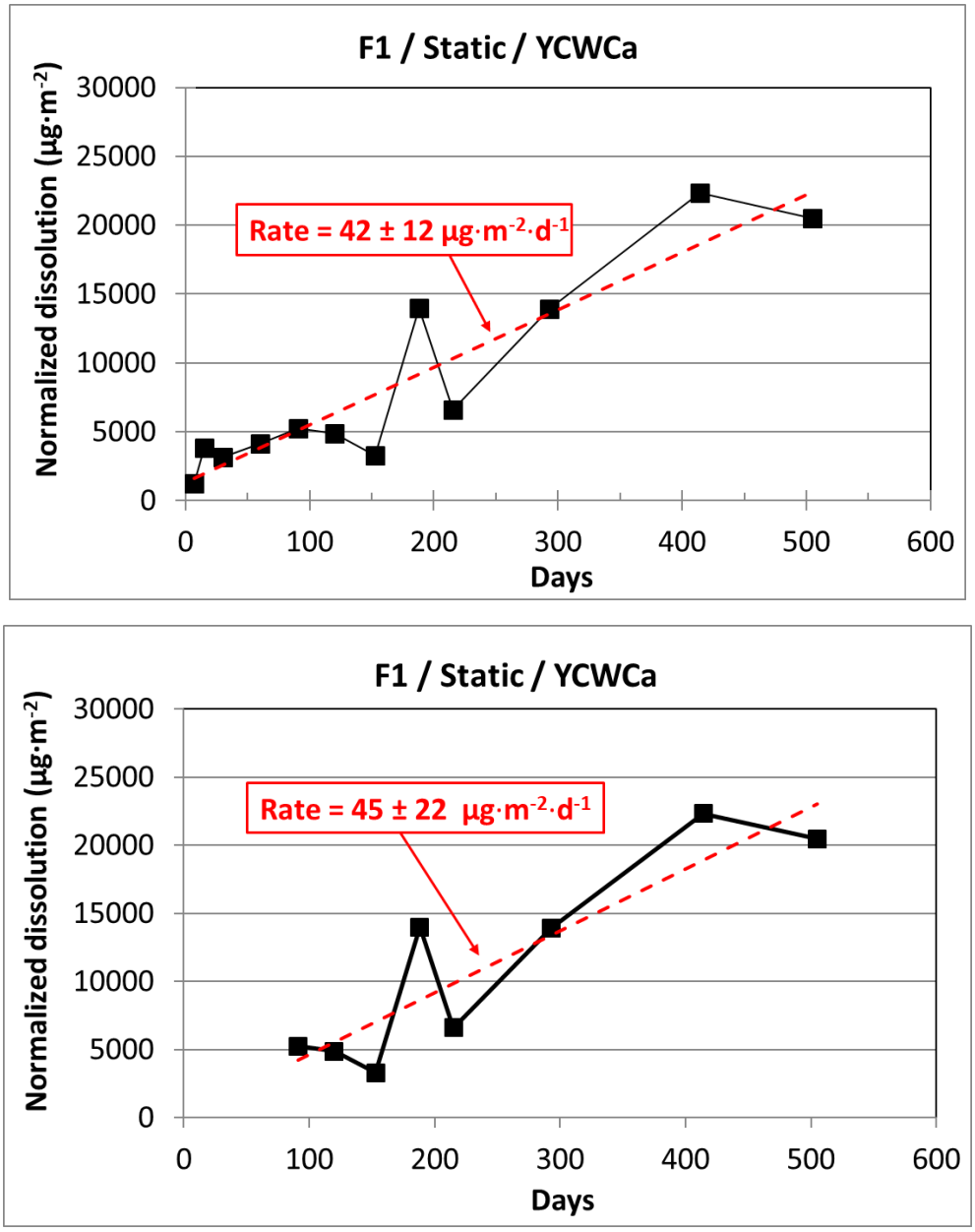

Figure 5-3: Evolution of the amount of uranium dissolved per m^2 of UO_2 in a static test with Pu-doped UO_2 powder F1 (100 – 200 µm) in YCWCa at ambient temperature for a surface/volume ratio of 6 m^{-1} (top: regression 0 – 500 days; bottom : regression 100 – 500 days), based on uranium concentrations in leachates that were not filtered.

The dissolution rates measured with F1 in YCWCa at an SA/V ratio of 6 m^{-1} are summarized in Table 5-1, together with the rates measured in ECW and OCW. Considering the uncertainties on the regression rates, there are no strong arguments to assume that the dissolution rate of fuel F1 is significantly different for the three cement waters.

The results thus suggest that the impact of the medium on the dissolution rate will be relatively small. Additional experiments are necessary to improve the rate estimations, to reduce the uncertainty intervals and to better understand the underlying mechanisms.

The dissolution rates in Table 5-1 may be biased because they were obtained with doped UO_2 in powder form, with a surface area that is not exactly known. The actual dissolution rate may be somewhat higher (see Section 4.2.3).

Table 5-1: Dissolution rates, expressed in $\mu g \cdot m^{-2} \cdot d^{-1}$, for Pu-doped UO_2 of type F1 (100 – 200 µm) in static tests with OCW, ECW and YCWCa at ambient temperature for a surface/volume ratio of 6 m^{-1} (Cachoir et al.,2015b; Cachoir et al.,2015c). The rates are based on uranium concentrations in leachates that were not filtered.

Type of Pu-doped UO_2	Medium	Dissolution rate (regression rate 0 – 500 days)	Dissolution rate (regression rate 100 – 500 days)
F1	OCW	68 ± 15	79 ± 24
F1	ECW	48 ± 8	54 ± 12
F1	YCWCa	42 ± 12	45 ± 22

5.3.2 Results for static tests with Pu-doped UO_2 F2, F4 and F6

For the doped UO_2 with lower activity (F2, F4 and F6), static tests were performed with an SA/V ratio of 130 m^{-1} in YCWCa (not in ECW or OCW).

For **fuel F2**, the dissolution rate was probably biased by colloid precipitation, although the colloids are less abundant than with fuel F1. The average dissolution rate between 0 and 602 days, and between 0 and 720 days (two different test containers) was 7.6 $\mu g \cdot m^{-2} \cdot d^{-1}$ ± 41% and 6.0 $\mu g \cdot m^{-2} \cdot d^{-1}$ ± 6%, resp.

The dissolution rate determined in static tests with **fuel F4** in YCWCa could not be distinguished from zero due to colloid precipitation.

Static tests with **fuel F6** in YCWCa resulted in regression rate of 0.28 ± 0.11 $\mu g \cdot m^{-2} \cdot d^{-1}$ (Figure 5-4) (Cachoir et al., 2015a), based on uranium concentrations in leachates that were not filtered. This most probably overestimates the long-term dissolution rate in anoxic conditions, because the sudden increase for last data point suggests a perturbation of the system. The data points until 450 days indicated a gradual decrease to much lower dissolution rates.

These dissolution rates may be biased because they were obtained with doped UO_2 in powder form, with a surface area that is not exactly known. The actual dissolution rate may be somewhat higher (see Section 4.2.3).

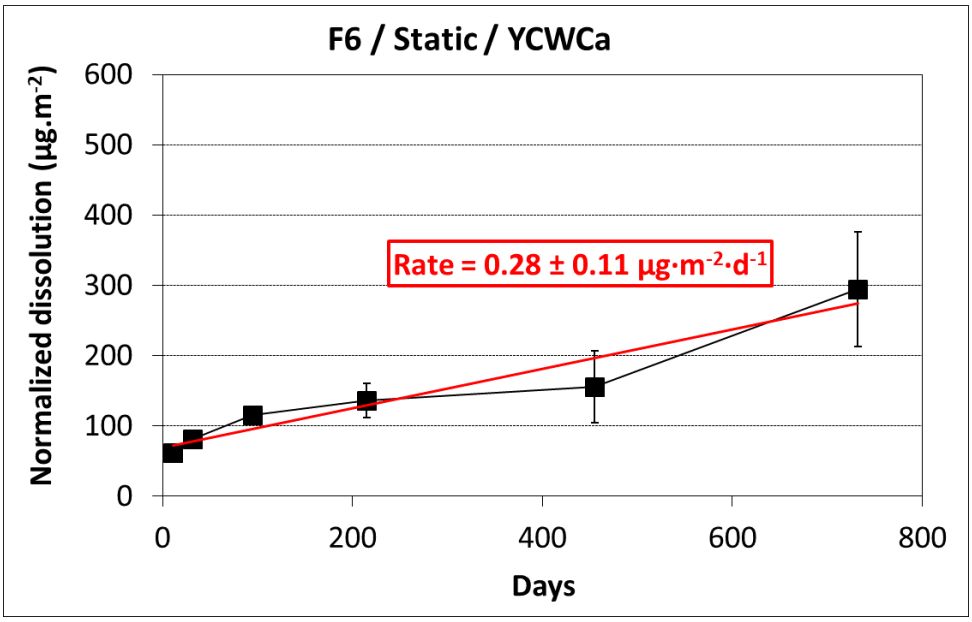

Figure 5-4: Evolution of the amount of uranium dissolved per m^2 of UO_2 in a static test with Pu-doped UO_2 powder F6 (50 – 100 µm) in YCWCa at ambient temperature for a surface/volume ratio of 130 m^{-1}, based on uranium concentrations in leachates that were not filtered.

To verify the suppression of the matrix dissolution by H_2 gas observed with real spent fuel (see Section 5.5), the dissolution of fuel F2 was also tested in autoclaves filled with YCWCa and 0.5 and 5 bar H_2 (0.4 or 0.04 mmol·L^{-1} H_2). The H_2 overpressure had no measurable effect on the dissolution rate. This may be due to the absence of catalytic epsilon particles. According to the Fuel Matrix Dissolution Model (FMDM), concentrations up to 0.4 mmol·L^{-1} H_2 would indeed have only a small effect on the fuel dissolution rate in absence of epsilon particles (Jerden et al., 2015). Nevertheless, experiments in other media showed that the UO_2 surface can also have a catalyzing effect, even without epsilon particles (Muzeau et al., 2009, Carbol et al., 2009b). A hypothetical mechanism for this catalysis is that O_2 and H_2 would both absorb to the same partly oxidized U(IV)-U(V) sites, where the H_2 donates an electron to the surface, reducing the U(V) back before it is oxidized to U(VI). If the surface is too oxidized, there will be no U(IV)-U(V) sites any more, so a requirement for the catalytic effect is that the surface is close to stoichimetric (Carbol et al. 2009b). Another factor that may explain the absence of a H_2 effect for the fuel F2 may be the high surface area of the F2 powder, leading to a disequilibrium between local concentrations of oxidizing and reducing species. According to Carbol (Carbol et al., 2009b), the surface has to be close to stoichiometric to have a catalyzing effect. An oxidized layer would have no catalyzing effect.

No static experiments were performed with fuel F2, F4 or F6 in ECW or OCW. The results for depleted UO_2 and fuel F1 suggest, however, that the cement water does not affect much the dissolution rate range. For this reason, the rates for fuel F2, F4 and F6 in YCWCa can be used as approximations for the dissolution rate in ECW and OCW, awaiting confirmation by additional experiments.

Because of the colloid formation, the dissolution rates measured with the Pu-doped UO_2 were less reliable. Therefore, dynamic tests were performed, where colloid formation is less prominent.

5.4 Dynamic tests with Pu-doped UO_2 in cement waters

Dynamic tests with fuels F1, F2, F4 and F6 were performed only in YCWCa so far. The detailed results can be found in the topical reports (Cachoir et al., 2015a; Cachoir et al., 2015b; Cachoir et al., 2015c). The 95% confidence intervals on the dissolution rates in the reference reports have been recalculated and are slightly smaller than the values given in these reports.

The continuous flow with U(IV) undersaturated water accelerates the non-oxidative dissolution, but the radiolytic oxidative dissolution is probably less affected. For more active fuels, where the oxidative dissolution is dominant, the effect of the water flow on the total dissolution rate should thus be small. On the other hand, the flow counteracts precipitation of U(VI) phases on the surface and the possible protective effect this might have. So the dissolution rate measured in these tests may still be higher than the net dissolution rate one would observe in static conditions. In spite of the continuous removal of dissolved U with the flowing leaching solution, there is still some colloid formation.

For **fuel F1**, with a three-step flow rate, going from 20 over 12 to 8 µl·min^{-1}, an average dissolution rate over the entire test duration of 12 ± 5 µg·m^{-2}·d^{-1} was found, based on uranium concentrations in leachates that were not filtered (Figure 5-5). The rate during the last 40 days (with flow rate 8 µl·min^{-1}) was slightly lower (9.1 ± 5.0 µg·m^{-2}·d^{-1}). The uranium concentration was between 10^{-7} – 10^{-8} mol·L^{-1} and thus dominated by radiolytic oxidative dissolution. This rate is about 4 times lower than the rate determined with static experiments at 6 m^{-1} (Table 5-1). To clarify this relatively large difference, further experiments are necessary. Part of the difference may be due to the uncertainty on the specific surface area of the UO_2 powder. The dynamic test was done with the 50 – 100 µm fraction, while the static test was done with the 100 – 200 µm fraction. The few available data from the particle distribution analyses suggest that the specific surface area of the 50 – 100 µm fraction was possibly overestimated (and the dissolution rate thus underestimated). For the 100 – 200 µm fraction no particle distribution analyses was performed (see Section 4.2.3).

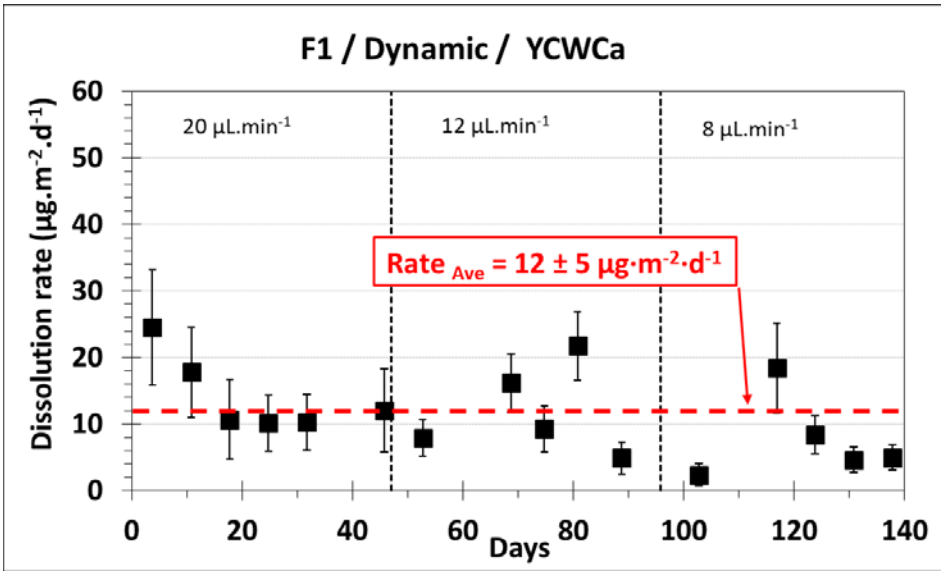

Figure 5-5: Evolution of the dissolution rate for the dynamic tests with Pu-doped UO_2 powder F1 (50 – 100 µm) at ambient temperature (flow rate 8 – 20 µl·min^{-1}), based on uranium concentrations in leachates that were not filtered

For **fuel F2**, two dynamic tests were performed.

- For the first test (with a flow rate of 8 µL·min^{-1}), analyses were performed on both ultrafiltered and unfiltered samples. Figure 5-6 only shows the dissolution rates for the unfiltered samples. The difference with the ultrafiltered samples (corresponding to dissolution rates of 1 to 2 µg·m^{-2}·d^{-1}) was small, except for the three data points around 7 µg·m^{-2}·d^{-1}, where there were apparently more colloids or small UO_2 particles in suspension. We thus have two different rate levels of 1.9 ± 0.6 µg·m^{-2}·d^{-1} for the samples without colloids, and 6.9 ± 0.6 µg·m^{-2}·d^{-1} for the samples with colloids.
- A second test (with a three-step flow rate, going from 20 over 12 to 8 µl·min^{-1}) resulted in an average dissolution rate of 39 ± 10 µg·m^{-2}·d^{-1}over the entire test duration, and a dissolution rate of 18 ± 15 µg·m^{-2}·d^{-1}over the last 40 days (with flow rate 8 µl·min^{-1}), based on uranium concentrations in leachates that were not filtered (Figure 5-7). The uranium concentration was close to 10^{-7} mol·L^{-1}, suggesting oxidative dissolution driven by radiolysis. The rate shows a decreasing trend, though. The dissolution rate for the last samplings was clearly lower than in the first samplings, and approaching the dissolution rate measured in the first test. The occasional very high dissolution rates around 80 µg·m^{-2}·d^{-}may be due to artifacts (pre-oxidation or small UO_2 particles in suspension), but they were included for the rate calculations.

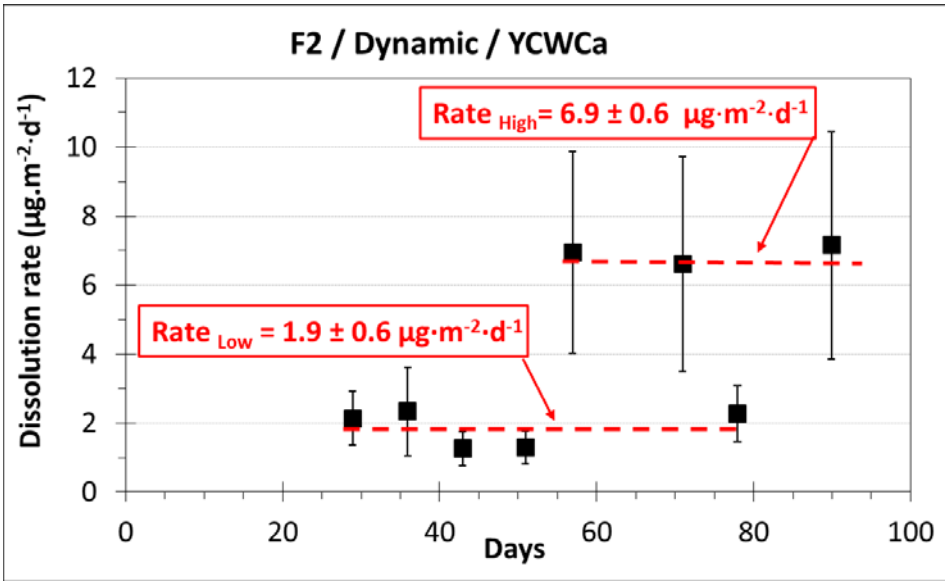

Figure 5-6: Evolution of the dissolution rate for the dynamic tests with Pu-doped UO_2 powder F2 (<100 µm) at ambient temperature – first experiment (flow rate 8 µL·min^{-1}), based on uranium concentrations in leachates that were not filtered

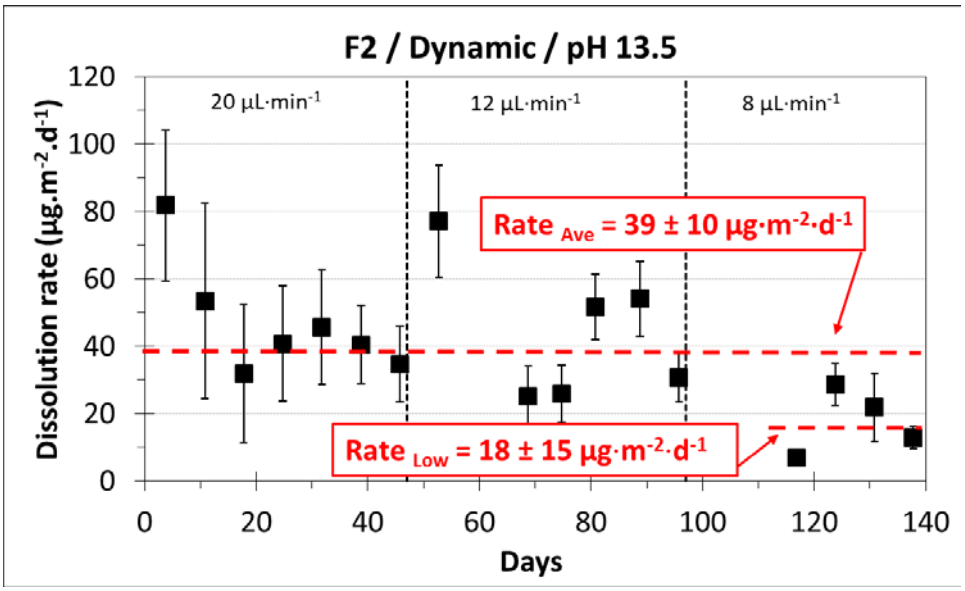

Figure 5-7: Evolution of the dissolution rate for the dynamic tests with Pu-doped UO_2 powder F2 (50 – 100 µm) at ambient temperature (flow rate 20 – 12 – 8 µl·min^{-1}), based on uranium concentrations in leachates that were not filtered

For **fuel F4**, (with a three-step flow rate, going from 24 over 12 to of 8 µl·min^{-1}), an average dissolution rate of 2.7 ± 0.6 µg·m^{-2}·d^{-1} was measured over the entire test duration (Figure 5-8). Between 60 and 80 days, a lower rate of 1.5 ± 0.3 µg·m^{-2}·d^{-1} was measured. Until 40 days, both ultrafiltered and unfiltered samples were taken. Figure 5-8 only shows for this period only the dissolution rates for the samples that were not filtered. The rates calculated from the ultrafiltered samples were only slightly different and are not shown. For the longer test duration, only ultrafiltered samples were analyzed. The calculated rate of 1.5 ± 0.3 µg·m^{-2}·d^{-1}, may thus underestimate the actual dissolution rate, but if there was little colloid formation also after more than 40 days (a hypothesis that is not unlikely, but whose correctness was not demonstrated by further measurements), the underestimation should be small.

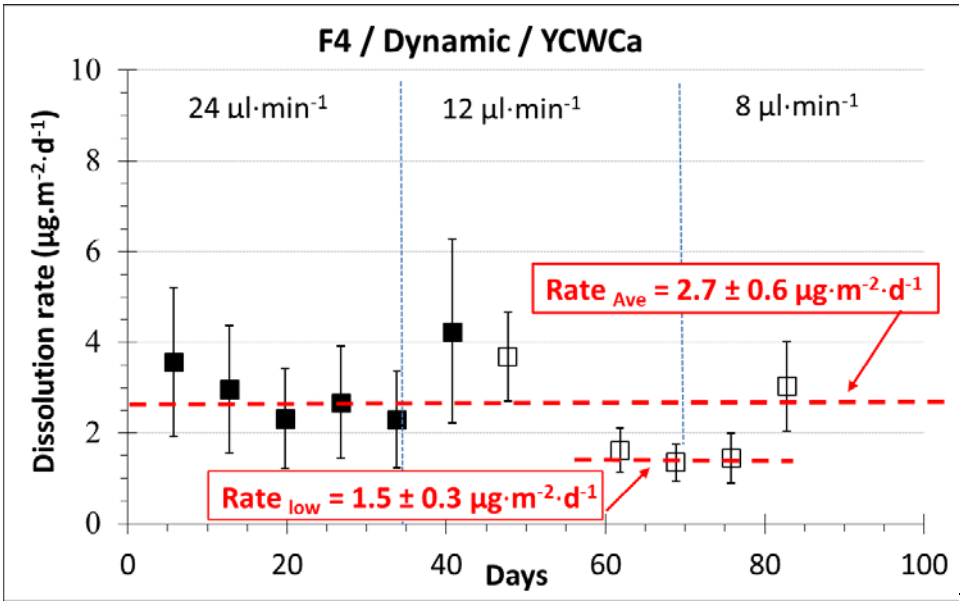

Figure 5-8: Evolution of the dissolution rate for the dynamic test with Pu-doped UO_2 powder F4 (50 – 100 µm) in YCWCa at ambient temperature (flow rate 24 – 12 – 8 µl·min^{-1}), based on uranium concentrations in leachates that were ultrafiltered (□) and that were not filtered (■)

For **fuel F6**, (with a three-step flow rate, going from 24 over 12 to of 8 µl·min^{-1}), the dissolution rate decreased with time and stabilized after more than 50 days at 0.16 ± 0.03 µg·m^{-2}·d^{-1} (Figure 5-9). The (ultrafiltered and not-filtered) U concentration decreased to <10^{-9} mol·L^{-1}, indicating non-oxidative dissolution.

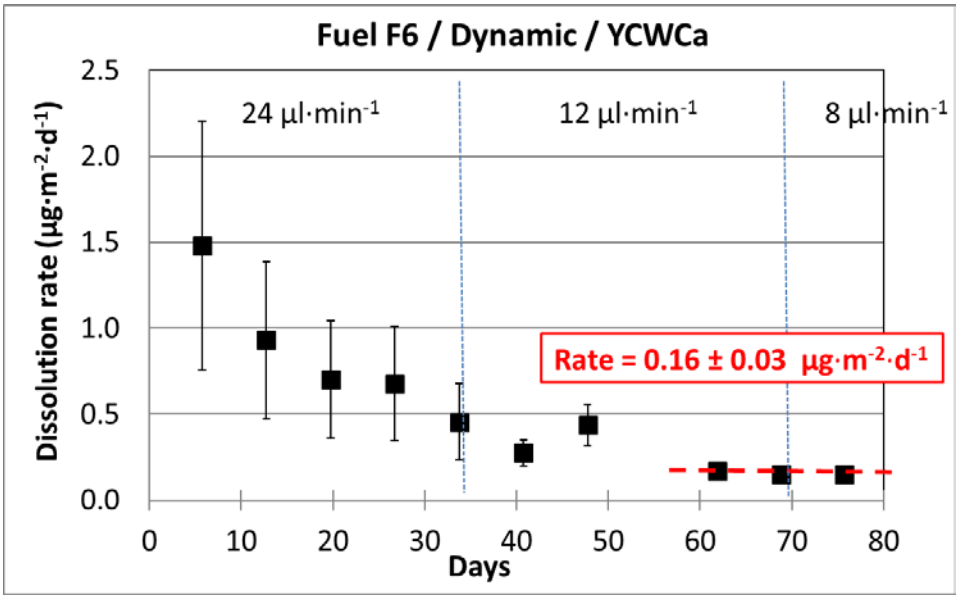

Figure 5-9: Evolution of the dissolution rate for the dynamic test with Pu-doped UO_2 powder F6 (50 – 100 µm) in YCWCa at ambient temperature (flow rate 24 – 12 – 8 µL·min^{-1}), based on uranium concentrations in leachates that were not filtered

Like for fuel F1, the dissolution rates given for F2, F4 and F6 may slightly underestimate the real rates, because of a possible overestimation of the surface area of the UO_2 powder (see Section 4.2.3).

5.5 Tests with spent fuel in cement waters

The following conditions were tested:

- Tests with clad fuel *segments* in ECW without an applied H_2 gas overpressure (Section 5.5.1)
- Tests with clad fuel *segments* in ECW and YCWCa with an applied H_2 overpressure up to 3.2 bar (Section 5.5.2)
- Tests with fuel *fragments* in ECW and YCWCa with an applied H_2 overpressure of 3.2 bar (Section 5.5.3).

The resulting dissolution rates are discussed hereunder. The rates are typically expressed as fractional dissolution rates, because the surface area of the fuel samples is not well known (see Section 4.2.3). ^{90}Sr is a relatively good dissolution indicator, because it is present in the UOX matrix and relatively soluble. Part of the ^{90}Sr is, however, segregated in the grain boundaries or in the gap between fuel and cladding, and can be leached preferentially. This can lead to an overestimation of the matrix dissolution rate. The rates are thus expressed in 'FIAP per day', based on the release of ^{90}Sr in the leachate. 'FIAP' is the *Fraction of the Inventory in the Aqueous Phase*, this is the fraction of the total ^{90}Sr inventory in the tested spent fuel sample found in

the solution (the total initial ^{90}Sr inventory of the fuel after 22 years cooling time was $4.2x10^{-6}$ mol·g^{-1} UO_2). Because *FIAP* is dimensionless, the units for the fractional dissolution rate '*FIAP·day^{-1}*' can also be written simply as '*day^{-1}*'.

5.5.1 Tests with fuel segments in ECW without applied H_2 gas overpressure

In ECW without H_2 overpressure, tests were done with and without addition of iron chips and magnetite as reducing agents. A dissolution rate based on ^{90}Sr release of about 1 x 10^{-7} FIAP·day^{-1} is reported (Loida et al., 2009a). This is illustrated in Figure 5-10. The same graph shows data for tests in Simple Young fluid (SYF) with Bure Clay, which were shown also in Section 3.3.4. The composition of SYF (KOH (9.033 g·L^{-1}) NaOH (2.606 g·L^{-1}) and $Ca(OH)_2$ (0.166 g·L^{-1}) is similar to the composition of YCWCa. The graph further shows that the dissolution rate in distilled water (DIW) was clearly higher than in the media with higher pH. Nevertheless, a fractional dissolution rate of 1 x 10^{-7} FIAP·day^{-1} is still relatively high (it would correspond to complete dissolution in 27000 years), suggesting oxidative dissolution. The addition of magnetite or Fe did not reduce the dissolution rate, probably because the passive layer formed on the Fe chip at high pH decreases its reducing capacity. The U and Tc concentrations were nevertheless relatively low ([U] = 2 – 3 x 10^{-9} mol·L^{-1} and [Tc] ≤ 7 x 10^{-9} mol·L^{-1}). Much of the U and Tc was absorbed on the autoclave wall. For comparison, in NaCl solutions with final pH 9.45 (without iron) and 10.3 (with iron), U concentrations were 1.5 x 10^{-6} and 2.8 x 10^{-8} mol·L^{-1}, respectively (Grambow et al., 2000).

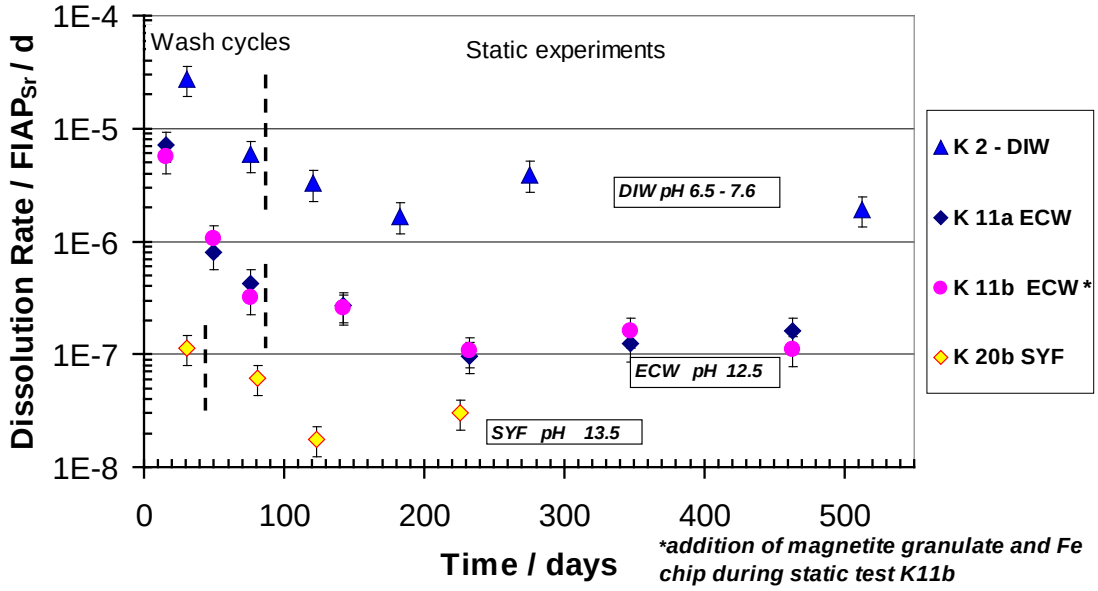

Figure 5-10: Matrix dissolution rates of spent nuclear fuel derived from the Sr release ($FIAP_{Sr}$ · d^{-1}) as a function of time obtained during corrosion experiments of spent fuel sample K 11a and K 11b in ECW at pH 12.5, sample K2 in DIW at pH 6.5 – 7.6, and sample K20a in SYF at pH 13.5 (Loida et al., 2009a)

5.5.2 Tests with fuel segments in ECW and YCWCa with applied H_2 gas overpressure

In these tests, the H_2 pressure was 1 bar in a first stage, and 3.2 bar in a second stage. This corresponds to dissolved H_2 concentrations of 0.8 mmol·L^{-1} and 2.5 mmol·L^{-1}, respectively. In ECW with H_2 overpressure, the dissolution rate based on ^{90}Sr release decreased with time to about 1x10^{-8} FIAP·day^{-1} (Loida et al., 2012). In a report from 2011 (Loida et al., 2011), a rate of 1.3 x 10^{-8} FIAP·day^{-1} is given for the same experiments. This is illustrated in Figure 5-11. In YCWCa, the ^{90}Sr concentration in solution decreased with time after 80 days because of adsorption on the wall of the autoclave, so a FIAP rate estimation based on ^{90}Sr was not possible (Figure 5-11 shows ^{90}Sr FIAP rates in YCWCa only up to 80 days). In the ECW, there was no adsorption of Sr on the vessel wall, probably because the sorption sites were saturated with Ca. The sum of the Sr in solution and the Sr on the vessel wall was the same in ECW and YCWCa (Loida et al., 2011). One can therefore conclude that the matrix dissolution rate was similar for both media.

A rate of 1 x 10^{-8} FIAP·day^{-1} for ^{90}Sr with 3.2 bar H_2 is lower than the rate in the tests with ECW without H_2 gas, where rates of about 1 x 10^{-7} FIAP·day^{-1} were measured. This confirms the favourable effect of H_2 on the fuel stability. Nevertheless, the FIAP rate was still relatively high in these tests with clad segments, and would imply a relatively short fuel time for the complete dissolution (order of magnitude 300000 years). On the other hand, the concentrations of the redox-sensitive radionuclides were typical for reducing conditions. Tc, Np, Pu, and U concentrations were in the order of magnitude 10^{-10} – 10^{-9} mol·L^{-1} or lower, both at 1 bar and 3.2 bar of H_2 gas. The final U concentration was 1.5 x 10^{-9} mol·L^{-1}in YCWCa and 1.9 x 10^{-10} mol·L^{-1} in ECW (Loida et al., 2012). The amount of U absorbed on the autoclave walls was much larger than the amount of dissolved U, though. The total amount of leached U was the same in both media. The low concentrations of redox sensitive species suggests very low concentrations of oxidizing species, implying that the FIAP rate for ^{90}Sr probably overestimates the real dissolution rate. A possible reason for this might have been the preferential Sr release from the gap in the experiments with clad segments. To test this hypothesis, tests were performed with isolated fuel fragments, leached without the cladding.

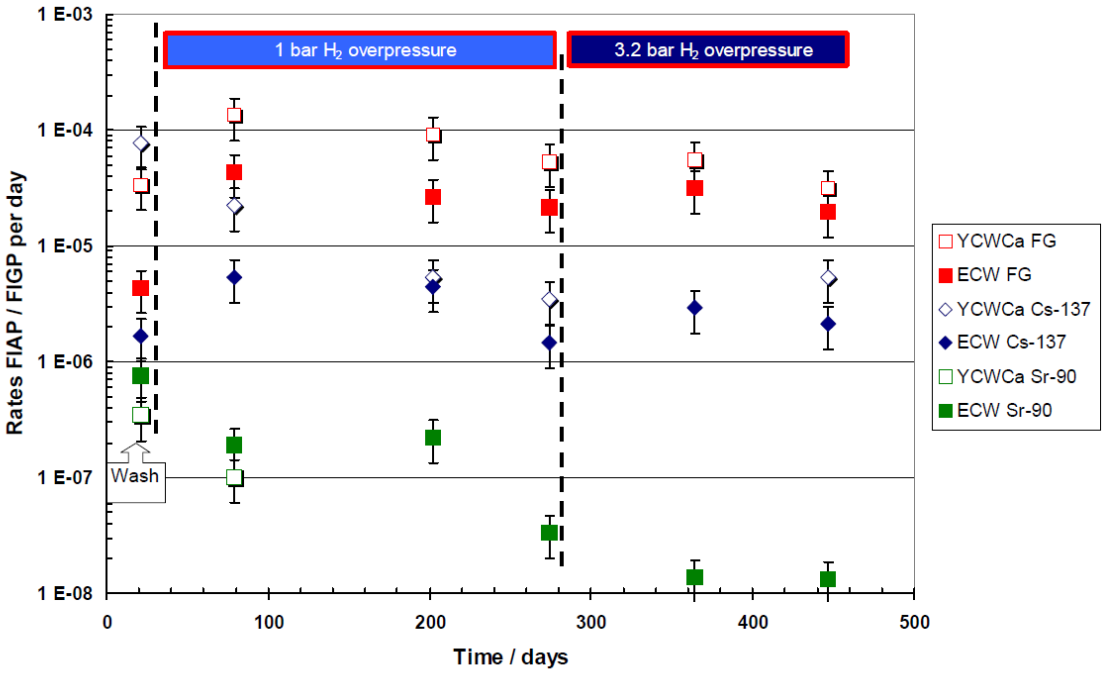

Figure 5-11: Matrix dissolution rates of spent nuclear fuel derived from the Sr release ($FIAP_{Sr}$ · d^{-1}) as a function of time obtained during corrosion experiments of spent fuel sample 2K11a in ECW water at pH 12.5, and sample 2K11 in YCWCa (tests with H_2 overpressure) (Loida et al., 2011)

5.5.3 Tests with fuel fragments in YCWCa with an applied overpressure of 3.2 bar H_2

To test the hypothesis that Sr release from the gap might bias the results, tests were performed in YCWCa with declad fuel fragments, prepared from the fuel segments that were tested previously (González et al., 2014). Here also, the sorption on the cell wall was very important for U (99% absorbed) and for Sr (82% absorbed). In this series, different containers were used for different test durations, which allowed to follow the evolution with time of the Sr sorption on the container wall. The disadvantage of using different containers for each test duration is that there was no continuous increase of the total released fraction (including the sorbed fraction) with time (Figure 5-12). Hence it was not possible to derive a precise mechanistically underpinned long term matrix dissolution rate. In an alternative approach, average dissolution rates were calculated based on the difference between the total Sr (dissolved plus sorbed) at the end of the test and at the start of the preleaching, or at the solution replacement after the preleaching. In this way, the fast increase of the FIAP in the first day of exposure is averaged over the entire test, and the decrease with time is masked. This results in calculated dissolution rates of order of magnitude 10^{-7} day^{-1}, corresponding to a time for complete dissolution of a few tens of thousands of years. The thus calculated average rate is certainly much higher than the long term rate, which could unfortunately not be quantified exactly. The low concentrations or redox-sensitive radionuclides (about 10^{-9} mol·L^{-1} for U, 10^{-10} to 2 x 10^{-9} mol·L^{-1} for Tc) suggest again effective reducing conditions just like in the tests with fuel segments. This means that the tests with fuel fragments confirmed the trends of the first series of tests (with fuel

segments), but the test did not yield a precise quantification of the very low long term dissolution rate.

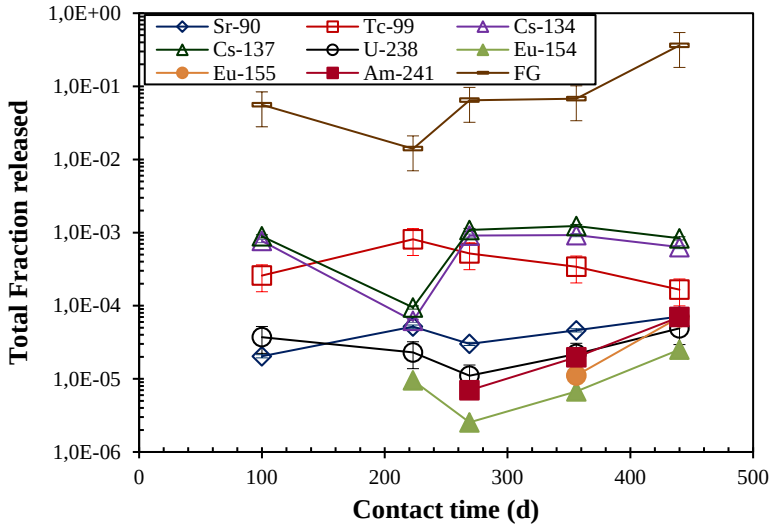

Figure 5-12: Total release fraction from spent fuel fragments (including preleached and sorbed fraction) as function of the total contact time in YCWCa with 3.2 bar H_2

5.6 Overview of matrix dissolution rates at high pH

Table 5-2 gives a complete overview of the dissolution rates measured at high pH, presented in Section 3.3 and Section 5. All these rates were measured at ambient temperature. There are no data available from tests with spent fuel or spent fuel analogues in cement-conditioned environment at high temperature. We refer to Section 3.2.6 for data obtained at higher temperature in other media.

Table 5-2: Overview of the fractional and surface normalized matrix dissolution rates of (α-doped) UO_2 and spent fuel at ambient temperature mentioned in Sections 5.1 to 5.5.

Ref.	Fuel	Medium	Redox	Test	SA diss. rate $\mu g \cdot m^{-2} \cdot d^{-1}$	Fract. diss. rate Day^{-1}	[U] $(mol \cdot L^{-1})$	Figure or table in this report
Loida et al., 2001	SNF	Brine pH 11	Anoxic	Static		1.7 – 2.4 $x10^{-4}$		Fig. 3-10
Loida et al., 2006	SNF	Cement water + Bure clay pH 13.02	Anoxic	Static		4.0 x 10^{-8}		Fig. 3-11
Cui et al., 2003a	UO_2	KOH and cement water (Lawrence solution	Anoxic	Static	Low, not quantified		10^{-6} – 10^{-7}	Fig. 3-12
Ollila et al., 2008	Depl. UO_2	NaCl/KOH pH 13	Sulphide, Fe(0)	Static	Low, not quantified		10^{-9}	Fig. 3-13
Cachoir et al. 2015	Depl. UO_2	YCWCa pH 13.5	Anoxic	Static	0.23 ± 0.21			Fig. 5-1
Cachoir et al. 2015	Depl. UO_2	YCWCa pH 13.5	Anoxic	Dynamic	0.10 ± 0.02		10^{-9}	Fig. 5-2
Cachoir et al., 2015	Depl. UO_2	ECW pH 12.5	Anoxic	Dynamic	1.0 ± 0.3 1.8 ± 0.9			Section 5.2
Cachoir et al., 2015	Depl. UO_2	OCW pH 11.5	Anoxic	Dynamic	2.3 ± 1.0			Section 5.2
Cachoir et al., 2015	Doped UO_2 Powder F1	YCWCa pH 13.5	Anoxic	Static	42 ± 12 45 ± 22			Fig. 5-3
Cachoir et al., 2015	Doped UO_2 Powder F1	ECW pH 12.5	Anoxic	Static	48 ± 8 54± 12			Tab. 5-1
Cachoir et al., 2015	Doped UO_2 Powder F1	OCW pH 11.5	Anoxic	Static	68 ± 15 79 ± 24			Tab. 5-1
Cachoir et al., 2015c	Doped UO_2 Powder F2	YCWCa pH 13.5	Anoxic	Static	(6.0 – 7.2) ± 10%			Section 5.3.2
Cachoir et al., 2015c	Doped UO_2 Powder F6	YCWCa pH 13.5	Anoxic	Static	0.28 ± 0.11			Fig. 5-4
Cachoir et al., 2015	Doped UO_2 Powder F1	YCWCa pH 13.5	Anoxic	Dynamic	12 ± 3		10^{-8}	Fig. 5-5
Cachoir et al., 2015	Doped UO_2 Powder F2	YCWCa pH 13.5	Anoxic	Dynamic	6.9 ± 0.6 1.9 ± 0.6 39 ± 10 18 ± 15		10^{-8} 10^{-7}	Fig. 5-6 Fig. 5-7
Cachoir et al., 2015	Doped UO_2 Powder F4	YCWCa pH 13.5	Anoxic	Dynamic	2.7 ± 0.6 1.5 ± 0.3		10^{-8}	Fig. 5-8
Cachoir et al., 2015c	Doped UO_2 Powder F6	YCWCa pH 13.5	Anoxic	Dynamic	0.16 ± 0.03		$<10^{-9}$	Fig. 5-9
Loida et al., 2009	SNF segment K11a	ECW pH12.5	Anoxic	Static	13 – 100	1 x 10^{-7}	2-3 x 10^{-9}	Fig. 5-10
Loida et al., 2012	SNF segment 2K11a(H_2)	ECW pH12.5	H_2	Static	2 – 13	~10^{-8}	2.1 x 10^{-10}	Fig. 5-11
Loida et al., 2012 Loida et al., 2011	SNF segment 2K11b(H_2)	YCWCa pH13.5	H_2	Static		Similar as for ECW (~10^{-8})	1.5 x 10^{-9}	Fig. 5-11
Gonzalez et al., 2014	SNF fragments	YCWCa pH13.5	H_2	Static		Low, not quantified	$<10^{-9}$	Fig. 5-12

6 Discussion

In this section we present a discussion of the effect of an OPC conditioned environment on the dissolution rate of spent fuel as compared to other conditions, based on the data available from the literature and the Belgian R&D programme, and see how the results can be used to estimate the long term dissolution rate of spent fuel in realistic conditions. The discussion is structured as follows :

- In Section 6.1, we select the most representative set of dissolution rates as a basis for the further discussion.
- In Section 6.2, we summarize the differences between the dissolution rates obtained in the three types of cement water that were investigated in the Belgian R&D programme.
- In Section 6.3, we compare the dissolution rates with the rates observed in other conditions.
- In Section 6.4, we focus on the threshold for oxidative dissolution in cement water.
- In Section 6.5, we discuss the artifacts due to the fact that the expected geological disposal conditions cannot be reproduced perfectly in laboratory conditions.
- In Section 6.6, we discuss the consequences of the observations for the long term evolution of the spent fuel.
- In Sections 6.7 to 6.12, we discuss some specific topics that are potentially relevant for the long term evolution in geological disposal conditions with an OPC conditioned environment, i.e. the minimum H_2 gas pressure required for the suppression of the fuel dissolution, the possible effect of colloid formation, the possible accelerated fuel dissolution due to secondary phase formation, the reducing capacity of cement water without H_2 gas, the potential effect of sorption of uranium on cement phases and metallic corrosion products, and the immobilization of released radionuclides in another form.

6.1 Selection of the most representative set of dissolution rates

In Section 5, a large set of dissolution rates determined in the Belgian R&D programme is given. In this Section 6.1, we select the most representative dissolution rates for comparison with rates obtained in other conditions. The selected rates should be representative for (α-doped) UO_2 or spent fuel at high pH and anoxic or reducing conditions. As most representative dissolution rates, we thus consider the rates from tests that were the least affected by oxidation by traces of atmospheric oxygen. This includes the tests with real spent fuel performed at KIT in autoclaves with H_2 gas (Section 5.5.2 and 5.5.3) and a selection of tests with α-doped UO_2. For the α-doped UO_2, the results from the dynamic tests were in most cases the most representative. From the available data set, minimum and maximum rates (R_{min} and R_{max}) are selected. The spread between these two can be considered as an indication of the total experimental uncertainty.

Table 6-1 summarizes the proposed rates R_{min} and R_{max}. In a topical report from 2015 (Cachoir et al., 2015a), these rates are called 'reference dissolution rates'. For all fuels, extra measurements would be useful to improve the rate estimation. As discussed further, these rates may still overestimate the dissolution rate of real spent fuel in geological disposal conditions.

Table 6-1: Reference dissolution rates proposed for the different Pu-doped UO_2 and depleted UO_2 in YCWCa

	Specific activity ($MBq \cdot g(UO_2)^{-1}$)	Simulated age (years)	R_{min} ($\mu g \cdot m^{-2} \cdot d^{-1}$)	R_{max} ($\mu g \cdot m^{-2} \cdot d^{-1}$)
F1	244	150	12 ± 3 (Figure 5-5)	79 ± 24 (Table 5-1)
F2	36	2.000	1.9 ± 0.6 (Figure 5-6)	39 ± 10 (Figure 5-7)
F4	17	11.000	1.5 ± 0.3 (Figure 5-8)	2.7 ± 0.6 (Figure 5-8)
F6	1.4	89.000	0.16 ± 0.03 (Figure 5-9)	0.16 ± 0.03 (Figure 5-9)
Depleted UO_2	0.01	$< 10^8$	0.10 ± 0.02 (Figure 5-2)	0.10 ± 0.02 (Figure 5-2)

The argumentation for the selection of values in Table 6.1 is as follows:

- For F1, the lowest rate was measured in the dynamic test, shown in Figure 5-5. This is taken as R_{min}. As R_{max}, we take the highest rate of Table 5-1, measured in static conditions in OCW, considering that the differences in regression rates between the three media are not significant.
- For F2, the lowest and highest rate measured with unfiltered leachates in the two dynamic tests are taken as R_{min} and R_{max} (see Figure 5-6 and Figure 5-7), knowing that the max rate of 39 $\mu g \cdot m^{-2} \cdot d^{-1}$ from the second experiment does not take into account the further decrease of the dissolution rate with time.
- For F4, the lowest and average rate measured in the dynamic test shown in Figure 5-8 are taken as R_{min} and R_{max}. The lowest rate was obtained for ultrafiltered samples, but because there were not many colloids in this test, it should not much underestimate the actual dissolution rate.
- For F6, the minimum and maximum rate are both derived from the dynamic test shown in Figure 5-9, resulting in a dissolution rate of 0.16 ± 0.03 $\mu g \cdot m^{-2} \cdot d^{-1}$, in which 0.03 $\mu g \cdot m^{-2} \cdot d^{-1}$ is the 95% confidence interval. A minimum estimation can be calculated as (0.16 - 0.03) $\mu g \cdot m^{-2} \cdot d^{-1}$, this 0.13 $\mu g \cdot m^{-2} \cdot d^{-1}$, and a maximum estimation as (0.16 + 0.03) $\mu g \cdot m^{-2} \cdot d^{-1}$, this is 0.19 $\mu g \cdot m^{-2} \cdot d^{-1}$. An alternative maximum is the rate measured in the static test of Figure 5-4, which is 0.28 ± 0.11 $\mu g \cdot m^{-2} \cdot d^{-1}$, but this high

dissolution rate is probably due to slow oxygen intrusion, unavoidable over such long test durations. The lower rate measured in the dynamic test is considered as more representative for anoxic conditions.

- For depleted UO_2, the minimum and maximum rate are both derived from the dynamic test shown in Figure 5-2, resulting in a dissolution rate of 0.10 ± 0.02 $\mu g \cdot m^{-2} \cdot d^{-1}$, in which 0.02 $\mu g \cdot m^{-2} \cdot d^{-1}$ is the 95% confidence interval. A minimum estimation can be calculated as (0.10 - 0.02) $\mu g \cdot m^{-2} \cdot d^{-1}$, this is 0.08 $\mu g \cdot m^{-2} \cdot d^{-1}$, and a maximum estimation as (0.10 + 0.02) $\mu g \cdot m^{-2} \cdot d^{-1}$, this is 0.12 $\mu g \cdot m^{-2} \cdot d^{-1}$. Like for F6, an alternative maximum is the rate measured in the static test, which is 0.23 ± 0.21 $\mu g \cdot m^{-2} \cdot d^{-1}$ (Figure 5-1), but the higher rate measured in the static test is probably due to slow oxygen intrusion. Hence, the lower rate of the dynamic test is considered as more representative for anoxic conditions.
- Because all reference dissolution rates in Table 6-1 were obtained with UO_2 powder for which the surface area may have been slightly overestimated, the rates may slightly underestimate the actual dissolution rate. For the few samples that were analysed, an underestimation by 20 – 40 % was estimated. This is the best estimation available of a possible bias related to the UO_2 surface area.

For ECW and OCW, the only experimental measurements available are the dynamic dissolution rates for depleted UO_2, which were 1 to 2 $\mu g \cdot m^{-2} \cdot d^{-1}$ (see Section 5.2). Because of the very short term of the experiments, these rates may overestimate the longer term rate, so they are probably rather maximum rate estimations. That is why they are not considered for the maximum rate. The doped fuels were not tested in ECW and OCW, so there are no direct rate measurements in these cement waters. The tests with depleted UO_2 and F1 showed little effect of the type of cement water. If this would be the case also for the doped fuels F2, F4 and F6, the rates measured with these fuels in YCWCa could be used as an approximation of the rates in ECW and OCW, but this needs experimental confirmation.

Figure 6.1 shows on a logarithmic scale the selected dissolution rates of the (Pu-doped) UO_2 in YCWCa as a function of the α-activity of the doped UO_2. The rate tends to increase with the increasing radiation field. The dissolution rate of the most active fuel F1 would be 100 – 1000 times higher than the dissolution rate of depleted UO_2 in the given test conditions.

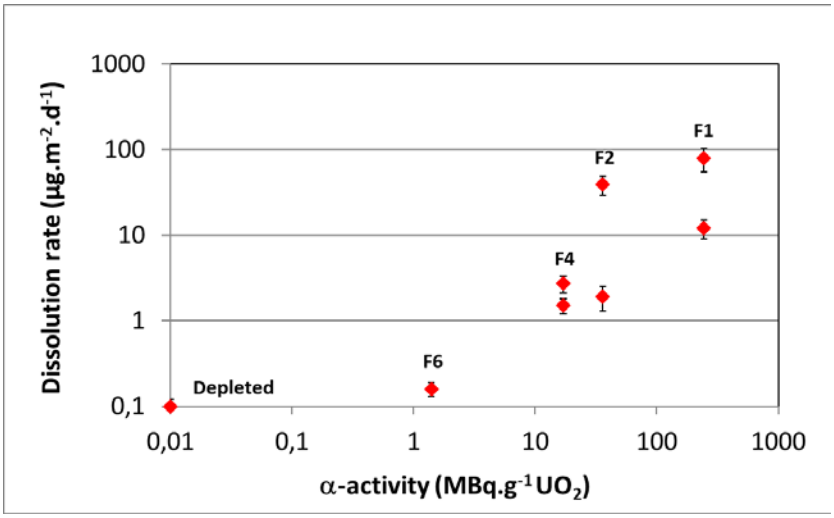

Figure 6-1: Dissolution rate as a function of the α-activity of (doped) UO_2 in YCWCa (pH 13.5)

The uranium concentrations in the dynamic tests were between 10^{-7} – 10^{-8} mol·L^{-1} for F1 and F2, about 10^{-8} mol·L^{-1} for F4, and around 10^{-9} mol·L^{-1} for F6 and depleted UO_2, indicating that the oxidative dissolution accelerates with increasing α-activity. The similar uranium concentration and dissolution rate of F6 and depleted UO_2 imply that F6 behaves almost the same as the depleted UO_2. For both types of UO_2, the dissolution is dominated by non-oxidative dissolution. The radiolytically driven oxidative dissolution rate is probably negligible, but there may be some continuous oxidation by traces of atmospheric oxygen.

6.2 Effect of the cement water composition on the dissolution rate

According to the reported dissolution rates, the composition and the pH of the cement water (young cement water, evolved cement water, or old cement water) have not much impact.

- The static tests with depleted UO_2 in cement waters (Section 5.1) showed similar rates for the three media.
- The dynamic tests with depleted UO_2 in the three cement waters (Section 5.2) showed similar dissolution rates. The dissolution rate was lower in the YCWCa than in the other media, but this may have been an artefact because the tests with evolved and old cement water were stopped much sooner.
- The static test with Pu-doped UO_2 F1 (Section 5.3) showed an apparently faster dissolution for OCW and ECW, but this difference was not significant, because of the data scatter.
- The static tests with real spent fuel (Section 5.5) in YCWCa and ECW with H_2 gas suggest a similar matrix dissolution rate (based on Sr release).

This does not mean that there is no impact of the water composition:

- The high Ca concentration in the ECW can lead to more colloid formation and precipitation (Section 6.8).
- Although the dissolution rate was similar within the experimental uncertainty in the three cement waters, the uranium concentrations in static tests with depleted UO_2 tend to be higher in YCWCa that in the other media (Cachoir et al, 2015c). The complexation of U(VI) with OH^- at pH 13, in agreement with the thermodynamically expected behaviour (Figure 3-5), might prevent the formation of a partly protective oxide layer, similar to the effect of dissolved carbonate. This may still have a dissolution accelerating effect in the presence of oxidants.

6.3 Comparison of dissolution rates within the Belgian R&D programme with other conditions

In this section, we compare successively the fractional and surface normalized dissolution rates measured within the Belgian R&D programme with the results obtained in the literature under different experimental conditions.

- **Comparison of fractional dissolution rates of spent fuel**

Figure 6-2, taken from publications by Loida (Loida et al., 2011; (Loida et al., 2012), shows the matrix dissolution rates of tests with real spent fuel in cement waters obtained within the Belgian R&D programme, together with the dissolution rates reported in literature for other media. The results for ECW are indicated by the red symbols. Data points for tests 'K11a' and 'K11b + Mt/Fe' present rates found in ECW without external H_2 gas, with or without magnetite and iron (Mt/Fe) (see Figure 5-10). Data points for '2K11a(H2)' present the rates found in Evolved Cement Water with external H_2 gas (see Figure 5-11). The other data points present rates from experiments in absence of H_2 overpressure in various waters, i.e. pure water, carbonate bearing granitic groundwater, saline solution or water from tufaceous formations) from Swedish (SKB), US-American (PNL), Canadian (AECL), and German (FZK-INE) projects.

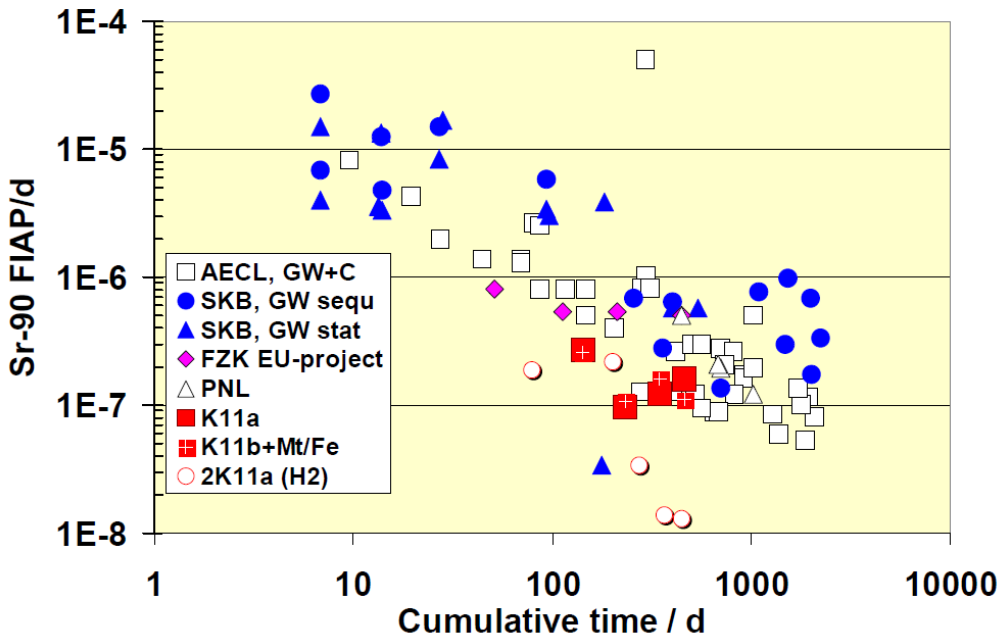

Figure 6-2: Matrix dissolution rates of spent nuclear fuel in terms of $FIAP_{Sr} \cdot day^{-1}$ as a function of time for tests reported in literature and in the Belgian R&D programme. Data points for K11a and K11b + Mt/Fe (= Magnetite/iron) present the rates found in ECW without external H_2 gas. Data points for 2K11a(H_2) present the rates found in ECW with external H_2 gas. The other data present rates from experiments in absence of H_2 overpressure in various waters. Figure taken from publications by Loida (Loida et al., 2011; Loida et al., 2012).

This graph shows that the dissolution rate in the ECW without H_2 (FIAP ~10^{-7} day^{-1}), is relatively low, compared to the dissolution rates in the other media, suggesting that the high pH is not unfavourable, and perhaps even favourable for the spent fuel stability. The exact reason for a possible favourable effect is not known, but it was suggested that the formation of a Ca rich precipitation layer or sorption of Ca^{2+} on the UO_2 surface may reduce the oxidative fuel dissolution (Loida et al., 2009b; Santos et al., 2006). The rates for the tests with H_2 gas are clearly lower, especially for the longer term data (~ 10^{-8} day^{-1}), corresponding to a H_2 pressure of 3.5 bars.

- **Comparison of surface normalized dissolution rates of spent fuel, depleted UO_2 and Pu-doped UO_2**

Figure 6-3 compares the dissolution rates of spent fuel, depleted UO_2 and Pu-doped UO_2 measured in cement waters for the Belgian R&D programme with the dissolution rates for other test conditions found in literature. The graph presents surface normalized dissolution rates for various types of depleted or UO_2 doped with α-emitters and spent fuel, as a function of the specific α-activity. The surface normalization of the spent fuel dissolution rates implies the estimation of the effective surface area, which has a relatively large uncertainty. The most relevant data points are shown in color. These are the rates measured with spent fuel in ECW (data from Figure 5-10 and Figure 5-11) and with depleted or doped UO_2 in YCWCa (data from Table 6-1). Also shown explicitly are rates in the range 0.3 – 3 $\mu g \cdot m^{-2} \cdot d^{-1}$ measured with depleted and doped UO_2 in anoxic and reducing conditions by Ollila et al. (the green diamonds in Figure 6-3) (Ollila et al., 2007), and the ranges 0.03 – 2.6 $\mu g \cdot m^{-2} \cdot d^{-1}$ and 0.02 – 5 $\mu g \cdot m^{-2} \cdot d^{-1}$ proposed in the MICADO project for the dissolution of (α-doped) UO_2 in reducing conditions and spent fuel in the presence of an overpressure of H_2 gas, respectively (Grambow et al., 2010). The other data, taken from a report from Cachoir (Cachoir et al., 2005) and originating from the European SFS project, represent data obtained at neutral pH under anoxic conditions (deaerated carbonated water, N_2 atmosphere, electrochemical tests) or oxidizing conditions. They correspond to the data that were shown already in Figure 3-3. The rates of VTT (Ollila et al., 2007) have been determined with an isotopic dilution method, assuming that there is a residual dissolution by exchange between uranium at the fuel surface and in the solution. With this method, dissolution rates are derived from constant U concentrations. There are methodological questions about this approach, but it nevertheless gives an estimation of the possible residual rate if this exchange mechanism would be relevant on the long term.

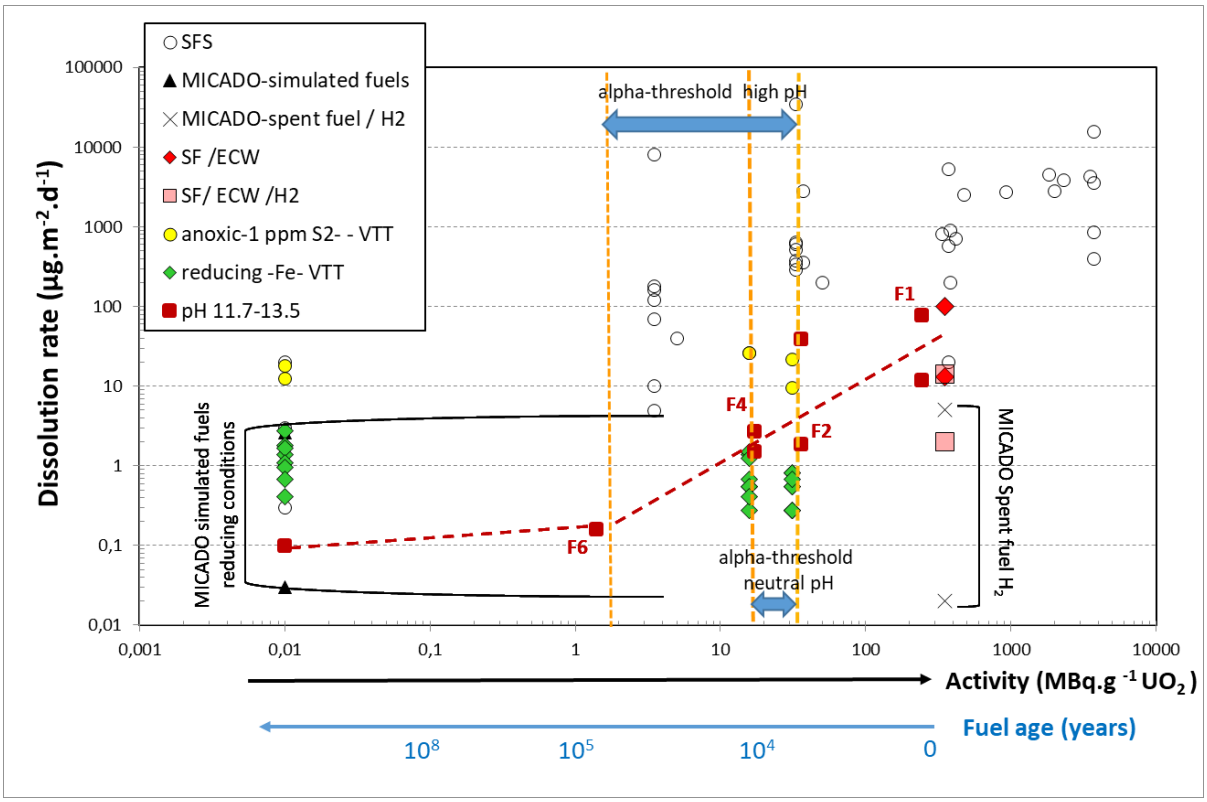

Figure 6-3: Fuel matrix dissolution rate as a function of specific α-activity, including data from literature and from the Belgian R&D programme. For the depleted UO_2 and for the Pu-doped UO_2 F2 and F4, and for the tests with spent fuel in cement waters, the range with the minimum and maximum rate estimation is shown (Cachoir et al., 2005; Loida et al., 2009a; Loida et al., 2011; Ollila et al., 2007; Cachoir et al., 2015a; Grambow et al., 2010). The tests in anoxic conditions at high pH showed that the α-threshold for radiolytic oxidative dissolution is situated between the activity of F6 and F4. In reducing conditions the threshold is expected to shift to higher specific fuel activities and might be as high as the activity of F2. With H_2 gas, it may even shift to the activity of fresh spent fuel (≥350 MBq·g^{-1}).

Figure 6.3 shows the following:

- The dissolution rate determined for depleted UO_2 (0.01 MBq·g^{-1}) in cement water is of the order of magnitude of 10^{-1} µg·m^{-2}·d^{-1}, and coincides well with the rates measured on undoped UO_2 at more neutral pH in reducing conditions (Ollila et al., 2007; Grambow et al., 2010). The dissolution rate for the Pu-doped UO_2 of type F6 (1.4 MBq·g^{-1}) falls in the same range.
- For doped UO_2 of type F4 (17 MBq·g^{-1}) and F2 (36 MBq·g^{-1}), the minimum rates in cement water are slightly higher than in the measurements of Ollila et al. with ^{233}U doped UO_2 (Ollila et al., 2007). This may be due to the fact that the conditions were more reducing in the tests by Ollila (Ollila et al., 2007), done with sulphide addition, whereas in the tests with F4 and F2, there was no reducing agent (the addition of iron did not effectively reduce the U concentrations in tests with depleted or Pu-doped UO_2 at high pH (Cachoir et al., 2015c)). The maximum rates measured in cement water are probably less representative, as they do not consider the further decrease with time in the experiments.

- For fuel F1, with an activity of 2.4 x 10^2 MBq·g^{-1} (simulating fuel of about 150 years), the minimum dissolution rate of 12 µg·m^{-2}·d^{-1} is an order of magnitude higher than the minimum for F2. The higher value of 79 µg·m^{-2}·d^{-1} may be biased because the F1 was tested in powder form. With pellets, the dissolution rate might have been lower.
- For spent fuel, the surface normalized dissolution rates in cement waters in Figure 6-3 have been calculated with the fractional dissolution rates reported for fuel segments by Loida (Loida et al., 2009a; Loida et al., 2011). For the tests with spent fuel, the effective specific surface area is not well known, though. We therefore indicate the range in which the normalized dissolution rate is expected to lie, using a low and a high estimation of the specific surface area of the fuel sample, i.e. respectively 10 cm^2·g^{-1} and 80 cm^2·g^{-1} (see Section 7). This is similar to the specific surface area used to calculate the dissolution rates of spent fuel in the MICADO project (Grambow et al., 2011). The resulting rates are indicated in Table 6-2.

Table 6-2: Fractional and surface normalized matrix dissolution rate of spent fuel in ECW and in ECW with H_2 overpressure as a function of specific surface area SA (Loida et al., 2009; Loida et al., 2011), and comparison with ranges proposed in MICADO (Grambow et al., 2010)

	Fractional rate (day^{-1})	Surface normalized rate (µg·m^{-2}·d^{-1})		
		Low SA 10 cm^2·g^{-1}	High SA 80 cm^2·g^{-1}	MICADO
ECW	1 x 10^{-7}	100	13	(0.03 – 2.6) (UO_2, reducing)
ECW + H_2	1.3 x 10^{-8}	13	2	0.02 – 5 (Spent fuel, H_2)

We thus find a surface normalized dissolution rate between 13 and 100 µg·m^{-2}·d^{-1} in ECW without imposed hydrogen gas, and a rate between 2 and 13 µg·m^{-2}·d^{-1} in ECW with 3.2 bar of imposed hydrogen gas pressure. This is relatively high compared to the ranges proposed in the MICADO project, which were 0.02 – 5 µg·m^{-2}·d^{-1} for spent fuel in the presence of H_2 gas for a specific surface area of respectively 71 and 10 cm^2·g^{-1}. With doped UO_2 (activity up to 314 MBq·g^{-1}) in reducing conditions (Fe metal, but without addition of H_2 gas) a range of 0.03 – 2.6 µg·m^{-2}·d^{-1} was proposed in MICADO (Grambow et al., 2011). The much higher dissolution rate with spent fuel in ECW can be ascribed to the higher activity of the spent fuel and the fact that the conditions were less reducing.

For the tests with spent fuel without H_2 gas, the relatively low *surface normalized dissolution rate* in ECW compared to the data from SFS, confirm the data of Figure 6-2, showing that the *fractional dissolution rate* was lower in ECW than in most other tests found in literature. In ECW, the formation of a precipitate on the fuel surface probably reduces the effective exposed surface area (Loida et al., 2009a; Loida et al., 2009b). So, as an overall indicator of the fuel stability, the fractional dissolution rate may be a better indicator. In the presence of H_2 gas, the surface normalized dissolution rate seems relatively high compared to the MICADO range. It

was suggested that the relatively high dissolution rate of fuel segments in the ECW with H_2 gas may be an artifact, due to the continued leaching of Sr from the gap between the cladding and the fuel pellet. The low concentration of redox-sensitive radionuclides in all tests with H_2 gas still suggest that there must have been very little oxidative dissolution. The relatively high dissolution rate in ECW with H_2 gas in Figure 6-3 may thus overestimate the long-term matrix dissolution rate.

6.4 Threshold for oxidative dissolution in cement water

Figure 6-3 further shows that the fuel dissolution rate tends to increase with increasing specific α-activity in cement waters, confirming the trend observed also in other media. The highest dissolution rate is observed for spent fuel without H_2 gas, with a rate in the range 13 to 100 $\mu g \cdot m^{-2} \cdot d^{-1}$. This young spent fuel has a high α-activity (~350 $MBq \cdot g^{-1}$ after 10 years), but also a high β-γ activity. For fuel F1, with lower α-activity (~244 $MBq \cdot g^{-1}$, and little β-γ activity, the minimum dissolution rate of 12 $\mu g \cdot m^{-2} \cdot d^{-1}$ would be slightly lower. For the less active types of UO_2, the estimated dissolution rate decreases further with decreasing activity, but for F6 (1.4 $MBq \cdot g^{-1}$) the dissolution rate is close to the rate for depleted UO_2 (0.01 $MBq \cdot g^{-1}$).

This suggests that for α-doped UO_2 in cement water conditions without H_2 overpressure the threshold α-activity under which the fuel dissolution rate does not further decrease, is situated between 17 $MBq \cdot g^{-1}$ (for F4) and 1.4 $MBq \cdot g^{-1}$ (for F6), corresponding to fuel ages of 11,000 to 89,000 years, respectively. For the tests at more neutral pH, this threshold would be situated between 18 and 33 $MBq \cdot g^{-1}$ (Muzeau et al., 2009). The exact threshold activity depends, however, on the reducing capacity of the medium rather than on the pH. The weak reducing capacity in the tests with F4 may explain why it dissolves relatively fast compared to the doped UO_2 tested by VTT (Ollila et al., 2007).

Below the α-threshold, the dissolution is assumed to be controlled by solubility, but the corresponding U concentration depends on the test conditions. The concentration level is lower in reducing conditions than in anoxic conditions. The uranium concentrations in the dynamic tests with F6 were lower than 10^{-9} $mol \cdot L^{-1}$, confirming that there is indeed very little uranium oxidation, and that we have predominantly non-oxidative dissolution, which should be solubility controlled. The tests with depleted UO_2 reported by Cachoir (Cachoir et al., 2015a; Cachoir et al., 2015b; Cachoir et al., 2015c) but also by Ollila (Ollila et al., 2008) thus give sufficient evidence to assume that we will have solubility control also at high pH when the fuel activity is low enough.

The threshold α-activity can be assumed to shift to higher activities when the conditions are more reducing. Tests with F4 in cement water with an effective reducing agent (e.g. dithionite) might decrease the radiolytic fuel oxidation and shift the threshold to the activity of F2, as in neutral pH conditions. To have a lasting effect, there should be a continuous supply with reducing species, though. The most important reducing species in a geological disposal environment with concrete and steel should be H_2 gas. The tests with spent fuel performed in the Belgian R&D programme show that H_2 is an effective reducing agent for spent fuel, also in cement water. In the presence of H_2, the uranium concentrations are so low that we can conclude that the threshold for oxidative dissolution is reached already with young spent fuel, a few tens of years after the end of the irradiation.

A test with F2 together with H_2 gas did not show a H_2 effect, for the reasons mentioned in Section 5.3.2.

6.5 Experimental artifacts resulting in dissolution rate overestimation under laboratory conditions

The dissolution rates reported in the previous sections can constitute a scientific basis to estimate the dissolution rate of real spent fuel in real disposal conditions. Although the laboratory tests are performed in conditions that approach as much as possible the expected long-term geological repository conditions for the most critical parameters, the dissolution rates measured in laboratory conditions are likely to be higher than the expected dissolution rates under the foreseen conditions. There are (1) general inevitable causes of rate overestimation, and (2) specific causes for rate overestimation related to the use of dynamic test cells. On the other hand, the dissolution rate may be underestimated due to fuel conversion (3). The possible under- or overestimation of the dissolution rate because of an over- or underestimation of the surface area was discussed already in Section 4.2.3.

(1) General causes of dissolution rate overestimation

There are several reasons for the systematic overestimation of the dissolution rate in tests with simulated fuels under laboratory conditions (Werme et al., 2004):

- The oxidative dissolution of UO_2 is very sensitive to traces of oxygen. Although the experiments are performed in conditions that minimize contamination with atmospheric O_2, the remaining oxygen traces will always cause some fuel oxidation. This causes an artificial increase of the dissolution rate, which is not expected under the foreseen repository conditions, where all traces of atmospheric oxygen will be consumed in the first years after the closure of the galleries.
- All experiments are necessarily performed with fresh spent fuel or simulated fuels, because real old fuel is not available. An important difference between the real fuel and the simulated fuels, is the fact that the real fuel contains within its UO_2 matrix also radionuclides from decay, fission and activation. There is evidence that the presence of these radionuclides decrease the dissolution rate of the UO_2. Indeed, as mentioned by SKB (SKB, 2010, p. 91), the increase of the concentration of fission products and actinides in the UO_2 matrix seems to compensate successfully for the increased radiation field (and surface area) of higher burnup fuel. Hence, the dissolution rate of simulated fuels probably overestimates the dissolution rate of a real spent fuel with a similar activity.
- The tested UO_2 particles, prepared by crushing of pellets, have fractured surfaces with high energy sites that will dissolve at a higher rate. Based on analogy with CeO_2, one could expect an increase of the dissolution rate with decreasing particle size for not-annealed UO_2. Annealing should decrease the number of high energy sites by removing the sharp edges (Corkhill et al., 2016).
- The specific geometry of the tested (Pu-doped) UO_2 samples powder may have an effect on the dissolution rate, because it can affect the concentration of radiolytical

products close to the UO_2 surface. Higher local concentrations of these radiolytical products might exist with UO_2 powder than with UO_2 pellets, because of the higher local SA/V with powder. This may have in influence on the surface normalized dissolution rate of UO_2 powder, compared to UO_2 pellets.

(2) Dissolution rate overestimation in dynamic leach cells

The UO_2 dissolution rates determined in dynamic leach cells within the Belgian R&D programme were not measured as intrinsic rates far from U(IV) saturation, but as steady state dissolution rates corresponding to the tested flow rates, which have to be compared with the flow rate under geological disposal conditions (Cachoir et al., 2015a; Cachoir et al., 2015b; Cachoir et al., 2015c). The dynamic leach cells with which most rates on (Pu-doped) UO_2 were measured, consist of narrow columns filled with a small amount of UO_2 powder, through which water is pumped (Figure 4-2). This specific set-up also has effects that tend to increase the dissolution rate, compared to the geometry under geological disposal conditions. This is valid both for the non-oxidative and the oxidative dissolution.

- Effect on non-oxidative dissolution: The non-oxidative dissolution rate from dynamic tests is increased by the continuous flow with water undersaturated with U(IV). The dissolution rate of 0.1 $\mu g \cdot m^{-2} \cdot d^{-1}$ measured with depleted UO_2, where there is no radiolytic fuel oxidation, is the result of a combination of this water flow and oxidation by traces of atmospheric oxygen. Under the expected repository conditions, the flow rate should be much smaller, and U(IV) saturation will be reached immediately. This should stop (or lower) the further non-oxidative dissolution. The dissolution rate of 0.1 $\mu g \cdot m^{-2} \cdot d^{-1}$ measured with depleted UO_2 can be used to estimate the increase of the dissolution rate due to the water flow for an old fuel like F6. For the more active fuels, with an oxidative dissolution rate that is an order of magnitude higher, the net effect of the water flow on the non-oxidative dissolution should be relatively small.
- Effect on oxidative dissolution: The water flow causes a removal of radiolytically generated H_2O_2 from the UO_2 surface where the H_2O_2 molecule was formed, but at the same time, the water flow brings this H_2O_2 molecule closer to the surface of the neighbouring UO_2 particles where it can react before it dissociates. To estimate the effect on the reaction efficiency of H_2O_2 with the UO_2 surface, specific studies should be done.

(3) Dissolution rate underestimation due to fuel conversion

The dissolution rates determined experimentally with depleted or low-activity UO_2 do not consider the possibility that the fuel may continue to release fission products, actinides and decay products even when the UOX surface is in dynamic equilibrium with the solution, saturated with U(IV), as a result of continued oxidative dissolution, followed by reduction and precipitation of the dissolved uranium species. This is the so called *fuel conversion* mentioned already in Section 3.1.1. Isotopic dilution tests suggested a possible conversion mechanism with a release rate between 0.05 and 2.6 $\mu g \cdot m^{-2} \cdot d^{-1}$ under reducing conditions and constant U concentrations (Ollilla et al., 2008; Grambow et al., 2010). However, these values must be considered as maximum values, considering that ongoing isotopic exchange considers only the outermost surface of the UO_2 and it is doubtful that isotopic exchange will continue for all atomic layers beneath the surface.

So, there are causes for over- and underestimation of the experimental UO_2 or spent fuel dissolution rate as an estimator of the dissolution rate under the expected geological repository conditions. The net effect is difficult to assess. However, natural analogues suggest that optimistic lifetimes of several millions of years may still underestimate the real fuel life time. For instance, the natural uraninites of Cigar Lake have an estimated age of 1.3×10^9 years (Section 3.4). This suggests that the dissolution rates measured in laboratory conditions probably overestimate the rate under the expected geological repository conditions.

Remark:
Experiments performed in the Belgian R&D programme after 2015, not included in this report, have confirmed the high sensitivity of UO_2 for oxidation by traces of atmospheric oxygen, especially at high pH. To avoid this, tests were done with reducing agents. Under certain conditions, these were indeed able to keep the U concentrations in the solubility range of U(IV), resulting in low dissolution rates.

6.6 Consequences for the long term evolution of the spent fuel

The measurements reported in the previous sections imply that the radiolytic oxidative matrix dissolution rate of α-doped UO_2 in absence of H_2 gas will decrease with time as a result of the decreasing specific α-activity, until the threshold activity is reached where the oxidative dissolution becomes negligible. In absence of other oxidants like airborne O_2, the further dissolution of the UO_2 will be only non-oxidative. Any further dissolution should be driven by processes that counteract the saturation of the solution with U(IV). This might be diffusion, convection, sorption, or secondary phase formation, but with the available knowledge, the dissolution rate should be much smaller than in the first, oxidative dissolution stage. The experiments with spent fuel and H_2 gas have given qualitative indications that H_2 gas has a similar favourable effect on the fuel stability in cement water as in pH neutral waters, leading to a very slow matrix dissolution. In other words, in the presence of H_2 gas, the threshold for radiolytic oxidation is reached already for young fuel. This fits also with the findings of Muzeau (Muzeau et al., 2009) with Pu-doped UO_2 (simulated age of 50 years and an activity of 365 $MBq.g^{-1}$), for which the dissolution was suppressed by 1 bar H_2, implying that the threshold activity would be higher than 365 $MBq \cdot g^{-1}$ (for today's fuel, the activity is in the range 100 – 1000 $MBq \cdot g^{-1}$, see Figure 3-2). The effect of H_2 gas on simulated fuel with a remaining α-activity but no β,γ-activity was tested at SCK•CEN with α-doped UO_2 F2 in YCWCa. These tests did not show a measurable suppressing effect of the H_2, though, perhaps because the UO_2 was added as a powder without epsilon particles (see Section 5.3.2).

The experimental program has given quantitative indications of the matrix dissolution rate that we can expect for real spent fuel in geological disposal conditions, but also made clear that the evolution of the matrix dissolution rate will depend on critical environmental parameters.

A major parameter is the H_2 concentration in the near-field. If this is high enough, a very low dissolution rate can be expected. A precise quantification of this very low matrix dissolution rate at high pH is not evident, though, because the first series of experiments with H_2 using clad fuel segments probably overestimates the dissolution rate (because of retarded Sr release from the gap between fuel and cladding, see Section 5.5.2), while in the next test series with

fuel fragments and H_2 gas, the variation of the Sr-release between the test containers was too large to determine a precise release rate (see Section 5.5.3). Because of the effective reducing conditions, the matrix dissolution rated is nevertheless assumed to be very low. Moreover, for extrapolation to long-term conditions, one should consider that the decrease of the β,γ activity will probably lead to a further decrease of the dissolution rate.

The effect of the decreasing activity can be estimated by model calculations that take into account the fuel activity for a given H_2 concentration. Calculations with such a model (Spahiu et al., 2001) suggest that the dissolution rate decreases by a factor 10 when the dose rate decreases by a factor 100 (Figure 6-4). This model included the effects of α and β radiation. The base case in these calculations is the dose rate of a young fuel (385 $Gy \cdot h^{-1}$). This implies that the long term rates would be at least 10 times lower than the rates that we measure on the spent fuels that are available today.

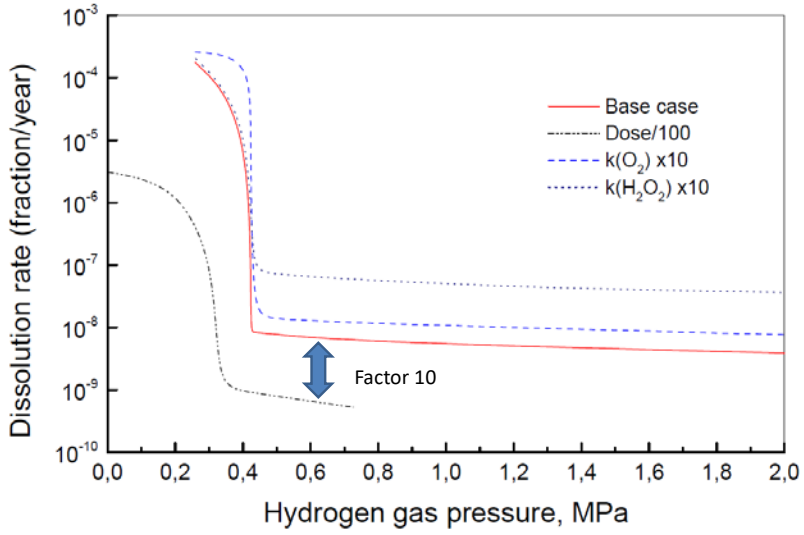

Figure 6-4: Dissolution rate calculated by modeling as a function of hydrogen gas pressure at constant dose rate for the base case, a 100 times lower dose rate, a 10 times higher reaction rate between oxygen molecules and uranium dioxide, and a 10 times higher reaction rate between hydrogen peroxide and uranium dioxide (Spahiu et al., 2001)

Pu-doped UO_2 with a simulated age of 1500 years dissolved at 6 $mg \cdot m^{-2} \cdot d^{-1}$ in γ-irradiated water with applied hydrogen gas pressure (Jégou et al., 2005), but at 0.2 $mg \cdot m^{-2} \cdot d^{-1}$ in deaerated water without γ radiation and without hydrogen gas (Jégou et al., 2004a). So the γ radiation accelerated the fuel dissolution by a factor 30, in spite of the presence of H_2 gas. Conversely, we can thus expect that the dissolution rate will decrease at least with a factor 30 after decay of the γ-emitters.

In the case of a complete suppression of the oxidative dissolution by the H_2 effect, the fuel will dissolve further by non-oxidative dissolution, controlled by the solubility of the UO_2, coupled to diffusion of U(IV) towards the far field. This would result in constantly decreasing dissolution rate, far below the detection limits of experimental measurements, but compatible with the long life time of natural analogues.

There may be a critical H_2 concentration below which the oxidation suppression effect is not strong enough anymore to stop the dissolution of young fuel. This minimum H_2 gas pressure is discussed more in detail in Section 6.7.

If the threshold would not be reached because the H_2 concentration is too low, higher matrix dissolution rates can be expected. In the complete absence of H_2 and with young spent fuel, this would lead to a high dissolution rate, as shown by the experiment with spent fuel in ECW without H_2 (Section 5.5.1 and Table 6-2). Because of the decreasing activity, the dissolution rate would also decrease further, as shown by the data in Figure 6-3. The rate range obtained with Pu-doped UO_2 in cement water (Table 6.1) gives an indication of the dissolution rate for old spent fuel in such conditions, but for the reasons given in Section 6.5, these rates may overestimate the dissolution rate of spent fuel in geological disposal conditions. At a given time, the threshold for radiolytic oxidative dissolution would still be reached. As shown in Figure 6-3, this threshold might be situated around an activity of 1.4 $MBq \cdot g^{-1}$, which would be lower than in other media, but on the other hand, the corresponding dissolution rate would also be lower than in other media. Once the threshold has been reached, the dissolution rates measured with depleted UO_2 are indicative for the dissolution rate of spent fuel.

The presence of metallic iron in the system at high pH without sufficient H_2 accumulation could also counteract the oxidative dissolution, but there is not much data to support this quantitatively. A stabilizing effect has been observed for UO_2 with a low activity (see Figure 3-13), but for more active UO_2, the reducing effect of metallic iron may be too small at high pH. This is discussed in more detail in Section 6.10.

All these rates were obtained at room temperature. Much less data are available for the dissolution rate of spent fuel in cement water at high temperature (see Section 3.2.6), but the available data suggests that a moderate temperature increase has not much effect in reducing conditions.

Most reference dissolution rates mentioned in Section 6.1, and that can be used to estimate the evolution of the dissolution rate of real spent fuel in disposal conditions, are surface normalized dissolution rates, expressed in $\mu g \cdot m^{-2} \cdot d^{-1}$. The application of these rates to real fuel requires the knowledge of the effective specific surface area of the spent fuel. This is discussed in Section 9 of this report. The combination of surface normalized dissolution rates that may already overestimate the *in situ* dissolution rate with conservative estimations of the specific surface area can lead to an important underestimation of the time required for the complete dissolution of a spent fuel pellet, considering the very high stability of natural analogues (Section 3.4).

6.7 Minimum H_2 gas pressure required for suppression of the fuel dissolution by radiolytic oxidation in cement water

In Section 3.3.2, we have given an overview of the dissolution rates measured with spent fuel in the presence of H_2 gas, from experiments reported in literature. We concluded that H_2 concentrations lower than 0.8 – 2.5 mmol·L^{-1} should still be effective.

The tests with spent fuel in ECW with H_2 gas (Loida et al., 2012; Loida et al., 2011) suggest that a lower H_2 concentration has less effect on the fuel dissolution than a higher H_2 concentration (Figure 5-11). This raises the question about the minimum H_2 pressure required for suppression of the oxidative fuel dissolution at high pH.

The tests with spent fuel in ECW with H_2 gas overpressure were performed with a H_2 pressure applied in 3 steps, from 0 bar over 1 bar to 3.2 bar (Loida et al., 2011). The evolution of the fuel dissolution rate with H_2, based on Sr in solution, is shown in Figure 6-5 (sample 2K11a ECW), including also the rate in ECW without external H_2 pressure (sample K11a ECW) and in distilled water (DIW). This graph collects data that were shown also in Figure 5-10 and Figure 5-11.

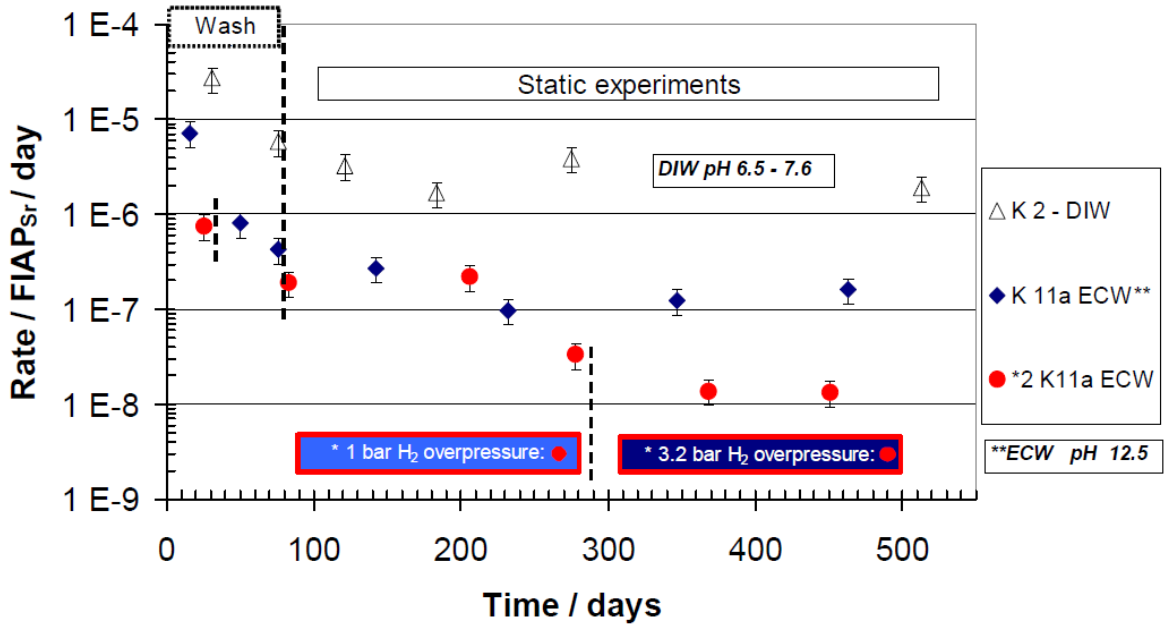

Figure 6-5: Matrix dissolution rates of spent nuclear fuel derived from Sr release ($FIAP_{Sr}$ · day^{-1}) in ECW with H_2 overpressure (2 K11a ECW), without H_2 overpressure (K11a ECW) and in distilled water (K2 – DIW) (Loida et al., 2011)

With 1 bar H_2 (0.8 mmol·L^{-1} H_2), the FIAP fractional dissolution rate decreased to 3.4 x 10^{-8} day^{-1}, but only gradually. With 3.2 bar H_2 (2.5 mmol·L^{-1}), the dissolution rate decreased further to about 1.4 x 10^{-8} day^{-1}. This suggests that 1 bar of H_2 had less effect than 3.2 bar, but the decrease of the rate with time suggests that the rate might have decreased further also with 1 bar of H_2 for longer test durations. Without H_2 gas (sample K11aECW), the long term dissolution rate was slightly higher than 10^{-7} day^{-1}. The pressure of 3.2 bar H_2 thus reduced the dissolution rate by a factor of 10, compared to ECW without H_2.

The concentration of redox sensitive species (Tc, Np, Pu and U) was similarly low at 1 bar and 3.2 bar. Final concentrations in ECW were $<5 \times 10^{-10}$ mol·L^{-1} for Tc and Pu and 2.1×10^{-10} mol·L^{-1} for U . Final concentrations in YCWCa were $<1 \times 10^{-10}$ mol·L^{-1} for Tc and Pu and 1.5×10^{-9} mol·L^{-1} for U. This suggests that the concentration of oxidants was not higher with 1 bar than with 3.2 bar, and that we thus can expect a similar fuel behaviour (and similar dissolution rate). In the ECW without H_2 gas, U concentrations were 10 times higher ($2 – 3 \times 10^{-9}$ mol·L^{-1}), so the addition of H_2 gas had a clear effect on the concentrations (Loida et al., 2009a).

So, in cement water, a H_2 concentration of 2.5 mmol·L^{-1} had a clear effect on the measured fuel dissolution rate, while a lower concentration of 0.8 mmol·L^{-1} had less effect on the dissolution rate, but a clear effect on the concentration of redox sensitive species. This confirms the trends mentioned in literature for other media, confirming a clear hydrogen effect for concentrations in the range 0.8 – 2.5 mmol·L^{-1} that was tested also in cement water. Unfortunately, the effect on the Sr-release in the evolved cement water was difficult to quantify, either due to possible Sr-release from the gap, or due to sorption on the autoclave.

The tests and calculations for other media suggest that even H_2 concentrations lower than 0.8 mmol·L^{-1} should still be effective. To verify this, experiments with lower H_2 pressure in highly alkaline conditions are necessary.

On the long term, the activity of the fuel will decrease with time. This might imply that for older fuel, less H_2 gas is sufficient to suppress the oxidative dissolution. Calculations with a radiolytic model (Spahiu et al., 2001) can be used to estimate this effect (see Section 6.6).

6.8 Possible effects of colloid formation in cement water

Tests with UO_2 in cement waters (Cachoir et al., 2015c) showed considerable colloid formation with U(VI) under certain conditions, but this is not expected with the real spent fuel for the following reasons:

- The colloids were observed only when the tests were done in conditions favouring the presence of U(VI). They were observed more specifically in tests with UO_2 powder, having a large surface area favouring oxidation by traces of oxygen, and even more with Pu-doped UO_2 powder, favouring radiolytic oxidation. In conditions where the U(VI) formation or concentration was lower, the amount of colloids was much lower. Few colloids were thus observed in tests with depleted UO_2 pellets (low surface area, no radiolytic oxidation) and in dynamic tests (where the U(VI) concentration was kept low by constant dilution). Because the solubility limit of potential U(VI) secondary phases with Ca, K or Na is exceeded, the observed colloids may be interpreted as secondary phase formation, although this is still a hypothesis that needs further confirmation.
- In tests with depleted UO_2 pellets (instead of powder), there were no colloids, except in the Evolved Cement water, which seems to be unstable because of the high Ca concentration. Also in the tests with real spent fuel, colloids were not observed. This fuel is broken in fragments of mostly millimeter size, with a surface area that is much smaller than for the fine UO_2 powders used in the experiments with Pu-doped UO_2 powders. Moreover, the precipitation of secondary Ca-containing phases on the fuel

surface further reduces the effective surface area (Loida et al., 2009a). Under the expected geological disposal conditions, the spent fuel will have a similar relatively low surface area. For this reason, the colloid formation with U(VI) observed in tests with a high UO_2 surface area is considered as an artefact, and is not expected to occur upon geological disposal.

It is nevertheless important to better understand the conditions under which colloids can be formed, to support the hypothesis that they will not be formed in situ. This topic needs to be investigated further.

6.9 Possible accelerated fuel dissolution due to secondary phase formation in anoxic or reducing highly alkaline conditions

Formation of clearly identifiable secondary uranium (IV) phases from UO_2 has not yet been observed for the tests performed in anoxic or reducing (with H_2) highly alkaline conditions within the Belgian R&D programme. Formation of such phases is not expected to accelerate the fuel dissolution. Secondary uranium (VI) phases may be formed (e.g. as colloids), but are also not expected to accelerate the fuel dissolution rate.

- *U(IV) phases*

In tests with realistic cement waters (maximum 0.5 $g \cdot L^{-1}$ of Ca), there is so far no indication for secondary uranium (IV) phase formation, but because the secondary phase formation is a very slow process, one should also look at natural analogues. Calcium incorporation has been observed in many natural uraninite samples (Duro et al., 2010, p. 63), and can lead to secondary uraninite formation.

Precipitated layers were found in the tests with spent fuel in ECW (pH 12.5), but these were not identified as U phases (Loida et al., 2009a).

Coffinite is frequently observed as a uraninite alteration product in nature, but is formed only in reducing conditions at relatively high temperature (>80 °C) and at sufficiently high Si concentrations of more than 10^{-3} – $10^{-3.5}$ $mol \cdot L^{-1}$ (Duro et al., 2010), this is equivalent to ~10 – 30 $mg \cdot L^{-1}$ or more. In the conditions tested so far in the Belgian R&D programme, coffinite formation is unlikely, because neither of these conditions are met:

- The temperature was much lower than 80 °C;
- The Si concentration in the cement waters was around 2.0 x 10^{-4} $mol \cdot L^{-1}$ (5.5 $mg \cdot L^{-1}$) see Table 4.2). There was no other source of Si in the experiments.

The presence of hardened OPC-based concrete should not favour the formation of coffinite, because the Si concentrations in the cement pore water are kept low by equilibrium with calcium-silicate-hydrate (C-S-H) phases. The equilibrium with C-S-H phases in concrete gives theoretical Si concentrations of 1.4 – 8.4 $mg \cdot L^{-1}$ (Wang, 2009). Therefore, the probability for coffinite formation seems to be small in the expected geological disposal conditions, also in the presence of cement phases.

If secondary U(IV) phases would be formed on the long term, it is apparently a very slow process, which should not lead to a significant increase of the fuel alteration rate, but it can be a relevant long term alteration mechanism.

- *U(VI) phases*

Although colloids with U(VI) were observed in some tests (see Section 6.8), the transformation of U(IV) into U(VI) at high pH is not expected if the conditions are sufficiently reducing. It is thus unlikely that the precipitation of secondary U(VI) phases can be a long term driving force for fuel dissolution under highly alkaline geological disposal conditions.

- In the radiolytic dissolution of uranium from the fuel, the oxidation is the rate determining step. The rate of dissolution of the U(VI) plays only a minor role. There are no indications that reprecipitation of U(VI) as a secondary phase would increase the overall dissolution rate.
- As mentioned in Section 3.2.9, secondary phases with U(VI) at high pH are reported only in tests where the U is in the U(VI) valence from the start. Starting from UO_2, the oxidation of U(IV) to U(VI) requires the continuous availability of oxidizing species. In the experiments performed in highly alkaline anoxic or reducing conditions, the concentration of airborne O_2 was at trace level. Under the expected geological disposal conditions, the airborne O_2 concentration should be negligible. After the irreversible consumption of the traces of oxidants, the redox potential should decrease further to the domain where U(IV) is stable. Radiolysis might provide oxidants as long as the threshold for oxidative dissolution is not reached. Afterwards, fuel oxidation should be negligible. The period during which secondary U(VI) phases can be formed, thus depends on the threshold activity for oxidative dissolution. In the presence of hydrogen gas, this threshold activity will be reached soon.

6.10 Reducing capacity of the cement water without H_2 gas

With metallic iron or Fe(II) species as reducing agent instead of hydrogen gas, the threshold for oxidative dissolution may be lower in high pH cement water than in pore or ground waters at neutral pH. This would imply that in cement water without H_2 gas, the oxidative dissolution continues longer, because it would take longer to reach the activity level where the oxidative dissolution stops.

The redox conditions in cement waters appear to be only weakly reducing, even in the presence of metallic iron or Fe(II) species. According to thermodynamic data, the solubility of Fe(II) species in solution in equilibrium with $Fe(OH)_2$ is in the range to 10^{-7} mol·L^{-1} to 10^{-5} mol·L^{-1} between pH 11 and 13. At neutral pH (around pH 8), the solubility is 10^{-3} mol.L^{-1} (Pourbaix, 1974). So, the Fe(II) concentrations are expected to be lower in cementitious conditions than at neutral pH. Measurements in cement paste show maximum dissolved Fe concentrations of about 10^{-7} mol·L^{-1} (Wersin et al., 2004). This means that the concentration of reducing Fe species is small. Moreover, because of the passivation layer on the steel surface at high pH, we can expect that the underlying metallic Fe(0) layer will be a less effective reductor than at neutral pH. These theoretical arguments are supported by the experimental evidence that the

addition of metallic iron in tests with UO_2 in cement water did not consistently decrease the U concentration in tests with UO_2, whereas a clear decrease is observed in clay water at neutral pH (Cachoir et al., 2015c). The ratio of U(IV)/U(VI) in solution was nevertheless relatively high in the cement waters. This suggests that the medium is still relatively reducing or at least not oxidizing. In the tests with spent fuel in ECW (Section 5.5.1), the addition of an iron chip did not significantly decrease further the U concentration (2 x 10^{-9} mol·L^{-1} with iron, 3x10^{-9} mol·L^{-1} without iron), but the Tc concentration was clearly lower with Fe, suggesting that the Fe still had a reducing activity (Loida et al., 2009a). Tests with UO_2 and Fe strips performed by Ollila (Olllila et al., 2008) showed a reducing capacity of the Fe comparable to sulphide up to pH 12. At pH 13 varying results were obtained for duplicate tests (Figure 3-13). It is anyway expected that metallic iron will consume oxidizing species, even at high pH. The large amount of iron in the near-field materials (from the structural assembly components, canister, insert and overpack) should therefore help to reduce fuel oxidation as long as metallic iron is present.

6.11 Effects of sorption of uranium on cement phases and metallic corrosion products in anoxic or reducing highly alkaline conditions

As discussed in Section 3.2.8, solids like the C-S-H phases in the concrete and the magnetite that would be formed by corrosion of steel near-field components have a certain sorption capacity for uranium (IV) or uranium (VI), but – given the low U concentrations expected in solution - it would take a large amount of solid to have a significant effect on the UO_2 dissolution. In the Belgian R&D programme, the possible effects of such sorption for the UO_2 or spent fuel dissolution was not studied, so it did not provide experimental data that could confirm the expected absence of a significant effect. A calculation was, however, performed with the distribution ratios given in the literature and realistic masses of concrete or magnetite (Lemmens et al., 2011). This calculation confirmed that the sorption of uranium on near-field materials would indeed involve only a very small fraction of the total amount of uranium in the fuel. The sorption of U(IV) may nevertheless be a mechanism for slow non-oxidative long-term fuel dissolution.

In real disposal conditions, the iron dissolving from the steel will interact with the concrete. The influence of the steel corrosion on the sorption characteristics of the concrete is not known. Due to the elevated temperature in the concrete in the thermal stage (50 – 100 °C), the cement phases may evolve. This may affect the sorption of uranium. Also this effect was not evaluated, but much higher distribution ratios would be required to have a potentially significant effect on the SNF stability.

Also the effect of limestone as a potential near-field material was not studied. In principle, limestone is expected to have no significant effect on the fuel dissolution, because $CaCO_3$ should be rather inert relative to the UOX matrix. The presence of carbonate could lead to uranyl carbonate precipitation, but this involves only the already oxidized U(VI). Precipitation of U(VI) is not expected to have much effect on the UOX stability, similar as for sorption of U(VI).

6.12 Immobilization of released radionuclides in another form

The radionuclides released by the fuel are expected to be immobilized in another form, and are thus not immediately available for transport into the near-field. This immobilization is not explicitly considered in a source term model based only on the matrix dissolution rate. The immobilization will become measurable only after significant dissolution of spent fuel, which was not observed in the tests performed within the Belgian R&D programme. Hence, the evaluation of this mechanism under high pH conditions is based on literature.

A discussion of the immobilization of released radionuclides is given by Duro (Duro et al., 2010). It is mentioned that the reducing capacity of the fuel surface is so high, that the radionuclides will not escape from the matrix system. If the fuel is gradually transformed into secondary U(IV) phases, these phases will most probably host the actinides and rare earth elements in the structure in the proportions released to solution. Oxidized released radionuclides (e.g. Pu) are expected to be reduced and thus become less soluble. Actinides, lanthanides, Zr, Nb and divalent cations are compatible with the uraninite structure and are likely to be re-incorporated in tetravalent secondary phases. Trivalent actinides and rare earth elements will probably also be incorporated in secondary U(IV) phases. The elements not likely to be incorporated in the secondary U products are mainly those present as epsilon particles or metallic inclusions in the spent fuel matrix, mainly Rb, Tc, Ru, Pd, Ag, Cd, Sn, and Te. These elements are very likely to be immobilized by the presence of steel and its anoxically produced corrosion products, such as hydrogen gas. Ra is expected to co-precipitate with divalent solid phases.

The thus formed secondary phases formed at high pH constitute a secondary barrier for the release of these radionuclides. The incorporated radionuclides will be available for transport only after their release from these secondary phases, driven by solubility or specific dissolution kinetics. A source term model that neglects the incorporation of radionuclides in locally precipitated secondary phases will therefore be pessimistic. The effect should be radionuclide-dependent. Its quantification requires further studies, which may be focused on the most problematic radionuclides.

7 Open issues and recommendations

The study of the alteration behaviour of spent fuel and its analogues in anoxic and reducing highly alkaline conditions has shown that the fuel matrix dissolves in agreement with the general UOX matrix dissolution model.

The typical cement water composition has some particular effects on the UO_2 dissolution, but nevertheless, the tests that have been performed with depleted UO_2, with α-doped UO_2 and with real spent fuel in cement waters suggest a fuel stability that is in good agreement with the dissolution rates reported in the literature for neutral pH conditions. The rate decreases with decreasing fuel activity in anoxic conditions, until a threshold α-activity is reached at which the radiolytic oxidation does not further accelerate the fuel dissolution. Tests with Pu-doped UO_2 suggest that this stage is reached after about 90000 years. In the presence of hydrogen gas, the dissolution rate is low even for young fuel. This suggests that that the fuel disposed in highly alkaline conditions can have a very long life time, like natural UO_2 analogues that have survived over very long periods of time, be it in other geochemical conditions.

Estimations of the effective surface area were based on literature data, because they are not expected to depend much on the disposal design.

The proposed extrapolated reference dissolution rates cover a range from high to low rates, each corresponding to specified conditions. The rates measured in laboratory conditions on simplified or fresh fuels probably overestimate the long-term dissolution rate expected under geological disposal conditions.

There are nevertheless some important remaining limitations or questions:

- Tests with spent fuel and 3.2 bar hydrogen gas have shown very low concentrations of redox sensitive species such as Tc and U, suggesting that there was no or very little oxidative dissolution. An exact determination of the long-term dissolution rate was not possible, though. The dissolution rates derived from the tests probably overestimate the long-term rates. The effect of low hydrogen gas concentrations (corresponding to low steel corrosion rates) has not well been quantified at high pH. Tests with simulated old fuel did not show a dissolution suppressing effect of H_2 gas, probably because the fuel did not contain catalyzing epsilon particles, combined with the use of UO_2 powder. All this complicates the selection of a realistic long term dissolution rate.
- The dissolution rate estimations of old fuel in cement water are based on tests with depleted UO_2 and Pu-doped UO_2. Although the results are in good agreement with dissolution rates measured in other media under similar redox conditions, the number of experiments at high pH is still small, and the experimental uncertainty on the measurements is relatively large. This is at least partly due to the use of UO_2 powder, which has a large surface area that is very sensitive to traces of atmospheric O_2. This can lead to high U(VI) concentrations that form colloids that may reprecipitate. The cement waters are not always stable and tend to form precipitates, which may co-precipitate uranium. It is not yet clear if colloid formation is relevant also for geological disposal conditions.

- Thermodynamically, the oxidation of UO_2 to U(VI) should be favoured at high pH. The complexation of U(VI) with OH^- might prevent the formation of a partly protective oxide layer, similar to the effect of dissolved carbonate. The experiments performed so far give little or no evidence that this actually occurs and would lead to a faster fuel dissolution, but this may be due to the limited accuracy of the experiments, which were developed to demonstrate general evolutions in relatively realistic but complicated media, without focusing on particular phenomena. The confidence in the results would increase by additional, more fundamental research, with specific experimental set-ups that focus on specific phenomena.
- So far, most tests for the Belgian R&D programme were done in young cement water. Less tests were performed in the evolved cement water, although it is likely that the fuel will come in contact with evolved cement water sooner or later. The high Ca concentration in the evolved cement water has particular effects (colloid formation, possible protective effect) that should be studied more in detail.
- In the current evaluation, the presence of the near-field materials is included only via their effect on the composition of the water in contact with the fuel. The tests were done without addition of the actual near-field materials, except for a few tests with iron and magnetite. Tests with cement phases or limestone aggregate were not done. On the other hand, literature data suggest that sorption of U(IV) on concrete or metallic corrosion products is assumed to have a negligible effect on the fuel behaviour.
- All tests in highly alkaline conditions performed so far were done at ambient temperature. There were no tests at higher temperature.
- Important uncertainties remain regarding the boundary conditions to which the fuel will be exposed under geological disposal conditions. Tests have been done so far with UO_2 or spent fuel in contact with large volumes of water, but in reality, the fuel will probably be covered by a thin film of water or be in close contact with near-field materials with a low porosity, i.e. steel or steel corrosion products and secondary phases originating from the concrete and precipitated in the primary container. The radiolytic processes may be affected by these conditions. Most of the energy of the α-particles could be lost by interaction with the solids, leading to less water radiolysis. Oxidizing species generated by radiolysis in the porous medium may not reach the fuel surface because the surface layer acts as a diffusion barrier.
- The long-term evolution of the exposed surface area of the fuel remains uncertain. If fuel oxidation occurs, one can expect grain boundary opening, which might lead to fuel degradation, but in presence of H_2 gas, oxidation should not occur. In these conditions, the exposed surface area has no importance.

8 References

Altmaier, M., Neck, V., Müller, N. and Fanghänel, Th. (2005) Solubility of U(VI) and formation of $CaU_2O_7.3H_2O_{(Cr)}$ in alkaline $CaCl_2$ solutions. Book of abstracts Migration 2005 (Avignon, France, September 18-23), 143.

Amaya, M., Grismanovs, V. and Tverberg, T. (2010) Changes of the surface-to-volume ratio and diffusion coefficient of fission gas in fuel pellets during irradiation. Journal of Nuclear Materials 402, 108-115.

Auclair, G. (2001) Détermination des rendements radiolytiques primaires alpha en milieu alcalin. Université Pierre et Marie Curie, Thesis, p. 260.

Bastiaens, W., Bernier, F. and Li, X.L. (2007) SELFRAC: Experiments and conclusions on fracturing, self-healing and self-sealing processes in clays. Physics and Chemistry of the Earth 32, 600-615.

Bauhn, L., Hansson, N., Ekberg, C., Fors, P. and Spahiu, K. (2018) The fate of hydroxyl radicals produced during H_2O_2 decomposition on a SIMFUEL surface in the presence of dissolved hydrogen. Journal of Nuclear Materials 507, 38-43.

Bruno, J. and Spahiu, K. (2014) The long-term effect of hydrogen on the UO_2 spent fuel stability under anoxic conditions: Findings from the Cigar Lake Natural Analogue study. Applied Geochemistry 49, 178-183.

Cachoir, C., Carbol, P., Cobos, J., Glatz, J.P., Grambow, B., Lemmens, K., Martinez-Esparza, A., Mennecart, T., Ronchi, C., Rondinella, V.V., Serrano-Purroy, D., Spahiu, K., Wegen, D. and Wiss, T. (2005) Effect of alpha irradiation field on long term corrosion rates of Spent Fuel. Report JRC-ITU-SCA-2005-01, Edited by B. Grambow.

Cachoir, C. and Mennecart, T. (2011) Estimation of the effective surface area of UOX (MOX) spent fuel in Supercontainer disposal conditions (status 2010). SCK•CEN ER-142.

Cachoir, C. and Mennecart, T. (2015a) Spent fuel dissolution in Supercontainer conditions, Period 2012-2014, SCK•CEN-ER-275.

Cachoir, C. and Mennecart, T. (2015b) Executive summary of the level 5 report "Spent fuel dissolution in Supercontainer conditions, Reporting period 2009-2012, SCK•CEN-ER-231", SCK•CEN-ER-285.

Cachoir, C. and Mennecart, T. (2015c) Spent fuel dissolution in Supercontainer conditions, Reporting period 2009-2012, SCK•CEN-ER-231.

Carbol, P., Cobos, J., Glatz, J.P., Ronchi, C., Rondinella, V.V., Wegen, D. and Wiss, T. (2005) The effect of dissolved hydrogen on the dissolution of ^{233U} doped UO_2(s), high burn-up spent fuel and MOX fuel, SKB TR-05-09.

Carbol, P., Fors, P., Gouder, T. and Spahiu, K. (2009a) Hydrogen suppresses UO_2 corrosion. Geochimica et Cosmochimica Acta 73, 4366-4375.

Carbol, P., Fors, P., Van Winckel, S. and Spahiu, K. (2009b) Corrosion of irradiated MOX fuel in presence of dissolved H_2. Journal of Nuclear Materials 392, 45-54.

Casas, I., de Pablo, J., Clarens, F., Gimenez, J., Merino, J., Bruno, J. and Martinez-Esparza, A. (2009) Combined effect of H_2O_2 and HCO_3^- on UO_2(s) dissolution rates under anoxic conditions. Radiochim. Acta 97, 485-490.

Cerrato, J.M., Barrows, C.J., Blue, L.Y., Lezama-Pacheco, J.E., Bargar, J.R. and Giammar, D.E. (2012) Effect of Ca^{2+} and Zn^{2+} on UO_2 Dissolution Rates. Environ. Sci. Technol. 46, 2731-2737.

Chapman, N. and Hooper, A. (2012) The disposal of radioactive wastes underground. Proc. Geol. Assoc. 123, 46-63.

Choppin, G., Liljenzin, J.-O., Rydberg, J. and Ekberg, C. (2013) Radiation effects on matter, in: Elsevier Inc. (Ed.), Radiochemistry and nuclear chemistry, 4th ed, pp. 209-238.

Clacher, A. and Berry, J. (2010) Sorption of Uranium(IV) and Uranium(VI) onto LLWR Near-Field Materials. Serco (UK), Serco/TCS/003623/001/03.

Corkhill, C.L., Bailey, D.J., Tocino, F.Y., Stennett, M.C., Miller, J.A., Provis, J.L., Travis, K.P. and Hyatt, N.C. (2016) Role of microstructure and surface defects on the dissolution kinetics of CeO_2, a UO_2 fuel analogue. ACS applied materials & interfaces 8, 10562-10571.

Cui, D.Q., Devoy, J. and Spahiu, K. (2003a) The surface precipitation during UO_2 leaching process, in: Finch, R.J., Bullen, D.B. (Eds.), Mat. Res. Soc. Symp. Proc. Materials Research Society, Warrendale, pp. 359-364.

Cui, D.Q., Spahiu, K. and Wersin, P. (2003b) Redox reactions of iron and uranium dioxide in simulated cement pore water under anoxic conditions, in: Finch, R.J., Bullen, D.B. (Eds.), Mat. Res. Soc. Symp. Proc. Materials Research Society, Warrendale, pp. 427-432.

Duro, L., Grivé, M., Bruno, J. and Pehrman, R. (2010) Information on potential longterm conversion mechanisms of ceramic spent fuel material in the late post-closure phase. AMPHOS R-2225.2.

Ekeroth, E., Roth, O. and Jonsson, M. (2006) The relative impact of radiolysis products in radiation induced oxidative dissolution of UO_2. Journal of Nuclear Materials 355, 38-46.

Eriksen, T.E., Shoesmith, D.W. and Jonsson, M. (2012) Radiation induced dissolution of UO_2 based nuclear fuel - A critical review of predictive modelling approaches. Journal of Nuclear Materials 420, 409-423.

Ewart, F.T., Smith-Briggs, J.L., Thomason, H.P. and Williams, S.J. (1992) The solubility of actinides in a cementitous near-field environment. Waste Management 12, 241-252.

Fellhauer, D., Neck, V., Altmaier, M., Lutzenkirchen, J. and Fanghanel, T. (2010) Solubility of tetravalent actinides in alkaline $CaCl_2$ solutions and formation of $Ca_4[An(OH)_8]^{4+}$ complexes: A study of Np(IV) and Pu(IV) under reducing conditions and the systematic trend in the An(IV) series. Radiochim. Acta 98, 541-548.

Ferry, C., Piron, J.P., Poulesquen, A. and Poinssot, C. (2007) Update of the Instant Release Fraction Model for UO_2 PWR fuels, pp. Presentation given at Spent Fuel Workshop 2007 (Böttstein, Switzerland).

Ferry, C., Piron, J.P., Poulesquen, A. and Poinssot, C. (2008) Radionuclides release from the spent fuel under disposal conditions: Re-evaluation of the Instant Release Fraction, in: Lee, W.E., Roberts, J.W., Hyatt, N.C., Grimes, R.W. (Eds.), Mat. Res. Soc. Symp. Proc. Materials Research Society, Warrendale, pp. 447-454.

Ferry, C., Piron, J.P. and Ambard, A. (2010) Effect of helium on the microstructure of spent fuel in a repository An operational approach. Journal of Nuclear Materials 407, 100-109.

Fors, P., Carbol, P., Van Winckel, S. and Spahiu, K. (2009) Corrosion of high burn-up structured UO_2 fuel in presence of dissolved H_2. Journal of Nuclear Materials 394, 1-8.

Forsyth, R. (1997) An evaluation of results from the experimental programme performed in the Studsvisk Hot cell Laboratory. SKB report TR 97-25.

Fujiwara, K., Yamana, H., Fujii, T., Kawamoto, K., Sasaki, T. and Moriyama, H. (2005) Solubility of uranium(IV) hydrous oxide in high pH solution under reducing condition. Radiochim. Acta 93, 347-350.

González-Robles, E., Loida, A., Müller, N., Bohnert, E., Herm, M., Montoya, V., Kienzler, B. and Metz, V. (2014) Investigation of the Corrosion Behaviour of Spent Nuclear Fuel Fragments in High pH Solutions under H_2 Overpressure. KIT-INE report.

Govers, R., Boulanger, D., Meert, K., Leinders, G. and Verwerft, M. (2018) Characterization of Belgian spent fuel assemblies. Open Report BLG-1142.

Grambow, B., Loida, A., Martinez-Esparza, A., Diaz-Arocas, P., De Pablo, J., Paul, J.L., Marx, G., Glatz, J.P., Lemmens, K., Ollila, K. and Christensen, H. (2000) Final Report for EC contract FI4W-CT95-0004, Long-Term Safety of Radioactive Waste Disposal: Source Term for Performance Assessment of Spent Fuel as a Waste Form. Report FZKA6420.

Grambow, B. and Giffaut, E. (2006) Coupling of chemical processes in the near field, in: Van Iseghem, P. (Ed.), Mat. Res. Soc. Symp. Proc. Materials Research Society, Warrendale, pp. 55-66.

Grambow, B. and Lemmens, K. (2008) Dissolution and release from the waste matrix. NF-PRO, 1-100.

Grambow, B. and Lemmens, K. (2010) Model uncertainty for the mechanism of dissolution of spent fuel in nuclear waste repository. MICADO European Commission. 6th Framework Programme of the European Commision.

Grambow, B., Ferry, C., Casas, I., Bruno, J., Quinones, J. and Johnson, L. (2011) Spent Fuel Waste Disposal: Analyses of Model Uncertainty in the MICADO Project. Energy Procedia 7, 487-494.

Gray, W. and Wilson, R.F. (1995) Spent fuel dissolution studies FY 1991 to 1994. Pacific Northwest Laboratory. PNNL 10540.

IAEA (1991) Evaluation of Spent Fuel as a Final Waste Form, Technical Reports Series.

IAEA (2011) Disposal of radioactive waste. Specific safety requirements, IAEA Safety Standards Series, SSR-5, IAEA, Vienna, Austria.

Janeczek, J., Ewing, R.C., Oversby, V.M. and Werme, L.O. (1996) Uraninite and UO_2 in spent nuclear fuel: A comparison. Journal of Nuclear Materials 238, 121-130.

Jégou, C., Broudic, V., Poulesquen, A. and Bart, J.M. (2004a) Effects of alpha and gamma radiolysis of water on alteration of the spent UO_2 nuclear fuel matrix, in: Oversby, V.M., Werme, L.O. (Eds.), Mat. Res. Soc. Symp. Proc. Materials Research Society, Warrendale, pp. 391-396.

Jégou, C., Peuget, S., Broudic, V., Roudil, D., Deschanels, X. and Bart, J.M. (2004b) Identification of the mechanism limiting the alteration of clad spent fuel segments in aerated carbonated groundwater. Journal of Nuclear Materials 326, 144-155.

Jégou, C., Muzeau, B., Broudic, V., Peuget, S., Poulesquen, A., Roudil, D. and Corbel, C. (2005) Effect of external gamma irradiation on dissolution of the spent UO_2 fuel matrix. Journal of Nuclear Materials 341, 62-82.

Jerden, J.L., Frey, K. and Ebert, W. (2015) A multiphase interfacial model for the dissolution of spent nuclear fuel. Journal of Nuclear Materials 462, 135-146.

Johnson, L. and Joling, L.H. (1982) The dissolution of irradiated fuel under hydrothermal conditions. Scientific Basis for Nuclear Waste Management IV, 321-327.

Johnson, L. and Shoesmith, D.W. (1988) Spent Fuel. Radioactive Waste Forms for the Future, W. Lutze and R. Ewing (Eds.), Elsevier Science Publishers B.V., 635-698.

Kelm, M. and Bohnert, E. (2002) Radiolysis and corrosion of ^{238}Pu-doped UO_2 pellets in chloride brine. Proc. Indian Acad. Sci.-Chem. Sci. 114, 697-704.

Kursten, B., Uniform corrosion evaluation of C-steel in cementitious cnvironments relevant to the supercontainer design: Summary of corrosion rates from available literature and O/N funded RD&D projects, report SCK•CEN-ER-094, SCK•CEN, Mol, Belgium (2018).

Le Lous, K., Constantin, S., Paul, J.L., Sambugaro, D. and Vernaz, E. (1998) Leaching of spent fuel and simulated fuel in the presence of environmental materials: integral experiments. Mat. Res. Soc. Symp. Proc 506, 191-198.

Lemmens, K., Mennecart, T. and Cachoir, C. (2011) Spent fuel dissolution in Belgian Supercontainer conditions: source term and compatibility. Mat. Res. Soc. Symp. Proc. 1475, 131-136.

Linklater, C.M., Albinsson, Y., Alexander, W.R., Casas, I., McKinley, I.G. and Sellin, P. (1996) A natural analogue of high-pH cement pore waters from the Maqarin area of northern Jordan: Comparison of predicted and observed trace-element chemistry of uranium and selenium. J. Contam. Hydrol. 21, 59-69.

Loida, A., Grambow, B. and Geckeis, H. (2001) Congruent and incongruent radionuclide release during matrix dissolution of partly oxidized high burnup spent fuel, in: Hart, K.P., Lumpkin, G.R. (Eds.), Mat. Res. Soc. Symp. Proc. Materials Research Society, Warrendale, pp. 417-426.

Loida, A., Kelm, M., Kienzler, B., Geckeis, H. and Bauer, A. (2006) The effect of nearfield constraints on the corrosion behavior of high burnup spent fuel, in: Van Iseghem, P. (Ed.), Mat. Res. Soc. Symp. Proc. Materials Research Society, Warrendale, pp. 473-480.

Loida, A., Gens, R., Metz, V., Lemmens, K., Cachoir, C., Mennecart, T. and Kienzler, B. (2009a) Corrosion behavior of High Spent Fuel in Highly Alkaline Solutions. Mat. Res. Soc. Symp. Proc. 1193, 597-604.

Loida, A., Müller, N., Metz, V., Soballa, E., Schild, D. and Kienzler, B. (2009b) Investigation of the Corrosion Behaviour of Irradiated Spent Fuel in High pH Solutions. Final Report January 2009.

Loida, A., Müller, N., Metz, V., Bube, C. and Kienzler, B. (2010) Investigation of the Corrosion Behaviour of Irradiated Spent Fuel in High pH Solutions. Progress report September 2010.

Loida, A., Müller, N., Metz, V., Schild, D., Soballa, E. and Kienzler, B. (2011) Investigation of the Corrosion Behaviour of Irradiated Spent Fuel in High pH Solutions. Draft Final report, 2011 (Internal report).

Loida, A., Gens, R., Bube, C., Lemmens, K., Cachoir, C., Mennecart, T. and Kienzler, B. (2012) Corrosion behavior of spent nuclear fuel in high pH solutions – Effect of hydrogen. Mat. Res. Soc. Symp. Proc. 1475, 119-124.

Lutze, W. and Ewing, R.C. (1988) Radioactive waste forms for the future. chapter 11 (L.H. Johnson and D.W. Shoesmith).

Maes, N., Wang, L., Delécaut, G., Beauwens, T., Van Geet, M., Put, M., Weetjens, E., Marivoet, J., Van der Lee, J., Warwick, P., Hall, A., Walker, G., Maes, A., Bruggemann, C., Bennett, D., Hicks, T., Higgo, J. and Galson, D. (2004) Migration case study: Transport of radionuclides in a reducing clay sediment (TRANCOM II). report EUR 21022, European Commission, Brussels, Belgium.

Martinez Esparza, A. (2009) Development of a Matrix Alteration Model (MAM), ENRESA Publicacion téchnica 01/2005 .

Mennecart, T., Cachoir, C. and Lemmens, K. (2012) UO_2 dissolution in high pH conditions of the Belgian Supercontainer. Mat. Res. Soc. Symp. Proc. 1475, 293-298.

Moroni, L.P. and Glasser, F.P. (1995) Reactions between cement components and U(VI) oxide. Waste Management 15, 243-254. DOI 10.1016/0956-053x(95)00022-r.

Muzeau, B., Jégou, C., Delaunay, F., Broudic, V., Brevet, A., Catalette, H., Simoni, E. and Corbel, C. (2009) Radiolytic oxidation of UO_2 pellets doped with alpha-emitters (Pu-238/239). Journal of Alloys and Compounds 467, 578-589.

NEA (2008) Moving forward with geological disposal of radioactive waste: a collective statement by the NEA Radioactive Waste Management Committee (RWMC).

Neck, V. and Kim, J.I. (2001) Solubility and hydrolysis of tetravalent actinides. Radiochim. Acta 89, 1-16.

Ollila, K. (2007) Dissolution of unirradiated UO_2 and UO_2 doped with ^{233}U in low- and high-ionic-strength NaCl under anoxic and reducing conditions, Deliverable 1.5.11 of NF-PRO.

Ollila, K. (2008) Solubility of UO_2 in the High pH Range in 0.01 to 0.1 M NaCl solutions Under Reducing Conditions. Final activity report for VTT (WP1.5).

Ollila, K. (2011) Influence of Radiolysis on UO_2 Fuel Matrix Dissolution Under Disposal Conditions. POSIVA (2011-27).

ONDRAF/NIRAS (2004) A review of corrosion and material selection issues pertinent to underground disposal of highly active nuclear waste in Belgium, Final report for ONDRAF/NIRAS prepared by the Corrosion Study Panel. ONDRAF/NIRAS, Brussels, Belgium.

ONDRAF/NIRAS (2013) Development and Demonstration (RD&D) Plan for the geological disposal of high-level and/or long-lived radioactive waste including irradiated fuel if considered as waste, State-of-the-art report as of December 2012, ONDRAF/NIRAS, Brussels, Belgium.

ONDRAF/NIRAS (2017) Design and construction of the supercontainer for category C waste, ONDRAF/NIRAS, Brussels, Belgium.

Parks, G.A. and Pohl, D.C. (1988) Hydrothermal solubility of uraninite. Geochimica et Cosmochimica Acta 52, 863-875.

Pastina, B. and LaVerne, J.A. (2001) Effect of molecular hydrogen on hydrogen peroxide in water radiolysis. J. Phys. Chem. A 105, 9316-9322.

Poinssot, C., Toulhoat, P., Grouiller, J.-P., Pavageau, J., Piron, J.-P., Pelletier, M., Dehaijdt, P., Cappelaere, C., Limon, R., Desgranges, L., Jégou, C., Corbel, C., Maillard, S., Faure, M.-H., Cicariello, J.-C. and Masson, M. (2001) Syntheses on the long term behavior of spent nuclear fuel. Commissariat à l'Energie Atomique 1+2, 1-622.

Poinssot, C. (2005) CEA - R - 6093 Final report of the European project Spent Fuel Stability under Repository Conditions: files with all reports on CD.

Poinssot, C., Ferry, C., Grambow, B., Kelm, M., Spahiu, K., Martinez, A., Johnson, L., Cera, E., De Pablo, J., Quinones, J., Wegen, D., Lemmens, K. and McMenamin, T. (2006) Mechanisms governing the release of radionuclides from spent nuclear fuel in geological repository: Major outcomes of the European Project SFS, in: Van Iseghem, P. (Ed.), Mat. Res. Soc. Symp. Proc. Materials Research Society, Warrendale, pp. 421-432.

Pourbaix, M. (1974) Atlas of electrochemical equilibria in aqueous solutions. National Association of Corrosion Engineers.

Röllin, S., Spahiu, K. and Eklund, U.B. (2001) Determination of dissolution rates of spent fuel in carbonate solutions under different redox conditions with a flow-through experiment. Journal of Nuclear Materials 297, 231-243.

Roth, O. and LaVerne, J.A. (2011) Effect of pH on H_2O_2 Production in the Radiolysis of Water. J. Phys. Chem. A 115, 700-708.

Roudil, D., Jegou, C., Broudic, V., Muzeau, B., Peuget, S. and Deschanels, X. (2007) Gap and grain boundaries inventories from pressurized water reactor spent fuels. Journal of Nuclear Materials 362, 411-415.

Roudil, D., Bonhoure, J., Pik, R., Cuney, M., Jegou, C. and Gauthier-Lafaye, F. (2008) Diffusion of radiogenic helium in natural uranium oxides. Journal of Nuclear Materials 378, 70-78.

RP.W&D.0034 (2004) Design Specification 253-A21/1.4, Behaviour of spent fuel in Boom Clay disposal conditions, programme 2004-2008, Research plan RPWD0034 in the framework of the research agreement with SCK•CEN reference CO 90 01 1467.01 and NIRAS/ONDRAF reference CCHO-2004-2470/00/00 between SCK•CEN and NIRAS/ONDRAF.

RP.W&D.0060 (2009) Spent fuel dissolution in supercontainer conditions: research programme 2009-2014, Research plan RP.W&D.0060 (O/N reference LTBC03-SF-01) in the framework of the research agreement with SCK•CEN reference CO-90-08-2214-00 and NIRAS/ONDRAF reference CCHO-2009-00940000 between SCK•CEN and NIRAS/ONDRAF.

Salah, S., Cachoir, C., Lemmens, K. and Maes, N. (2006) Static dissolution tests of alpha-doped UO_2 under repository relevant conditions: Influence of Boom Clay and alpha-activity on fuel dissolution rates, in: Van Iseghem, P. (Ed.), Mat. Res. Soc. Symp. Proc. Materials Research Society, Warrendale, pp. 481-488.

Santos, B.G., Noël, J.J. and Shoesmith, D.W. (2006), The influence of calcium ions on the development of acidity in corrosion product deposits on SIMFUEL, UO_2, . Journal of Nuclear Materials 350, 320-331.

Shoesmith, D.W., Sunder, S., Bailey, M.G. and Miller, N.H. (1996) Corrosion of used nuclear fuel in aqueous perchlorate and carbonate solutions. Journal of Nuclear Materials 227, 287-299.

Shoesmith, D.W., Hocking, W.H., Ikdea, B.M., King, F., Noël, J.J. and Sunder, S. (1997) Application of electrochemical methods in the development of models for fuel dissolution and container corrosion under nuclear waste disposal conditions. Can .J. Chem 75, 1566-1584.

Shoesmith, D.W. and King, F. (1998) A Mixed-Potential Model for the Prediction of the Effects of Alpha-Radiolysis, Precipitation and Redox Processes on the Dissolution of Used Nuclear Fuel, Ontario Hydro, Nuclear Waste Management Division. Report 06819-REP-01200-MPM-R00.

Shoesmith, D. W. (2000) Fuel corrosion processes under waste disposal conditions. *Journal of Nuclear Materials*, vol. 282, pp. 1-31.

Shoesmith, D.W. (2008) The Role of Dissolved Hydrogen on the Corrosion/Dissolution of Spent Nuclear Fuel. NWMO Report No NWMO TR-2008-19.

SKB (2010) Data report for the safety assessment SR-site. Technical report TR-10-52.

SKB (2011) Long-term safety for the final repository for spent nuclear fuel at Forsmark, SKB. TR-11-01.

Spahiu, K. and Sellin, P. (2001) SR 97: Spent fuel alteration/dissolution and the influence of near field hydrogen, in: Hart, K.P., Lumpkin, G.R. (Eds.), Mat. Res. Soc. Symp. Proc. Materials Research Society, Warrendale, pp. 765-772.

Spahiu, K., Cui, D.Q. and Lundstrom, M. (2004) The fate of radiolytic oxidants during spent fuel leaching in the presence of dissolved near field hydrogen. Radiochim. Acta 92, 625-629.

Sunder, S., Boyer, G.D. and Miller, N.H. (1990) XPS studies of UO_2 oxidation by alpha radiolysis of water at 100 °C. Journal of Nuclear Materials 175, 163-169.

Sunder, S. and Shoesmith, D. (1991) Chemistry of UO_2 fuel dissolution in relation to the disposal of used nuclear fuel, Report AECL-10395.

Sutton, M., Warwick, P., Hall, A. and Jones, C. (1999) Carbonate induced dissolution of uranium containing precipitates under cement leachate conditions. J. Environ. Monit. 1, 177-182.

Thomas, L.E., Beyer, C.E. and Charlot, L.A. (1992) Microstructural analysis of LWR spent fuels at hight burnup. Journal of Nuclear Materials 188, 80-89.

Tits, J., Fujita, T., Tsukamoto, M. and Wieland, E. (2008) Uranium(VI) uptake by synthetic calcium silicate hydrates, in: Lee, W.E., Roberts, J.W., Hyatt, N.C., Grimes, R.W. (Eds.), Mat. Res. Soc. Symp. Proc. Materials Research Society, Warrendale, pp. 467-474.

Van Geet, M., Bastiaens, W. and Ortiz, L. (2008) Self-sealing capacity of argillaceous rocks: review of laboratory results obtained from the SELFRAC project. Physics and Chemistry of the Earth 33, S396-S406.

Wang, L. (2009) Near-field chemistry of a HLW/SF repository in Boom Clay - scoping calculations relevant to the supercontainer design. SCK ER-17.

Weetjens, E., Marivoet, J., Govaerts, J. and Leterme, B. (2012) Preparatory safety assessment: Conceptual model description of the reference case, First full draft, SCK•CEN, Mol, Belgium.

Werme, L.O., Johnson, L.H., Oversby, V., King, F., Spahiu, K., Grambow, B. and Shoesmith, D.W. (2004) Spent fuel performance under repository conditions: A model for use in SR-Can. SKB TR-04-19 Technical report.

Wersin, P., Johnson, L.H. and Schwyn, B. (2004) Assessment of redox conditions in the near field of nuclear waste repositories: Application to the swiss high-level and intermediate level waste disposal concept, in: Oversby, V.M., Werme, L.O. (Eds.), Mat. Res. Soc. Symp. Proc. Materials Research Society, Warrendale, pp. 539-544.

WNA (2017) Nuclear Fuel Fabrication. World Nuclear Association, London, UK.

Wu, L., Beauregard, Y., Qin, Z., Rohani, S. and Shoesmith, D.W. (2012) A model for the influence of steel corrosion products on nuclear fuel corrosion under permanent disposal conditions. Corrosion Science 61, 83-91.

Yu, L., Rogiers, B., Gedeon, M., Marivoet, J., De Craen, M. and Mallants, D. (2013) A critical review of laboratory and in situ hydraulic conductivity measurements for the Boom Clay in Belgium. Applied clay Science 75-76, 1-12.

9 Annex 1 : Literature data about the specific surface area of UO_2 and spent fuel

To express the dissolution rate of spent fuel or (α-doped) UO_2 per unit of surface area, the ***effective specific fuel surface area*** has to be known (see Section 3.2.7).

The effective specific fuel surface area is the specific fuel surface area that is contributing to the release of radionuclides. This includes the external surface area of the fuel pellets and the internal surface of the cracks and accessible grain boundaries of the pellets. It is expressed in units of surface area per unit of fuel mass. The fuel surface is an important parameter in the interpretation of experiments, if the dissolution step is rate determining (oxidative dissolution). The total oxidative dissolution will be proportional to this effective surface area. For solubility controlled non-oxidative dissolution, the surface area is irrelevant. Because there are good arguments to assume that the long term dissolution is solubility controlled, the long term evolution of the surface area is in principle not important. Nevertheless, it cannot be excluded that a surface dependent residual rate exists.

Hence, efforts were made to estimate the specific surface area of spent fuel and UO_2 or SIMFUEL samples used in experiments. This work was summarized in the MICADO project. Because the specific surface area will depend much on the sample preparation, a wide range of values is obtained, as illustrated in Figure 9-1 (Grambow et al., 2010). This figure compares the specific surface area calculated from sample geometry and measured by BET. The slope of the linear regression line corresponds to the surface roughness factor. An average roughness factor λ = 3.5 (uncertainty 2.6 to 9) can be deduced for irradiated fuel.

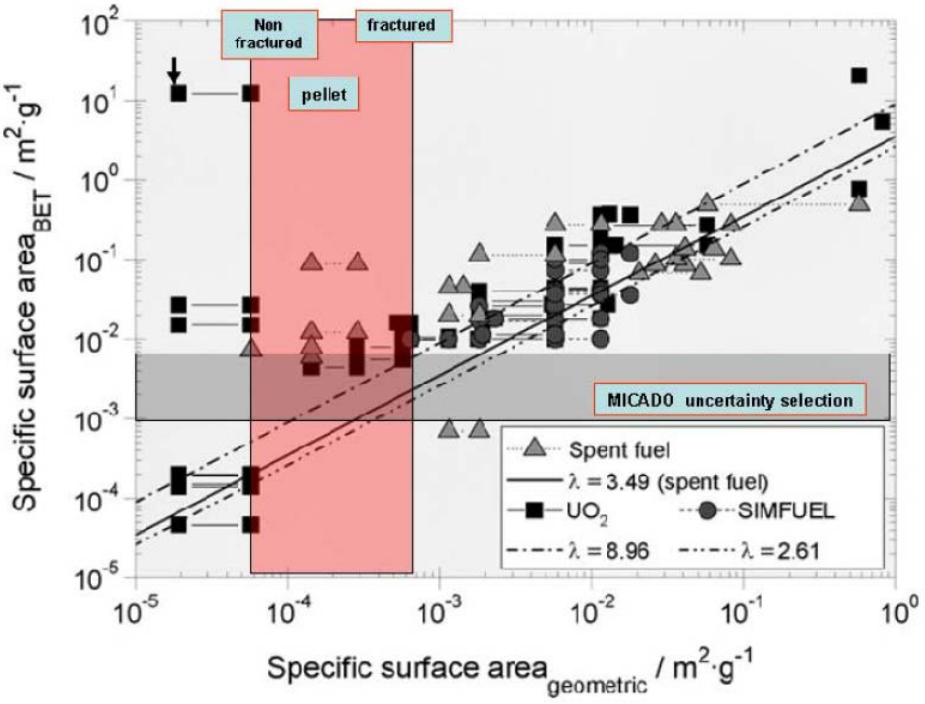

Figure 9-1: Specific surface area of various samples of spent fuel, UO_2 and SIMFUEL: comparison of specific surface area as calculated from sample geometry and as measured by BET. The slope of the linear regression line corresponds to the surface roughness factor. An average roughness factor λ = 3.5 (uncertainty 2.6 to 9) can be deduced for irradiated fuel.

Hereunder, we summarize the surface areas mentioned in literature, referring to the review of data by Cachoir (Cachoir et al., 2011) and the MICADO project (Grambow et al., 2010; Grambow et al., 2011). Specific surface areas can be measured, or calculated assuming a certain surface roughness and varying contributions from the grain boundaries. These different approaches lead to a certain range of the estimated specific surface area, from which a minimum and maximum can be selected. These values are given for spent fuel pellets or fragments in their current state. The effective specific surface area can change with time during the experiments, and is expected to change also gradually in geological disposal conditions.

- *Minimum specific surface area*

The lowest value taking into account the surface roughness factor without the grain boundaries for fragments of realistic size is 6 or 7.2 $cm^2 \cdot g^{-1}$. This may underestimate the real surface area, because the grain boundaries are expected to contribute to the dissolution as well (for irradiated fuel). This value was proposed by Cachoir (Cachoir et al., 2011) as minimal estimation of the effective surface area.
In the MICADO project (Grambow et al., 2010; Grambow et al., 2011), a rounded off minimum value of 10 $cm^2 \cdot g^{-1}$ fuel was proposed as minimum. This is a rather low value, based on the geometric surface area of representative large (mm size) fragments (2.5 $cm^2 \cdot g^{-1}$), corrected for surface roughness by a factor 3, and including some accessible grain boundary surface.

Remark:
The value of 10 $cm^2 \cdot g^{-1}$ fuel proposed in the MICADO project (Grambow et al., 2010; Grambow et al., 2011) as minimum can best explain the experimental observations. Indeed, the value of 10 $cm^2 \cdot g^{-1}$ fuel gives dissolution rates for spent fuel that are comparable to dissolution rates on α-doped UO_2 in similar test conditions. For example, typical fractional dissolution rates of spent fuel under reducing conditions are in the range of 10^{-9} day^{-1} (Carbol et al., 2005). With a specific surface area of 10 $cm^2 \cdot g^{-1}$, this corresponds to normalized dissolution rates of about 1 $\mu g \cdot m^{-2} \cdot d^{-1}$. This value is similar to the dissolution rate measured on α-doped UO_2 in reducing conditions, using the isotopic dilution method (Ollila et al., 2007) (see Figure 6-3), and in dynamic tests in (reducing) Boom Clay water (Poinssot et al., 2005). Similar conclusions can be drawn for tests in oxic conditions: when specific surfaces larger than 10 $cm^2 \cdot g^{-1}$ fuel are used to convert fractional release rates from spent fuel to surface area normalized rates, the resulting rates in oxic conditions are around or below the lower boundary of the dissolution rate for unirradiated UO_2. A better agreement is reached with the specific surface area of 10 $cm^2 \cdot g^{-1}$ fuel. A relatively low specific surface area like 10 $cm^2 \cdot g^{-1}$ fuel also fits with the experimental observation that the fractional dissolution rate decreased in certain tests from 10^{-4} $year^{-1}$ to 3×10^{-7} $year^{-1}$, probably by the formation of solid precipitates, blocking water access to fracture surfaces (Forsyth et al., 1997). For these reasons, the specific fuel surface of 10 $cm^2 \cdot g^{-1}$ is considered by Cachoir (Cachoir et al., 2011) as a good estimation for the present fuels.

- *Maximum specific surface area*

Most measured and calculated surface areas found in literature and summarized by Cachoir (Cachoir et al., 2011) are higher than 10 $cm^2 \cdot g^{-1}$. The highest reported specific surface area measured on relevant fuel fragments is a BET surface area of 120 $cm^2 \cdot g^{-1}$. This value is high compared to other BET measurements on similar samples. SCK•CEN estimations suggest that

a surface area of 120 $cm^2 \cdot g^{-1}$ is much higher than the average corrected geometric surface area, which was 66 $cm^2 \cdot g^{-1}$. Nevertheless, the BET measurement of 120 $cm^2.g^{-1}$ on relevant fuel fragments cannot be simply discarded just because it is too high. The high value may be realistic for specific samples, due to a large grain boundary contribution. It is, however, probably not representative for the average fuels. The surface area of 120 $cm^2 \cdot g^{-1}$ would thus be a very pessimistic reference value.

In het MICADO project (Grambow et al., 2010; Grambow et al., 2011), a maximum specific surface area of 71 $cm^2 \cdot g^{-1}$ is proposed, which is the average BET measurement on fuel fractions of the relevant size, but omitting the highest value of 120 $cm^2 \cdot g^{-1}$.

In the topical report from Cachoir (Cachoir et al., 2011), the average of the BET measurements on fuel fragments or pellets of relevant size including the high value of 120 $cm^2 \cdot g^{-1}$ is calculated as well. This gives a value of 80 $cm^2 \cdot g^{-1}$. This value assumes a high accessibility of the grain boundaries. It is relatively high, because it was obtained with declad fuels, for which the accessibility of the surfaces is believed to be higher than for clad fuel. Indeed, the surface normalized dissolution rate in oxidizing conditions was 8-10 times lower for clad fuel than for unclad fuel.

Table 9-1 summarizes the proposed reference specific surface areas.

Table 9-1: Minimum and maximum reference specific surface area of spent UOX fuel

Minimum	Maximum
6 $cm^2 \cdot g^{-1}$	80 $cm^2 \cdot g^{-1}$

Remarks:

- A specific surface area of 10 $cm^2 \cdot g^{-1}$ is a plausible estimation of the fuel surface also for the pellets that were used in the Belgian R&D programme with cement water. The surface normalized dissolution rate of spent fuel at high pH without H_2 overpressure is 100 $\mu g \cdot m^{-2} \cdot d^{-1}$ for a specific surface area of 10 $cm^2 \cdot g^{-1}$ (Table 6-2). This is higher than the dissolution rate of α-doped fuel F1 (12 – 79 $\mu g \cdot m^{-2} \cdot d^{-1}$, see Table 6-1), which can be expected because F1 does not have a significant β,γ–activity. With the specific surface area of 80 $cm^2 \cdot g^{-1}$, the calculated dissolution rate would be 13 $\mu g \cdot m^{-2} \cdot d^{-1}$ and thus similar as for fuel F1, or even lower, implying that the β,γ activity would have no effect on the fuel dissolution rate, which is unlikely. Moreover, the fuel surface was covered by precipitates in ECW. This may also reduce the effective surface area.
- The given range for the specific surface area can be compared with the measurements based on the release of short-lived gaseous isotopes, shown in Figure 3-9. For higher burnup fuels an SA/V of 400 to 1200 cm^{-1} is given. With a fuel density of approximately 10 $g \cdot cm^{-3}$, this corresponds to 40 to 120 $cm^2 \cdot g^{-1}$. This would be higher than the best estimate of 10 $g \cdot cm^{-2}$. This implies that the fine structured rim surface that is responsible for the large specific surface area of high burnup fuel apparently does not contribute to the matrix dissolution, because the porosity in the rim zone would not be interconnected.

- In the MICADO project (Grambow et al., 2010), a best estimate specific surface area of 40 $cm^2 \cdot g^{-1}$ was proposed as the mathematical average between the proposed minimum (10 $cm^2 \cdot g^{-1}$) and the proposed maximum (71 $cm^2 \cdot g^{-1}$). This average can, however, not be linked clearly to the expected phenomenology. It may be too low on the long term, when the grain boundaries may contribute more because the dissolution on the external surface decreases, or when the fuel physically disintegrates. It may be too high on the short term, when the accessible surface area is lower due to protection by the cladding and surface decreasing effects such as observed by Forsyth (Forsyth et al., 1997).
- In the MICADO project (Grambow et al., 2010), distinction was made between the external surface area of the fuel pellets (the large cracks), where the dissolution reactions are less hindered by transport, and the internal surface area (the narrow cracks), where there is more hindrance. The quantification of this effect is, however, still very difficult, and relevant mostly for the first stage of radiolytic oxidative dissolution. Moreover, the external surface of the pellets may still be covered by a cladding, and thus subjected to limited accessibility. Therefore, we propose not to make this distinction for the selection of reference surface areas under geological disposal conditions.
- For MOX fuel, the surface area would be lower than for UOX, because 85% of its surface would have no accessible grain boundaries.

Expected long-term evolution of the effective surface area

The initial surface area is an intrinsic fuel property, independent from the disposal design. It depends on the number of particles and their size distribution, but also on the surface roughness.

The fuel surface area is expected to change, but only very gradually. For this reason, the surface area measured on today's fuels can be considered as the surface area at the time of contact with ground water and during the major part of the fuel life time. In this section, we give the argumentation that supports this assumption. A detailed discussion of the involved aspects with a full list of references is given in the topical report from Cachoir (Cachoir et al., 2011). A summary is given hereunder.

After disposal of the fuel, the effective surface area can evolve further with time. This will be a very slow evolution, which will become potentially significant only on the very long term.

This evolution can in principle be influenced by environmental factors: (1) external pressure, (2) opening of grain boundaries by intergranular cracking, (3) fuel oxidation, and (4) fuel dissolution.

(1) The external pressure could damage fuel rods when the overpack has become mechanically unstable. This might in principle break up the fuel, but because the spent fuel already consists of millimeter size fragments that can be dislocated to accommodate to imposed pressures, it is not evident that this will lead to further fragmentation. We did not find specific publications devoted to this problem in the open literature.

(2) In the course of the storage and disposal of the spent fuel, the gradual opening of the grain boundaries by intergranular cracking, caused by He accumulation, could increase the accessible grain boundary surface. He pressure could cause intergranular cracking on the (very) long term, but the available data suggest that the critical pressure for microcracking will not be reached (Ferry et al., 2008; Ferry et al., 2010; Roudil et al., 2008), and that the fuel matrix can resist to very high gas bubble pressures (Thomas et al., 1992). Moreover, because microcracks should be sufficient to release the pressurized He, this should not cause a significant increase of the specific surface area. Similar conclusions can be drawn for the rim zone, but the degree of confidence is smaller in this case (Grambow et al., 2008).
In addition, it is not clear whether the opening of the grain boundaries would actually lead to an increase of the reactive surface area and alteration rate. If the accessible water volume near the grain boundaries is not large enough, α-particles may produce only insignificant amounts of radiolytic species. Mass transfer processes are much slower in fractures, while cementation processes by reaction products will be much more important.

(3) Oxidation of spent fuel seems to increase the grain boundary accessibility, but this has no effect on the leach rate. The formation of secondary phases with oxidized uranium can cause a volume expansion. This can cause the complete fuel disintegration. However, extensive fuel oxidation is not expected under the anticipated storage and disposal conditions (in Belgium and in the other European disposal concepts). Therefore, enhancement of the surface area by oxidation is not considered important in the assessment of the effective surface area.

(4) Fuel alteration at the grain boundaries after water intrusion might also cause microcracking. This will depend on the nature of the spent fuel, the local oxidant concentration and the duration of contact with water. The long-term evolution of the effective surface area under the influence of fuel alteration processes remains, however, difficult to predict. Currently there are no models available to describe the evolution of the grain boundaries over hundreds of thousands of years. One can nevertheless assume that on the very long term, the fuel dissolution will cause a decrease of the effective surface area, because the dissolving spent fuel fragments will gradually get smaller.

On the shorter term, the dissolution of the fuel in contact with water appears to increase the specific surface area of spent fuel particles, even without grain boundary opening. This has, however, no effect on the leach rate. Hence this effect is not considered in the assessment of the effective surface area.

There is experimental evidence for these hypotheses: the accessibility of fuel fragment surfaces strongly decreases with time (Forsyth et al., 1997), and even if the BET surface increased after fuel oxidation, the fuel dissolution rate was not affected (Gray et al., 1995), so the contribution of the opened grain boundaries was apparently small.

On the other hand, precipitation layers can reduce the accessibility of the fuel surface. Shoesmith describes how the accumulation of secondary phases in grain boundaries appears to block the further dissolution of CANDU fuel (Shoesmith et al., 1996). The principle of protection by a precipitation layer is also considered in the recent Fuel Matrix Dissolution Model (Jerden et al., 2015). The tests with spent fuel in ECW showed the precipitation of

secondary Ca phases on the fuel surface. The resulting decrease of the effective surface area may explain the relatively low fractional dissolution rates (see Fig. 6-2) (Loida et al., 2009b).

So, there are no evident mechanism that could cause a fast increase or decrease of the effective fuel surface area in reducing conditions. Surface increasing and decreasing effects will partly compensate. Important changes can be expected only on the very long term, when the fuel has very much degraded. As suggested by natural analogue studies, this may happen only over geological timescales. Moreover, long term changes of the fuel surface area will have little effect on the fuel stability, because - when the threshold for oxidative dissolution has been reached - the further dissolution is probably solubility controlled. For this reason, a constant effective fuel surface area, based on the measurements on today's fuels can be assumed for the largest part of the life time of the fuel. By selecting a suitable range, the uncertainties about a potential increase can be included.